AD

DEVELOPMENT OF HIGH-ENERGY BATTERIES FOR ELECTRIC VEHICLES

Progress Report for the Period

July 1970—June 1971

By

E. J. Cairns
R. K. Steunenberg
J. P. Ackerman
B. A. Feay
D. M. Gruen
M. L. Kyle
T. W. Latimer
J. N. Mundy
R. Rubischko
H. Shimotake
D. E. Walker
A. J. Zielen
A. D. Tevebaugh

July 1971

Prepared for

The Division of Advanced Automotive Power Systems Development
Environmental Protection Agency
Ann Arbor, Michigan

Chemical Engineering Division
ARGONNE NATIONAL LABORATORY
9700 South Cass Avenue
Argonne, Illinois
60439

Work performed under an agreement between the ENVIRONMENTAL PROTECTION AGENCY, Office of Air Programs, Division of Advanced Automotive Power Systems Development, and the United States Atomic Energy Commission.

Argonne National Laboratory
Chemical Engineering Division
9700 South Cass Avenue
Argonne, Illinois
60439

DEVELOPMENT OF HIGH-ENERGY BATTERIES FOR ELECTRIC VEHICLES

Progress Report for the Period July 1970 - June 1971

by

E. J. Cairns
R. K. Steunenberg
J. P. Ackerman
B. A. Feay
D. M. Gruen
M. L. Kyle
T. W. Latimer
J. N. Mundy
R. Rubischko
H. Shimotake
D. E. Walker
A. J. Zielen
A. D. Tevebaugh

July 1971

Prepared for
the Division of Advanced Automotive Power Systems Development
Environmental Protection Agency
Ann Arbor, Michigan

FOREWORD

This is the second annual technical progress report of a research and development program conducted by the Chemical Engineering Division of Argonne National Laboratory under an agreement between the United States Atomic Energy Commission and the Environmental Protection Agency, Office of Air Programs, Division of Advanced Automotive Power Systems Development. The period covered by this report is July 1, 1970, through June 30, 1971.

The long-term goal of this program is to develop the technology for the construction and testing of a lithium/sulfur battery suitable for powering an electric family automobile. The immediate goals are the development and scale-up of single lithium/sulfur cells, followed by the development and testing of small (1-2 kW) batteries.

Overall program management is the responsibility of Dr. R. C. Vogel, Division Director, and Dr. A. D. Tevebaugh, Associate Division Director. Technical direction is provided by Dr. E. J. Cairns, Section Head, and Dr. R. K. Steunenberg, Group Leader. The project officer for OAP is Mr. Charles E. Pax.

TABLE OF CONTENTS

		Page
ABSTRACT		1
SUMMARY		2
I.	INTRODUCTION	6
II.	INVESTIGATIONS OF LITHIUM/SULFUR CELLS	9
	A. Experimental Procedure	9
	B. Results and Discussion	13
	C. Conclusion	26
III.	SUPPORTING LABORATORY INVESTIGATIONS	30
	A. Phase Equilibrium Studies of Electrolyte-Containing Mixtures	30
	B. Studies of Sulfur-Bearing Species in Molten Alkali Halides	33
	1. Electrodes	34
	2. Direct Sulfide Analysis in Molten Salt	35
	3. Electrochemical Generation of S^{2-}	36
	4. Spectrochemical Studies	38
	5. Analysis of Frozen Eutectic Samples	38
	C. Solid-Electrolyte Studies	38
	1. Li_2O-MgO-Al_2O_3 System	39
	2. Li_2O-La_2O_3-Al_2O_3 System	40
	3. Sodium β- and β"-Alumina	41
	4. Conductivity	43
	D. Cathode Material Studies	44
	E. Mass-Transport Studies	47
IV.	MATERIALS TESTING AND FABRICATION	52
	A. Experimental Procedure	52
	B. Metallic Components Studies	53
	C. Seals and Insulating Component Studies	59
	D. Development and Fabrication of Ceramic Insulators	61
	1. Lithium Aluminate	62
	2. Lithium-Aluminate Sintering Studies	62
	3. Cell Insulator Production	63
	E. Cathode Current Collector Development	66

TABLE OF CONTENTS

	Page
V. ELECTRIC AUTOMOBILE PERFORMANCE CALCULATIONS	67
A. Cell Design	67
B. Method of Calculating Automobile Performance	69
C. Results and Discussion	76
D. Lithium Reserves	79
VI. STATUS AND FUTURE PLANS	80
REFERENCES	82
APPENDIX: SUMMARY OF PERFORMANCE OF CELLS OPERATED IN FISCAL YEAR 1971	84

LIST OF ILLUSTRATIONS

No.	Title	Page
1.	Schematic Diagram of a Typical Unsealed Laboratory Cell.	10
2.	Schematic Diagrams of Some Cathode Current Collector Designs . . .	13
3.	Schematic Diagram of a Mixed Cathode	15
4.	Typical Voltage-Current Density Curve for a Lithium/Sulfur Cell With a Laminated Cathode Having All-Stainless-Steel Laminae. . . .	16
5.	Typical Voltage-Capacity Density Curve for a Lithium/Sulfur Cell With a Laminated Cathode Having All-Stainless-Steel Laminae. . . .	17
6.	Voltage-Capacity Density Curves for a Lithium/Sulfur Cell With a Laminated Cathode Having Porous Graphite and Stainless Steel Feltmetal Laminae.	18
7.	Voltage-Capacity Density Curves for a Lithium/Sulfur Cell With a Comb-Type Cathode.	19
8.	Voltage-Capacity Density Curves for a Lithium/Sulfur Cell With an Enclosed Laminated Cathode.	20
9.	Capacity Density as a Function of Cycle Number for a Lithium/ Sulfur Cell With an Enclosed Laminated Cathode	21
10.	Voltage-Capacity Density Curves for a Lithium/Sulfur Cell With a Reservoir Cathode.	21
11.	Voltage-Capacity Density Curves for a Lithium/Sulfur Cell With an Enclosed Reservoir Cathode.	22
12.	Capacity Density as a Function of Cycle Number for a Lithium/ Sulfur Cell With a Mixed Cathode	24
13.	Voltage-Capacity Density Curves for a Lithium/Sulfur Cell With a Mixed Cathode.	24
14.	Voltage-Capacity Density Curves for a Lithium/Sulfur Cell With a Mixed Cathode Containing a Niobium Expanded-Mesh Spiral Current Collector.	25
15.	Schematic Drawing of a Sealed Lithium/Sulfur Cell.	26
16.	Phase Diagram of the Pseudo-ternary System Li_2S-S(LiBr-RbBr) . . .	30
17.	Molten-Salt Cell Assembly for Sulfide-Ion Investigations	34
18.	Precipitation Titration Curve for S^{2-} With Generated Ni^{2+}; Experiment LK-4.	35

LIST OF ILLUSTRATIONS

No.	Title	Page
19.	The Potential of the Ni/Ni^{2+} Electrode as a Function of S^{2-} Concentration.	37
20.	Ionic Conductivity of Aluminate Samples.	44
21.	Schematic Diagram of the Lithium Electrode Test Cell	48
22.	Typical Voltage-Time Behavior of a Li/LiCl-KCl/Li-Al Cell at 425°C and at a Current Density of 0.25 A/cm^2	48
23.	Lithium/Sulfur Test Cell	51
24.	Corrosion Rates of Metals Exposed to 20 at. % Li-S Mixtures at 375°C.	53
25.	Schematic Diagram of a Chromium-Plated Cell.	55
26.	Voltage-Capacity Density Curves for a Chromium-Plated Li/S Cell With LiBr-RbBr Electrolyte	56
27.	Voltage-Capacity Density Curves for a Chromium-Plated Li/S Cell With LiF-LiCl-KCl Electrolyte.	58
28.	Corrosion Rates of Electrical Insulators in Molten Lithium at 375°C.	61
29.	Photograph of a Rubber Die and Sealing Plug.	65
30.	Photograph of Isostatically Pressed $LiAlO_2$ Insulator Rings	65
31.	Specific Energy and Schematic Design of a Li/LiCl-KCl/Li in S Square Laminated Sealed Cell	68
32.	Conceptual Li/S Cell Design Used in Automobile Performance Calculations	70
33.	Voltage-Capacity Density Data and Empirical Curves for Li/S Cells With Laminated Cathodes.	74
34.	Driving Profiles With Corresponding Power Profiles for the Automobile of Table XXII	75
35.	Electric Automobile Ranges for Selected Driving Profiles	78
36.	Effect of Automobile Velocity on Range for Constant Velocity Driving.	78

LIST OF TABLES

No.	Title	Page
I.	Lithium/Sulfur Battery Development Program Goals.	8
II.	Physical Properties of Molten-Salt Electrolytes	10
III.	Physical Characteristics and Electrical Performance of Two Mixed-Cathode Cells	23
IV.	Construction and Performance Characteristics of a Sealed Lithium/Sulfur Cell	27
V.	Performance of Some Typical Lithium/Sulfur Cells.	29
VI.	Phases Present at Selected Compositions in the System Li_2S-S-(LiBr-RbBr).	31
VII.	Solubility of L_2 in L_3 for Various Electrolytes at 360 and 400°C	32
VIII.	Titration of S^{2-} in LiCl-KCl Eutectic with a Nickel Anode; Evaluation of Ni/Ni^{2+} Formal Potential and NiS Solubility Product	36
IX.	Starting Compositions (in wt %) of Li_2O-MgO-Al_2O_3 Specimens . .	40
X.	Weight Loss and Density of Li_2O-MgO-Al_2O_3 Compositions Fired at 1700 and 1800°C.	40
XI.	Starting Compositions (in wt %) of Li_2O-La_2O_3-Al_2O_3 Specimens .	41
XII.	Weight Losses and Densities of Li_2O-La_2O_3-Al_2O_3 Compositions Fired at 1500, 1650, and 1700°C	41
XIII.	Fired Densities of Monofrax H Specimens	42
XIV.	Effect of Milling Time on Unfired and Fired Densities of Alcoa β-alumina	42
XV.	Electrical Conductivities of the Two Immiscible Liquid Phases in the Sulfur-Rich Region of the Thallium-Sulfur Phase Diagram	46
XVI.	Summary of Lithium Electrode Cell Tests	49
XVII.	Corrosion of Aluminum and Ferritic Stainless Steel in LiCl-KCl Electrolyte and 20 at. % Li-S Mixtures at 375°C	55
XVIII.	Performance of a Chromium-Plated Li/S Cell.	57
XIX.	Corrosion Rates of Electrical Insulators in Molten Lithium. . .	60

LIST OF TABLES

No.	Title	Page
XX.	Characteristics of $LiAlO_2$ Powders	62
XXI.	Characteristics of Sintered $LiAlO_2$ Ceramic Bodies	64
XXII.	Electric Automobile Characteristics	69
XXIII.	Weight and Material Cost Breakdown for Conceptual Cell and Battery Design	71
XXIV.	Electric Automobile Performance Under Selected Driving Profiles	77

DEVELOPMENT OF HIGH-ENERGY BATTERIES FOR ELECTRIC VEHICLES

by

E. J. Cairns, R. K. Steunenberg, J. P. Ackerman, B. A. Feay, D. M. Gruen, M. L. Kyle, T. W. Latimer, J. N. Mundy, R. Rubischko,* H. Shimotake, D. E. Walker, A. J. Zielen, and A. D. Tevebaugh

ABSTRACT

The objective of the High-Energy Battery Development Program at Argonne National Laboratory is to develop the technology required to construct secondary batteries having the performance capabilities required for pollution-free electric automobiles. Batteries for this application should have an energy-storage capability of 220 W-hr/kg and be able to deliver power at a peak rate of 220 W/kg. Their cost should not exceed about $10/kW-hr of energy storage capability. Lithium/sulfur cells using a molten lithium halide-containing electrolyte and operating at 360 to 390°C have achieved capacity densities of up to 0.52 A-hr/cm^2 (above 1 V) at a current density of 0.52 A/cm^2. These results are consistent with the specific energy and specific power goals, but the cycle life (currently hundreds of cycles) and the sulfur electrode performance require further improvement.

The cell development program is supported by laboratory studies in various areas. The solubility of cathode materials in various electrolytes and the identity of the soluble species are being studied. Preliminary results indicate that electrolytes containing only fluoride and chloride anions have the lowest solubility for sulfur-bearing species. Investigations of various additives to sulfur indicate that thallium may be useful in reducing the vapor pressure and increasing the conductivity of sulfur. A survey of candidate solid electrolytes has led to the investigation of the lithium form of β-alumina. Mass transport studies have shown that an improved cycle life of the lithium electrode (hundreds of cycles) can be obtained by using LiF-LiCl-KCl electrolyte and by minimizing the concentration of various impurities in the cell.

The investigation of the corrosion rates of various materials at 375°C has shown that chromium and molybdenum had low corrosion rates in 20 at. % Li in S, and lithium aluminate, beryllia, aluminum nitride, yttria, thoria, $Y_3Al_5O_{12}$, and $MgO \cdot Al_2O_3$ had low corrosion rates in lithium. Work has begun on the preparation of various forms of some of these materials, with most of the effort on $LiAlO_2$ shapes.

Battery design and performance calculations carried out for a 1075-lb Li/S battery in a 4300-lb (curb weight) electric automobile indicate that a range of 88 to 225 miles can be expected under realistic driving conditions, depending on the driving profile and accessory load.

---

*Resident Associate from Gould, Inc.

SUMMARY

Investigations of Lithium/Sulfur Cells

Experimental studies of small cells of the types Li/LiX/S and Li/LiX/P_4S_{10}, where LiX represents a low-melting salt mixture containing lithium halides, operating at ~375°C have indicated that these cells show promise for meeting the requirements of a low-cost, high-specific-energy and high-specific-power battery for electric automobile propulsion. The immediate goals of the cell program are to produce laboratory cells with a specific energy of 220 W-hr/kg and a specific power of 220 W/kg. These goals, when related to single-cell performance, imply a capacity density (at the 1-hr rate) of 0.4 A-hr/cm^2, a sulfur utilization near 70%, a capacity per unit volume of cathode of 1.0 A-hr/cm^3, and for the battery to be economical, a cycle life of over 1000 cycles.

During the last year, significant progress in cell design and performance has been made. As a result of the investigation of a number of new cathode current collector designs, laboratory cells have demonstrated capacity densities (at the 1-hr rate) of up to 0.52 A-hr/cm^2. Other cells, operating at lower current densities and capacity densities, have demonstrated a cycle life of more than 800 discharge-charge cycles (over 1100 hr of operation). Although these results are encouraging, the capacity per unit volume (currently <0.5 A-hr/cm^3), the sulfur utilization (currently 30 to 50%), and the retention of good performance levels over long cell lifetimes must be improved in order to satisfy the requirements for practical electric vehicle batteries.

Phase Equilibrium Studies of Electrolyte-Containing Mixtures

In order to minimize possible difficulties caused by transport of cathode material through the electrolyte of lithium/sulfur cells, the mutual solubilities of several electrolyte-cathode material combinations are being determined. This information will be used to select the optimum electrolyte and cell operating temperature range.

The present aim of the experimental program is to determine the pseudo-ternary phase diagram of the Li_2S-S-electrolyte system using various candidate cell electrolytes such as LiBr-RbBr, LiCl-LiI-KI, LiF-LiCl-LiI, LiCl-KCl, and LiF-LiCl-KCl. Initial indications are that the system is similar to the Li_2Se-Se-electrolyte system, which has been studied in some detail. There are apparently one solid-phase and three liquid-phase fields in the diagram. The complete phase diagram has not yet been determined, but it is clear from the results gathered so far that salt mixtures containing only the small anions (chloride and fluoride) are the desirable cell electrolytes if the choice is made solely on solubility considerations.

Studies of Sulfur-Bearing Species in Molten Alkali Halides

The goals of this research are to study the molten salt chemistry, electrochemistry, and spectroscopy of the sulfur-sulfide-polysulfide system. Sulfide solutions free of elementary sulfur have been prepared at 400 and 450°C in LiCl-KCl eutectic salts by electrolysis with a nickel sulfide cathode: $NiS + 2\ e^- = Ni + S^{2-}$. (The reverse reaction, or precipitation

titration with a nickel anode, has been used for coulometric *in situ* sulfide analysis.) The results have yielded solubility data on Li_2S and NiS and the formal potential of the Ni/Ni^{2+} couple. It has been demonstrated that the Ni/Ni^{2+} couple can serve as a sulfide ion monitor and that the calculated concentrations so obtained are in agreement with the coulometric generation values. A "standard" sulfide solution was prepared electrochemically, and it is being used in a spectrophotometric study of sulfur, sulfide, and polysulfide species. Analytical methods for sulfide and total sulfur in solid salts are under evaluation. Excellent results have been obtained for sulfide ion using an Orion silver/sulfide specific ion electrode for potentiometric end-point detection in argentometric titrations in alkaline ammoniacal solutions.

Solid Electrolyte Studies

Solid electrolytes that are capable of adequate lithium-ion transport in lithium/sulfur cells are being investigated as alternate electrolytes to the molten salt in current use. The Li_2O-MgO-Al_2O_3, Li_2O-La_2O_3-Al_2O_3, and sodium β- and β"-alumina systems have been studied. The activation energies for the lithium-containing materials were between 17 and 21 kcal/mol. Conductivity was found to be linear when plotted as log conductivity versus 1/T and in the range of 10^{-8} to 10^{-3} ohm^{-1} cm^{-1} in the temperature range of 350 to 900°C. The conductivities of the sodium aluminates show a curved relationship and an activation energy of ∿5 kcal/mol when plotted on similar coordinates. Conductivities in the range of 10^{-4} to 10^{-1} ohm^{-1} cm^{-1} were measured in the temperature range from 350 to 900°C. This conductivity of the sodium aluminates is lower than anticipated and it is expected that with improved fabrication techniques a conductivity near 10^{-1} ohm^{-1} cm^{-1} at 400°C can be obtained. The molten-salt electrolytes in current use have conductivities near 1 ohm^{-1} cm^{-1}. None of the solid-electrolyte data obtained to date appears sufficiently promising to warrant cell operation with these electrolytes. Consequently, this investigation will concentrate on determining the materials systems, and the methods of producing them, that show promise as solid lithium-ion conductors.

Cathode Materials Studies

Although the small-scale tests have shown that elemental sulfur alone can be used as the active cathode material in lithium/sulfur cells, the use of an additive to increase its electronic conductivity or decrease its vapor pressure may prove beneficial. Iron does not appear to be a useful additive because of the slow dissolution rate of iron sulfides in sulfur. The addition of thallium to liquid sulfur results in the formation of two liquid phases. The lower-density, sulfur-rich phase has a conductivity of $\sim 10^{-9}$ ohm^{-1} cm^{-1}; the higher-density, thallium-rich phase has a much higher conductivity of $\sim 4 \times 10^{-1}$ ohm^{-1} cm^{-1} at 367°C. Thallium may be a useful additive if it is effective at low concentrations. Sulfur containing a proprietary additive, which was obtained from a commercial source, has a relatively high conductivity of 1.4×10^{-3} ohm^{-1} cm^{-1} at 158°C, but it does not appear to be suitable for use in the cathodes of lithium/sulfur cells because of its tendency to release gases at cell operating temperatures. It also appears that the additive and the sulfur tend to segregate.

Mass-Transport Studies

In an effort to improve the cycle life of the lithium anode in lithium/sulfur cells, a study has been undertaken on the transport characteristics of lithium between a lithium electrode of the type used in cells and a Li-Al counter electrode. Four cells were operated. The first three cells using LiCl-KCl, LiCl-LiI-KI and LiCl-LiI-KI electrolytes and Al_2O_3 electrical insulators, failed in less than 10 cycles (100 hr) of operation. The principal mode of failure was due to lithium not soaking into the Feltmetal during charging. This characteristic appeared to be strongly affected by the presence of contaminants such as traces of moisture or corrosion products resulting from lithium attack on the Al_2O_3 in the electrolyte.

In the operation of the fourth cell, an effort was made to eliminate contaminants. The electrolyte, LiF-LiCl-KCl, contained no iodide salt (normally among the salts most difficult to obtain in an anhydrous form), and the cell insulator was changed to BeO, which is less susceptible to lithium attack than is Al_2O_3. This cell operated well for 480 hr and 138 cycles, after which 10 g of LiCl-LiI-KI was added. The resulting bubbling indicated the presence of moisture and the performance of the cell rapidly deteriorated. Under proper operating conditions, the present lithium anode, comprised of lithium in Felcmetal (Huyck Metals Co., Type 302 stainless steel, 90% porosity, 67-μm pore size), appears capable of good cycle life.

In order to increase the capacity density of the sulfur cathode, a study of various cathode designs and materials has been undertaken. An attempt to develop a cell with a quartz housing failed because the quartz was too susceptible to lithium attack. Preliminary tests with a new cell design have been encouraging.

Materials Testing and Fabrication

The corrosion resistance of various materials to simulated cell environments is being studied to identify materials with potential usefulness for cell applications. Two different classes of materials resistant to cell conditions are being studied. Corrosion-resistant materials possessing good electrical conductivity are required to serve as current collectors and housings. Corrosion-resistant, electrically insulating materials are required to prevent short-circuit contacts within the cell. Among the conductive materials that were tested at 375°C in 20 at. % Li-S mixtures, molybdenum and chromium had low corrosion rates in both short-term (100-300 hr) and long-term (600 hr) tests. Molybdenum, in particular, has been used in many of the experimental cells for periods up to several hundred hours and has shown good corrosion resistance under these conditions.

The austenitic stainless steels, such as Types 2RK65, 347, and 205 (15 wt % Mn), had low corrosion rates in short-term tests, but much higher rates in the longer tests. The nickel-base alloys, such as Inconels 702 and 600 and Hastelloy X, as well as Zircaloy-2, showed similar behavior. The corrosion rate of aluminum by 20 at. % lithium-sulfur mixtures has proved to be highly variable, with rates ranging from 0.01 to 2.4 mm/yr in 600-hr tests. It is suspected that these variations are associated with the nature of a surface film that is formed during the exposure. Tantalum, iron,

titanium, nickel, and beryllium showed poor corrosion resistance to lithium-sulfur mixtures and have been excluded from consideration for use in the cathodes of lithium/sulfur cells.

Beryllia, the most corrosion-resistant insulator tested, showed variable rates that were dependent upon the purity and method of fabrication. High-purity (>99.9%), hot-pressed beryllia showed the best corrosion resistance. Thoria, aluminum nitride, yttria, $Y_3Al_5O_{12}$, $MgO \cdot Al_2O_3$, $LiAlO_2$, and boron nitride also had corrosion rates less than 0.5 mm/yr. Boron nitride had a relatively low corrosion rate, and it maintained its physical integrity, but it was attacked by a mechanism that caused it to become electrically conductive. This phenomenon has also been observed when boron nitride was used in test cells.

A program to produce electrical insulators in the sizes and shapes required for testing in operating cells has been initiated. Lithium aluminate ($LiAlO_2$), 90 wt % Y_2O_3-10 wt % Eu_2O_3, and Y_2O_3 bodies have been produced successfully and will be tested under cell conditions.

Electric Automobile Performance Calculations

Calculations of the performance characteristics that might be obtained from an electric automobile powered by a lithium/sulfur battery have been made. The calculations were based on a vehicle of 2086-kg (4600-lb) test weight powered by a 488-kg (1075-lb) battery. The electrical performance of the battery was assumed to be identical (per unit of electrode area) to that obtained from experimental laboratory cells. In the battery design allowances were made for the casings, thermal insulation and other items that are peculiar to an operational battery which were not included in the cell tests. The method of calculation differed from others of this kind in that specific cognizance was taken of the fact that the deliverable energy from the battery depends upon the power level of its operation. The results indicate that the present performance of laboratory cells is sufficient to permit a range of about 142 to 362 km (88 to 225 miles) for an electric family automobile, depending upon the accessory load and the driving conditions. These ranges are adequate to suggest that lithium/sulfur batteries possess the potential for this application. The power levels of the cells are satisfactory, but an effort should be made to increase the available specific energy of the batteries in order to extend the range of the vehicle.

I. INTRODUCTION

Research on lithium/chalcogen cells began at Argonne National Laboratory in 1967 as a result of an energy conversion program directed toward the development of thermally regenerative bimetallic galvanic cells for the direct conversion of heat to electricity. Power densities over 3 W/cm^2, current densities over 1 A/cm^2, and plateau voltages over 1.5 V were obtained from lithium/tellurium and lithium/selenium cells using a low-melting lithium halide electrolyte. This performance indicated the potential utility of lithium/chalcogen cells as secondary (electrically rechargeable) energy storage devices capable of delivering high power and energy per unit weight of cell. Lithium is well-suited for use as an anode because of its low weight per unit of electricity delivered, low affinity for electrons, and high electrochemical reactivity. The chalcogens (tellurium, selenium, and sulfur) are attractive as cathode materials because they have high affinities for electrons, high electrochemical reactivity, and reasonably low weight per unit of electricity delivered.

The OAP program on lithium/sulfur cells began at ANL in February of 1969 with a modest experimental program on cells of the types Li/LiX/Li in S and Li/LiX/Li in P_xS_y to determine if these cells could meet the requirements of a low-cost, high-specific-energy and high-specific-power battery for electric automobile propulsion. The lithium/sulfur and lithium/P_xS_y cells were selected for investigation because the cost and availability of these materials, relative to the other chalcogens, made these systems the most attractive for electric automobiles and similar mass-market applications.

Between February 1969 and June 1970 about 30 lithium/sulfur and lithium/phosphorus sulfide (P_xS_y) laboratory cells were tested. These small-scale ($\sim$1-cm^2 electrode area) cells were operated at current densities from 0.3 to 1 A/cm^2 to determine if capacity densities of about 0.4 $A\text{-}hr/cm^2$ were feasible. These current-density and capacity-density goals were estimates of the requirements of a battery in an electric automobile under urban driving conditions. The cells exhibited capacity densities from 0.1 to 0.2 $A\text{-}hr/cm^2$ at a current density of 0.5 A/cm^2. Sulfur utilization was usually less than 35%. Sulfur utilization is defined on the basis of the reaction

$$2\ Li + S \rightarrow Li_2S$$

where 100% utilization indicates that all the sulfur has been converted to Li_2S. While 100% utilization is unobtainable in an operating cell, the sulfur utilization figure is useful in comparing various cell designs and cathode geometries. A utilization of 50-70% (above a 1-V cut off) is desirable for a high-specific-energy cell in which a high percentage of the cell weight is devoted to reactants and a lesser percentage to housing, current collector, insulators, and other electrochemically inactive components.

Cell performance during the first year of the program was limited by two main factors, (1) the low diffusion rate of the cell reaction products away from the sulfur-electrolyte interface and (2) the low electronic conductivity of sulfur. The most significant findings of the initial phase of the program were (1) the lithium sulfur system appeared more promising

for further development than either the Li/P_4S_{10} or Li/P_4S_3 systems, (2) cell geometry and current-collector design greatly influenced cell performance, and (3) the cells operated at acceptable current densities, but capacity density, cycle life, and sulfur utilization required further improvement.

Corrosion tests (~600 hr, 375°C) of potential materials of construction for lithium/sulfur cells, including some representative austenitic and ferritic stainless steels, manganese-chromium stainless steels, nickel-base alloys and pure elements, indicated that only molybdenum, chromium, and niobium showed corrosion rates sufficiently low for use in cells of anticipated lifetimes greater than 1000 hr.

Experimental work has been carried out at a significantly higher level since July, 1970, when the funding level was increased and several tasks were added to the program. The major emphasis continues to be cell and battery development, but the increased funding permits the experimental program to undertake the following supporting studies necessary for further cell development:

(1) The solubility of sulfur-bearing species in various electrolytes and that of electrolytes in the cathode material are being measured in order to select the best electrolyte, cathode compositions, and operating temperature of the cells.

(2) Studies of sulfur-bearing species in molten alkali halides are being conducted to aid in understanding the chemical processes occurring in an operating cell.

(3) Exploratory work was initiated on solid electrolytes which may prove more suitable for some lithium/sulfur cell application than the alternative liquid electrolyte.

(4) Although it appears that elemental sulfur alone can be used satisfactorily as the active cathode material in lithium/sulfur cells, the use of an additive to increase its electronic conductivity and/or decrease its vapor pressure is being studied since it may increase the electrical performance (specific power and specific energy) of the cell.

(5) Interfacial phenomena, as they relate to the wetting of current collectors and the containment of lithium and sulfur, and mass-transfer effects occurring within a cell are being investigated. For example, in an effort to improve the cycle life of the lithium anode in lithium/sulfur cells, a study was undertaken on the transport characteristics of lithium between a lithium electrode of the type used as the anode in the laboratory cells and an aluminum-lithium counter electrode. Various electrode designs, electrode materials, and electrolytes were evaluated. Successful operation of an experimental cell for over 200 cycles indicated that under the proper conditions a long cycle life can be achieved.

(6) Materials evaluation has been performed by means of simple screening tests for initial identification of promising materials. Emphasis is now being directed toward the successful utilization of aluminum, titanium, or chromium-plated structures, which will probably be necessary for low-cost, light-weight batteries.

(7) Electrical insulator tests have demonstrated the usefulness of BeO, $LiAlO_2$, and Y_2O_3 for cell application, but additional work on alternative insulators and better methods of fabrication into cell components is necessary.

The goals for the cell program have been restated to provide additional insight into the relationship between the performance achieved in laboratory cells and what might be expected of an automobile battery constructed from similar cells. Table I presents both the battery and single-cell performance goals. These single-cell goals were developed from an analysis of the energy and power requirements of an automobile operated under urban conditions (see Section V).

The present laboratory cell performance fails to meet the prescribed goals, particularly in the areas of capacity per unit volume of cathode, sulfur utilization, cycle life, and lifetime. Consequently, the principal objective of the cell program during the past year has been to increase the capacity density, sulfur utilization, and lifetime of the laboratory cells. The principal variables investigated during the year are the design of, and materials used for, the cell cathode structure.

TABLE I. Lithium/Sulfur Battery Development Program Goals

Assembled Battery	
Specific Energy (at the 4-hr rate)	200 W-hr/kg
Specific Power (at the 1-hr rate)	200 W/kg
Cost[a]	$10/kW-hr
Lifetime	3-year minimum
Cycle Life	300-1000 cycles
Single Cell	
Specific Energy	220 W-hr/kg
Specific Power	220 W/kg
Cost[a]	$9/kW-hr
Capacity Density (at 1-hr rate)	0.4 A-hr/cm^2
Sulfur Utilization (above 1-V cut off)	70%
Capacity per Unit Volume of Cathode	1.0 A-hr/cm^3
Cycle Life	1000 minimum

[a]Capital equipment cost of installed capacity; not direct energy cost.

II. INVESTIGATIONS OF LITHIUM/SULFUR CELLS

(H. Shimotake, M. L. Kyle, F. J. Martino, R. Rubischko)

Liquid-electrolyte cells with lithium anodes, molten-halide salt electrolytes, and sulfur-containing cathodes are being operated at temperatures from 370 to 400°C to determine the cell configuration, materials, and operating conditions necessary to achieve capacity densities of about 0.4 A-hr/cm^2 at current densities near 0.4 A/cm^2. Other near-term objectives are to increase the cycle life of the cells to about 1000 cycles at these performance levels and to increase the sulfur utilization to the range of 50-70%. These goals for cell performance were chosen as necessary to meet the performance requirements of a battery for an electric automobile having a range of 200 miles under practical driving conditions (see Section V).

The attempts to increase the capacity density of the cells have centered around the design of the cathode. Since diffusion of the product in the cell cathode appeared to be a limiting feature of the initial cell design, several designs which increased the interfacial cathode area were tested. These cell designs are intended to increase the area over which product diffusion can occur. A higher interfacial cathode area should increase cell performance since more of the sulfur is available to the reaction sites at the sulfur-electrolyte interface. This should result in an increase of the sulfur utilization and a decrease in the diffusional overvoltage caused by the product layer at the sulfur-electrolyte interface.

The other main cathode design problem investigated was how to decrease sulfur loss from the cathode, which would increase the cycle life of the cells. Earlier cells exhibited lifetimes of less than 48 hr because sulfur was lost from the cathode during operation. Recent tests identified the mechanism of sulfur loss, and the cell design was modified to substantially reduce these losses and increase cell lifetime.

A. Experimental Procedure

Approximately 50 experimental cells of various designs were tested during the last year (July 1970 - June 1971). A generalized version of the cells is illustrated schematically in Fig. 1.

The main features common to all of the cells were an anode consisting of a stainless steel Feltmetal* current collector soaked with liquid lithium, a porous cathode current collector soaked with liquid sulfur or P_4S_{10}, and a molten-salt electrolyte containing lithium halide. The geometric areas of the electrodes used in these cells were 0.7 to 2.6 cm^2, and the interelectrode distance was usually 1.0 cm. The operating temperatures were in the range 370 to 400°C.

---

*A product of Huyck Metals Co.

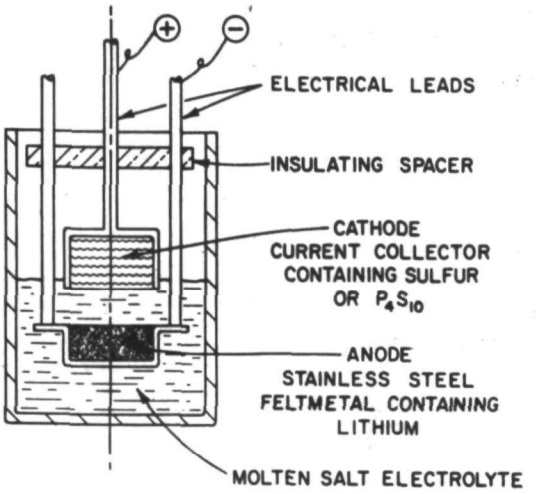

Fig. 1. Schematic Diagram of a Typical Unsealed Laboratory Cell

A typical cell assembly procedure was as follows. The anode current collector was soaked in molten lithium (Foote Mineral Co., 99.98% purity) at 550°C, the excess lithium was removed, and the electrode was cooled to room temperature and placed in the anode holder (a stainless steel cup with current and voltage leads attached). The cathode was prepared similarly, soaking the cathode current collector in sulfur at a temperature near 160°C where sulfur has a low viscosity. The sulfur was N. F. sublimed grade from the Mallinckrodt Chemical Works. The P_4S_{10} (obtained from the Hooker Chemical Co.) was purified by recrystallization from CS_2. The electrolyte was melted in an alumina or niobium crucible and the anode was immersed, followed by the cathode. The cell was then ready for electrical performance measurements. All of the above procedures, including operation of the cell, were performed in a glovebox containing a high-purity (< 2 ppm each of O_2 and N_2, < 1 ppm H_2O) helium atmosphere.[1] The compositions, melting points, and densities of the electrolytes used in the cell tests are listed in Table II; all of the electrolytes are eutectic compositions. The electrolytes used in these tests were normally prepared from anhydrous materials of purity greater than 99.5%. The eutectic mixture was premelted and mixed at a temperature slightly above the melting point of the lowest-melting constituent and contacted with molten lithium at about 50°C above the eutectic melting point. The lithium contacting was performed to remove any residual

TABLE II. Physical Properties of Molten-Salt Electrolytes

Composition, mol %	Melting Point, °C	Density at 380°C, g/cm^3	Reference
58.8 LiCl-41.2 KCl	352	1.68	2
59.0 LiBr-41.0 RbBr	278	2.85[a]	3
11.7 LiF-29.1 LiCl-59.2 LiI	340.9	2.77	4
8.5 LiCl-59.0 LiI-32.5 KI	260	2.92[a]	4
3.5 LiF-56.0 LiCl-40.5 KCl	346	1.68	5

[a]Estimated.

water and heavy metal ions. The lithium-contacted salt was filtered through porous quartz frits to remove the Li_2O and other solids in the electrolytes.

The cell reaction during discharge involves the electrochemical oxidation of lithium at the anode

$$Li \rightarrow Li^+ + e^-$$

transport of lithium ion through the electrolyte, and its reaction with sulfur at the cathode to form Li_2S

$$2Li^+ + S + 2e^- \rightarrow Li_2S$$

The maximum amount of electrical energy that can be delivered by the cell is determined by the quantities of lithium and sulfur in the electrodes. An excess of lithium was used in all of the cell tests, and the amount of sulfur in the cathode was usually 0.3 to 0.6 g/cm^2, which corresponds to a capacity density of 0.5 to 1.0 A-hr/cm^2, assuming Li_2S to be the final reaction product.

The assembled cells were placed in a furnace well which was attached to the floor of the helium-atmosphere glovebox. The furnace temperature was held constant by a controller at about 380°C for most of the experiments. Electrical connections to the cell were made by four wires, two for cell voltage and the other two for cell current readings. The wires were fed through the glovebox wall by means of a hermetically sealed connector to external metering equipment.

Usually, two types of electrical performance measurements were made. Voltage-current density data were obtained from short-time measurements, in which the cell voltage (at various current densities) was observed within a few seconds after the circuit was closed. Voltage-time measurements, used in determining the capacity densities (A-hr/cm^2) of the cells, were performed at constant current. The constant discharge and charge currents were obtained with the aid of a regulated dc power supply.

In most cases discharge data were taken from the fully charged condition; state of charge was determined by the open-circuit voltage of the cell. Charge data were obtained from the partially or totally discharged cells. The cells were usually discharged to a cut-off voltage of 1 volt, and left on open circuit for a prescribed period of time (about 10 minutes) before charge was begun. After the cell was charged to a prescribed cut-off voltage, it was left on open circuit for a prescribed period of time (about 10 minutes) which was then followed by the next discharge-charge cycle.

In the cycle-life tests, the cell was usually connected to a meter relay that automatically opened the circuit and reversed the polarity of the power supply when the cell reached a pre-set cut-off voltage, thereby causing the cell to be charged and discharged at prescribed current densities. Frequent measurements were made of IR-free voltages by interrupting the current for a short time.

The cell capacity was calculated from the discharge current and the duration of the cell discharge. The charge accepted by the cell was

similarly determined. The charge-storage capability of the cell is reported in terms of the capacity density by dividing the cell capacity (A-hr) by the projected cathode area. The cell capacity density can be expressed mathematically as follows:

$$q = \int i \, dt$$

where

q = capacity density, A-hr/cm^2

i = current density, A/cm^2

t = duration of cell operation, hr

The average voltage of the cell (volts) during the specified discharge or charge was determined from the following:

$$\overline{V} = \frac{\int V \, dt}{t}$$

where

V = cell voltage, volts.

The voltage-current density data were gathered by taking voltage readings (with a digital voltmeter having a 50-msec response time) at a predetermined current within a few seconds after closing the circuit. Because of the rapidity of the measurement there was a negligible overvoltage due to diffusion of reactants or products. The internal resistance of the cell was calculated from the following equation:

$$R = \frac{dV}{A \, di}$$

where

R = cell internal resistance, ohm

i = current density, A/cm^2

A = projected cathode area, cm^2

The cells were disassembled after testing to relate the condition of the cell to its electrical performance characteristics, to establish causes of failure, and to identify corrosion problems. Frequently samples of cathode products, electrolyte, structural materials, anode materials, and insulators were taken and examined by means of X-ray diffraction, microscopy and wet-chemical analysis. A mass balance was also made for some cells for the materials contained in the cells. Photographic techniques were used to record the appearances of cell cross sections and cell parts as well as the cell assembly.

B. Results and Discussion

The principal variables investigated in the cell tests were the cathode current collector design and the materials used for its construction. An earlier series of experiments[6] had been conducted on porous metal structures for use as the cathode current collector. The materials that were tested in those investigations included stainless steel Feltmetal and Fibermetal* and chromium foam.† Although considerably better short-term electrical performance was obtained with the Feltmetal and Fibermetal than with the chromium foam, stainless steel is not a suitable cathode current collector material because of its poor corrosion resistance to lithium-sulfur mixtures. Therefore two additional materials, molybdenum foam§ and porous graphite or carbon, were investigated for this application. Graphite in particular has the desirable characteristics of corrosion resistance, electrical conductivity, light weight, low cost, and durability.

Several different cathode designs that were used in the experimental cells are illustrated in Fig. 2. The objective of the laminated design (Fig. 2a) was to provide an extended interfacial area between the sulfur

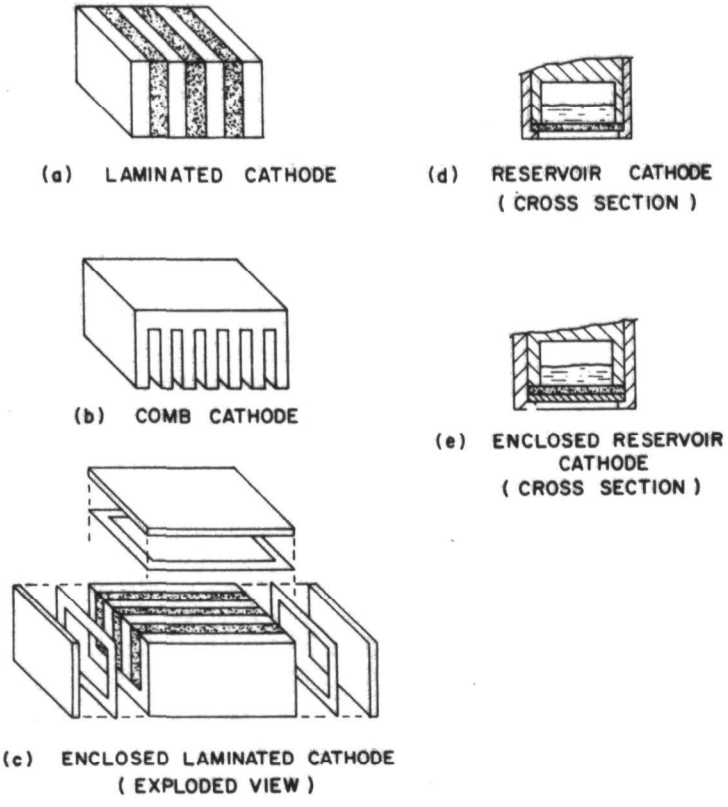

Fig. 2. Schematic Diagrams of Some Cathode Current Collector Designs

*A product of Brunswick Corp.
†A product of Astro Met Associates, Inc.
§A product of Spectra-Mat, Inc.

and the electrolyte. In the first design, this cathode consisted of alternating layers of stainless steel Feltmetal filled with sulfur and electrolyte, respectively. The later designs employed alternating layers of molybdenum foam, which is wet preferentially by the electrolyte, and porous graphite or carbon, which is wet preferentially by the sulfur. The comb design (Fig. 2b) embodies the same concept, but in this case the electrolyte-containing current-collector layers were eliminated in an attempt to decrease the cathode weight and to allow better access of the electrolyte to the sulfur at the surface of the graphite current collector.

The laminated and comb designs both resulted in reasonably good initial electrical performance, but they lost their capacity rapidly. The loss in capacity was attributed to the escape of sulfur from the cathode structure, which was confirmed in a special series of experiments. These experiments showed that sulfur extrudes from porous carbon and disperses into the molten-salt electrolyte, which becomes a yellow color. Upon freezing, the salt was an orange to yellow color, and when it was heated to 600°C the color gradually disappeared, presumably because of the vaporization of sulfur. The loss in capacity of the laminated and comb cathodes was therefore believed to result from the escape of sulfur from the current collector into the electrolyte and subsequent vaporization of the sulfur.

In order to minimize the migration of sulfur into the electrolyte, the enclosed laminated cathode in Fig. 2c was tested. If the sulfur entered the electrolyte as a dispersion rather than as a true solution, the process might be inhibited by surrounding the cathode by a porous layer that is wet preferentially by the electrolyte. This approach was shown to be successful first in a series of specific experiments for this purpose and later in enclosed laminated cathode cells which exhibited greatly extended lifetimes and showed little evidence of sulfur loss.

The reservoir cathode, shown in Fig. 2d, consisted of a thin, porous current collector that confined liquid sulfur within a reservoir. As sulfur was consumed by the cell reaction at the current collector-electrolyte interface, additional sulfur was wicked through the current collector to the site of the reaction. The purpose of this design was to minimize the volume and weight of the current collector. However, significant sulfur losses occurred, probably by the same mechanism as that in the laminated and comb designs (Figs. 2a and 2b). This problem was overcome in the same way, by interposing a porous molybdenum layer, which is wet preferentially by the electrolyte (Fig. 2e).

An attempt to increase the capacity density of the lithium/sulfur cell by intimately mixing the sulfur in the cathode with conductive materials such as carbon powder or metal fibers and electrolyte has been initiated. The major potential advantage of this design, called the "mixed-cathode" design, is that it is intended to increase the electrochemical reaction area, thereby increasing the cell capacity. A schematic drawing of the mixed cathode is shown in Fig. 3. The experimental cell housing was borosilicate glass tubing for ease of construction, but metal housings could also be used.

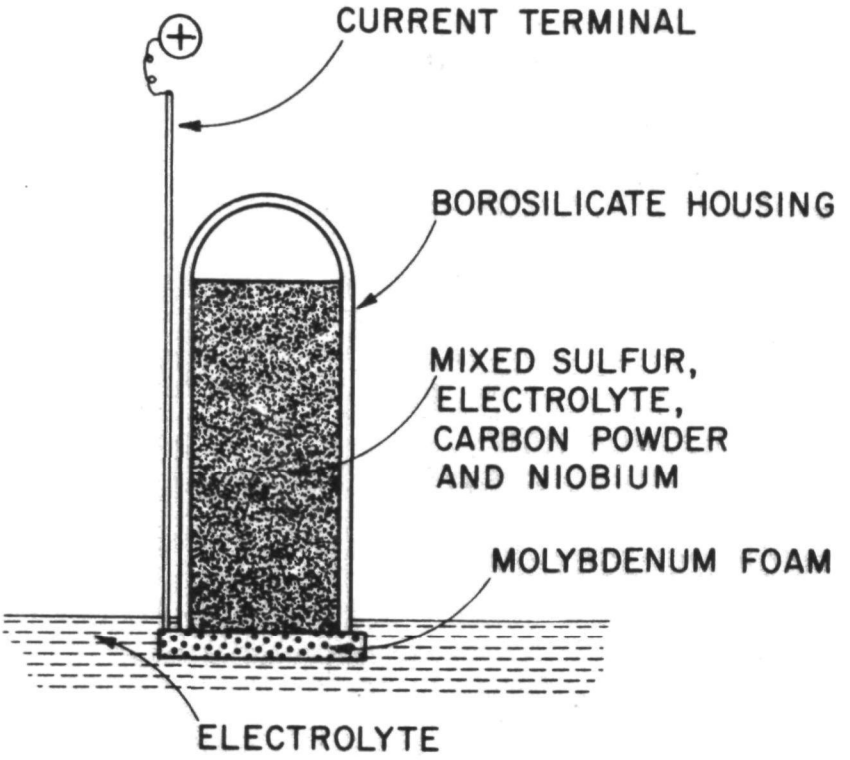

Fig. 3. Schematic Diagram of a Mixed Cathode

Detailed construction and performance data for all the small-scale cells operated during the last year are listed in the appendix. The results of these tests will be discussed by groups of cells which have common characteristics.

Lithium/sulfur cells were tested which utilized the laminated cathode configuration shown in Fig. 2a in which the laminae were 80 to 85% porous Type 302 or 304 stainless steel, with mean pore sizes in the range 25 to 40 μm. Alternate layers were filled with electrolyte and with sulfur. The laminae were 11 mm x 11 mm of various thicknesses in the range 0.07 to 0.16 cm and were mounted in a stainless steel housing. The cathode area used in current-density and capacity-density calculations is defined as the area of the cathode projected upon the anode, including both sulfur and electrolyte elements. The thickness of the elements was varied in these tests since it was expected that thin sulfur elements would produce improved sulfur utilization as the distance over which diffusion must proceed is diminished. The electrolyte elements were considered to serve only as a means of providing a continuous phase for lithium-ion transport to the sulfur-electrolyte interface. Voltage-current density and voltage-capacity density data that are considered to be typical for these cells are shown in Figs. 4 and 5. The best performance achieved with a laminated cathode configuration was 0.52 A-hr/cm^2 at 0.52 A/cm^2 with a sulfur utilization of 25%, assuming that 100% utilization corresponds to conversion of all of the sulfur to Li_2S. Several difficulties with this type of cathode were encountered, the most severe being that the capacity density decreased markedly

after 2 or 3 cycles. Examination of the cathode components after testing indicated that considerable corrosion of the stainless steel elements had occurred. The significant decrease in capacity density that took place with cycling was attributed to the formation of corrosion products and the loss of sulfur from the cathode structure by diffusion or dispersion into the electrolyte. It was noted that thinner sulfur-bearing elements permitted greater utilization of the available sulfur, but the corrosion and sulfur vaporization problems still limited the cell life to a few cycles.

Since corrosion of the cathode current collector appeared to be a severe problem, an alternate current-collector material was desired. It was found that porous graphite and carbon were readily wet by sulfur and were corrosion resistant to the lithium/sulfur cell environment. These structures were not wet by the majority of molten-salt electrolytes used in the cell tests. These characteristics made it possible to create a laminated cathode in which the containment of the sulfur could be greatly improved and the formation of corrosion products reduced. A series of cells were fabricated using porous graphite (Poco Graphite, Inc., Grade AX Fuel Cell Carbon, 64% porosity, 1.4-μm pore size) as sulfur-bearing elements and porous stainless steel (Huyck Metals Corp., Type 302 stainless steel, 80% porosity, 30-μm pore size) as electrolyte-bearing elements. These elements

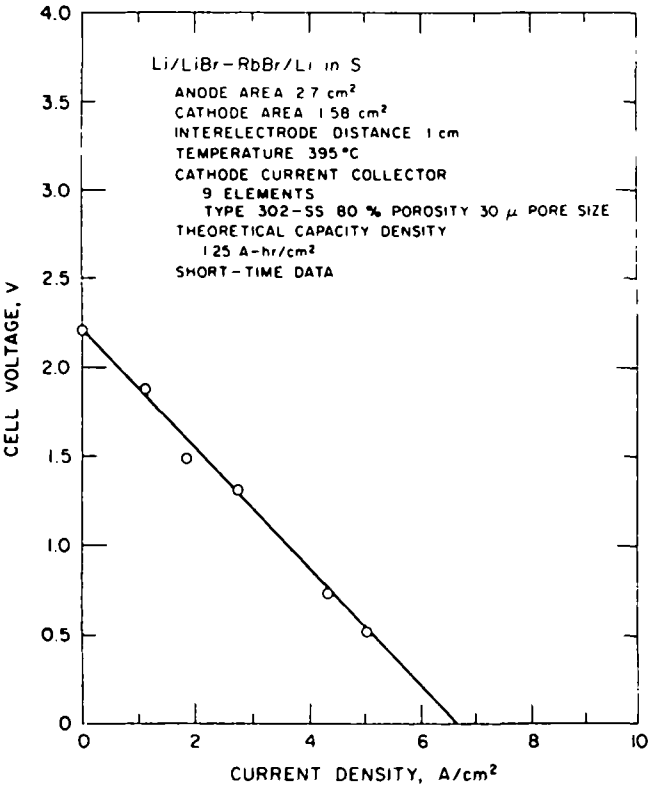

Fig. 4. Typical Voltage-Current Density Curve for a Lithium/Sulfur Cell With a Laminated Cathode Having All-Stainless-Steel Laminae

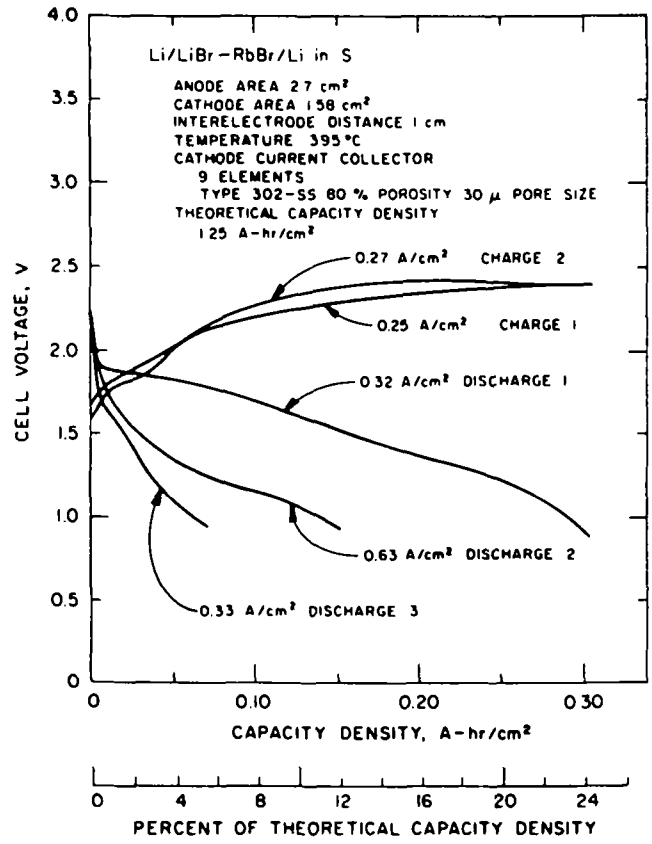

Fig. 5. Typical Voltage-Capacity Density Curve for a Lithium/Sulfur Cell With a Laminated Cathode Having All-Stainless-Steel Laminae

were contained in a stainless steel housing. The capacity density and cycle life of test cells containing such cathode structures were better than those for cells with all-stainless-steel cathode current collectors. Voltage-capacity density data of the best cell of this series are shown in Fig. 6. On the sixth discharge at 0.25 A/cm^2, a capacity density of 0.34 A-hr/cm^2 with 45% sulfur utilization was achieved above a 1.0-V cut off. Operation of this cell was voluntarily discontinued after the sixth cycle and the cell was disassembled. As in other cells of this type, excessive corrosion of the stainless steel electrolyte elements was observed.

The next cathode design did not contain any stainless steel Feltmetal. A porous-graphite comb structure as shown in Fig. 2b was tested. The first discharge yielded 0.40 A-hr/cm^2 at a current density of 0.53 A/cm^2 with 28% sulfur utilization above a 1.0-V cut off. However, subsequent discharges yielded much lower capacity densities as shown in Fig. 7. It is noteworthy that the cell voltage during discharge was significantly higher than in previous cells due to the lower internal resistance of this cell. It appeared that the absence of the electrolyte-containing elements permitted more rapid transport of sulfur from the porous carbon into the bulk electrolyte. A second cell of identical configuration was constructed and P_4S_{10} was

substituted for sulfur. Some improvement in performance was noticed, and the rate of deterioration with cycling was reduced, but the conclusions remained unchanged.

The next series of laminated-cathode cells tested was designed to eliminate the corrosion problems associated with the use of stainless steel. The cathode design was the laminated configuration except that in this series of cells the electrolyte-bearing elements were molybdenum foam (Spectra-Mat, Inc., ,5% porosity, 25-μm pore size). The graphite elements were filled with P_4S_{10} and all the elements were contained in a niobium housing rather than the stainless steel housing used previously. Although the capacity density of these cells was somewhat lower than that of the earlier cells, the cycle life was substantially increased. The first cell operated for 17 cycles (three days) and was frozen and restarted twice without difficulty. Another cell operated continuously for 35 cycles. The capacity density, however, decreased during operation.

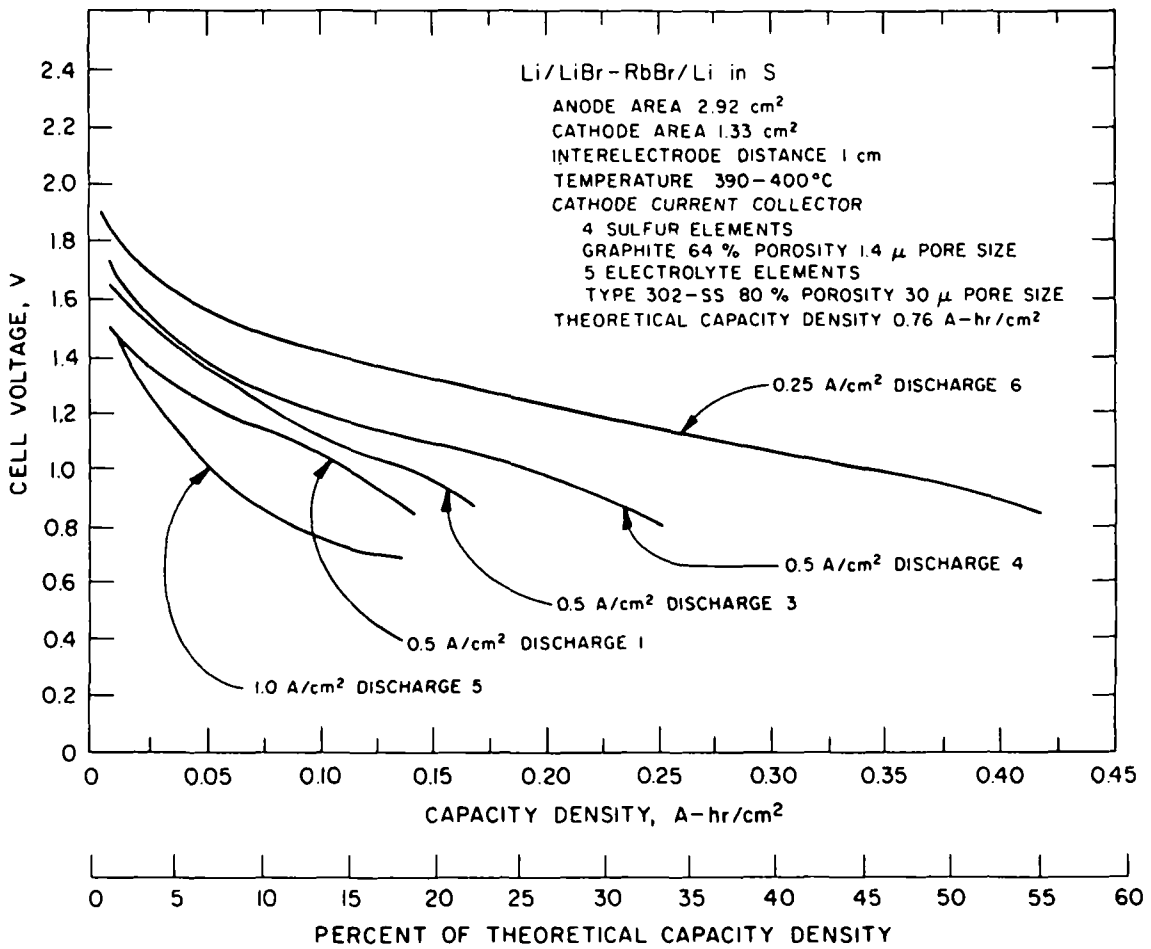

Fig. 6. Voltage-Capacity Density Curves for a Lithium/Sulfur Cell With a Laminated Cathode Having Porous Graphite and Stainless Steel Feltmetal Laminae

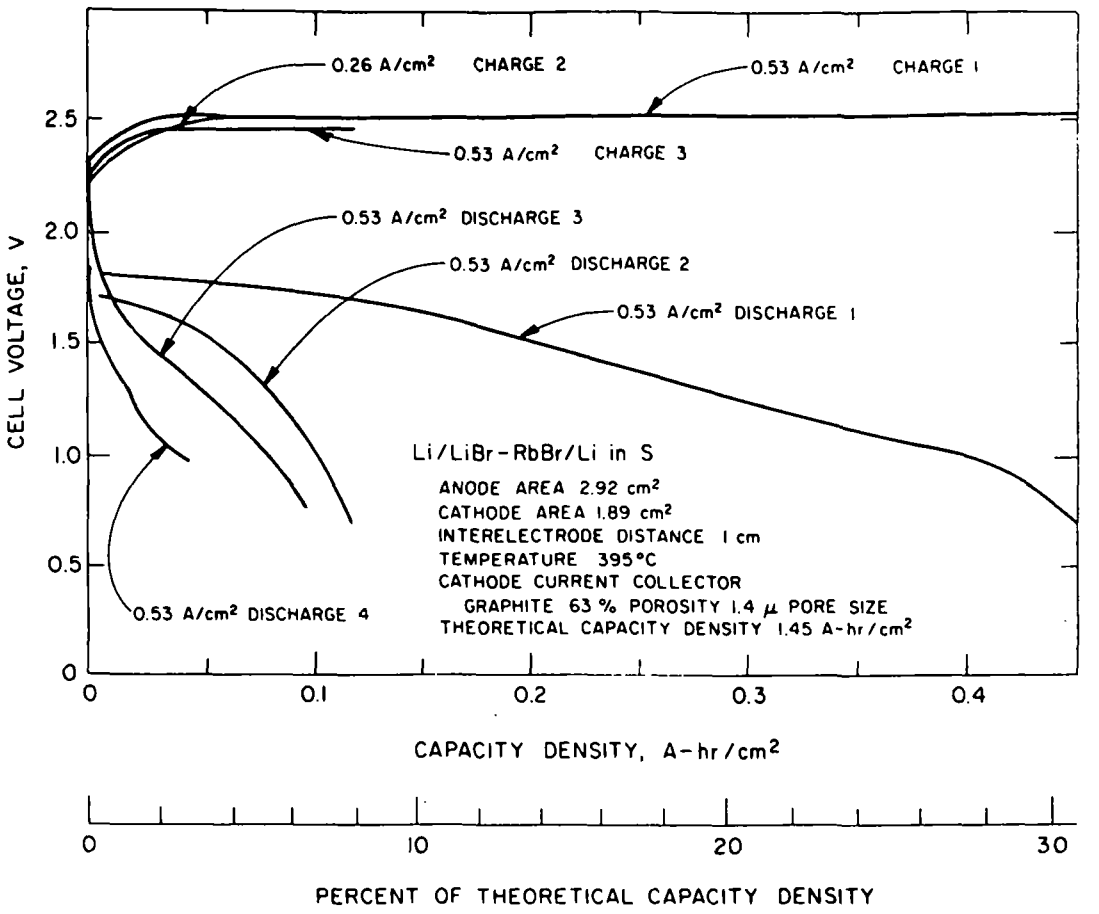

Fig. 7. Voltage-Capacity Density Curves for a Lithium/Sulfur Cell With a Comb-Type Cathode

In order to prevent the escape of sulfur (or P_4S_{10}), a cathode current collector of an enclosed laminated configuration was designed and fabricated (see Fig. 2c). In this configuration the sulfur-bearing, porous-graphite elements were completely surrounded by porous-molybdenum elements filled with electrolyte. This design reduced the sulfur loss into the electrolyte, with the result that the cell operated for over 800 cycles. The best capacity density for this cell was 0.16 A-hr/cm^2 (above a cut-off voltage of 1.0 V), at a current density of 0.20 A/cm^2 with 49% sulfur utilization. Selected voltage-capacity density data for this cell are shown in Fig. 8. The trend of sulfur utilization was downwards, averaging 30% over the first 10 cycles, 25% in the next 60 cycles, and about 15% over the following 100 cycles. The capacity density-cycle number performance of the cell is presented in Fig. 9. The decrease in capacity density was attributed to the fact that lithium was being lost from the anode current collector. The cell capacity was recovered by replacing the lithium anode.

In another series of experiments, the concept of using a sulfur reservoir in the cathode was evaluated. In the reservoir configuration (see Fig. 2d) the cathode is a pool of sulfur which is contained by a thin porous-graphite housing. The purpose of this design is to increase the capacity per unit volume of cathode (A-hr/cm^3). During discharge, sulfur should wick

through the graphite current collector to the graphite-sulfur-electrolyte interface at a rate sufficient to sustain the cell reaction. If the reaction product, Li_2S, diffuses back into the sulfur pool at an adequate rate, this type of cell design would be very attractive and should have a high specific energy. The voltage-capacity density curves for the first reservoir cell are shown in Fig. 10. It is noteworthy that the capacity density, 0.28 A-hr/cm^2, achieved in the first cycle required that sulfur from the reservoir be utilized. However, the capacity decreased to 0.05 A-hr/cm^2 by the 5th cycle and when the cathode was disassembled the reservoir was found to be filled with electrolyte; no sulfur was present.

Based upon the experience gained with the cell just discussed, two design modifications were made: (1) Grafoil* seals were used to contain the sulfur and to prevent leakage of electrolyte into the reservoir, and (2) a porous-metal element filled with electrolyte was placed in front of the porous-graphite current collector. (See Fig. 2e.) One such cell was operated for 803 cycles (1100 hr). The 193rd discharge yielded 0.55

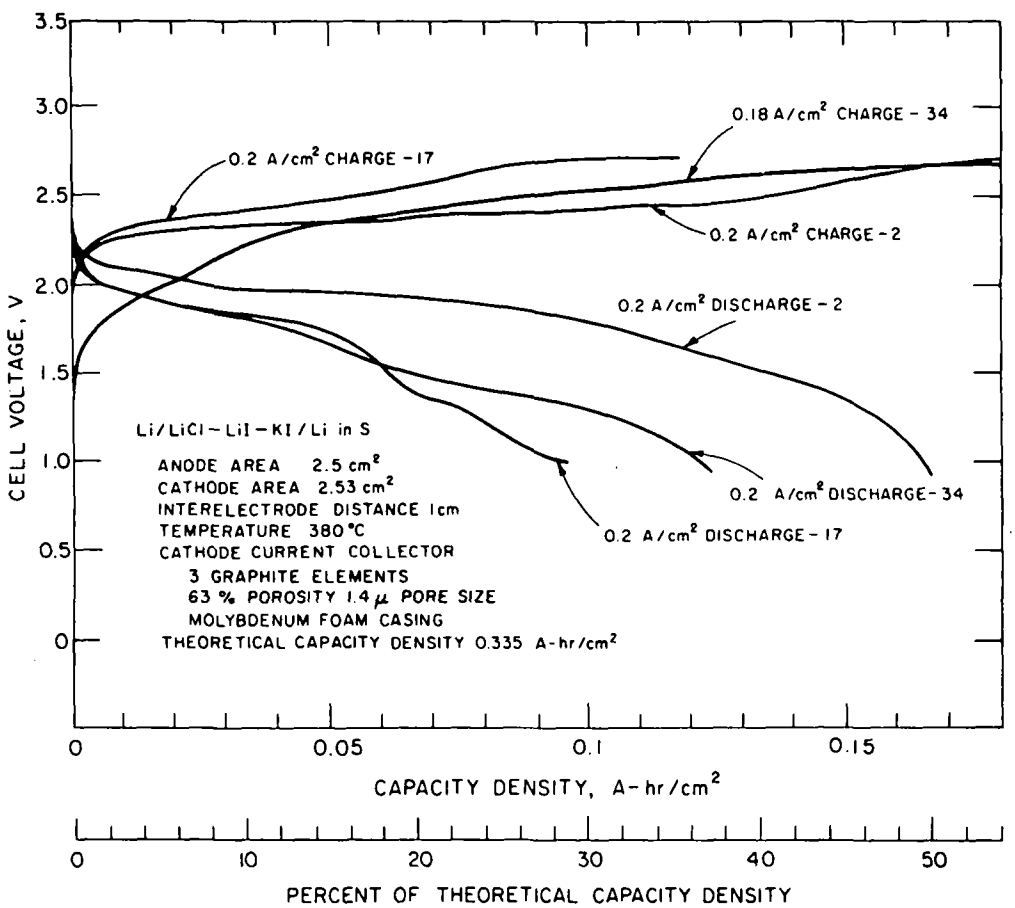

Fig. 8. Voltage-Capacity Density Curves for a Lithium/Sulfur Cell With an Enclosed Laminated Cathode

*Product of the Union Carbide Corp.

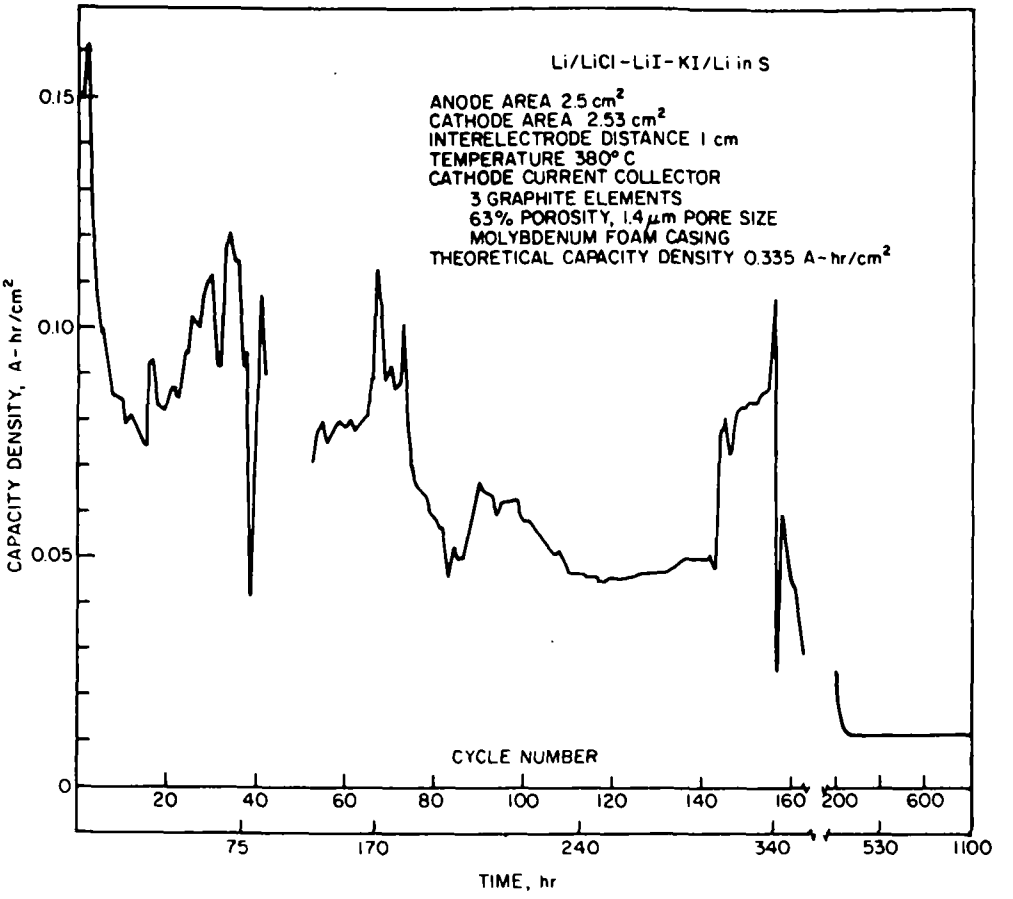

Fig. 9. Capacity Density as a Function of Cycle Number for a Lithium/Sulfur Cell With an Enclosed Laminated Cathode

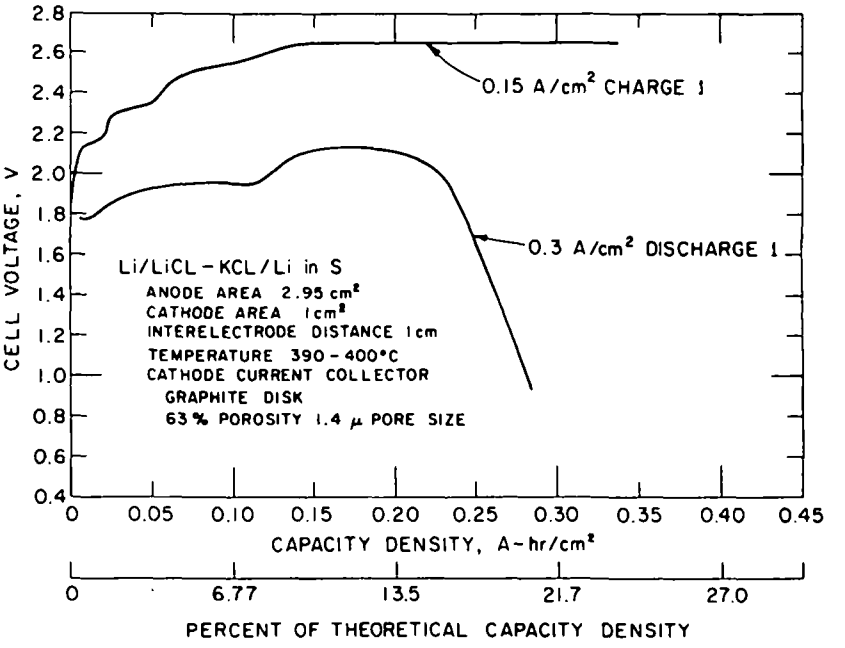

Fig. 10. Voltage-Capacity Density Curves for a Lithium/Sulfur Cell With a Reservoir Cathode

A-hr/cm^2 at 0.165 A/cm^2 with 27% sulfur utilization; the 207th cycle yielded 0.52 A-hr/cm^2 at 0.27 A/cm^2 with 26% sulfur utilization; and the 209th cycle yielded 0.15 A-hr/cm^2 at 0.48 A/cm^2 with 8% sulfur utilization. The voltage-capacity density data for this cell are shown in Fig. 11.

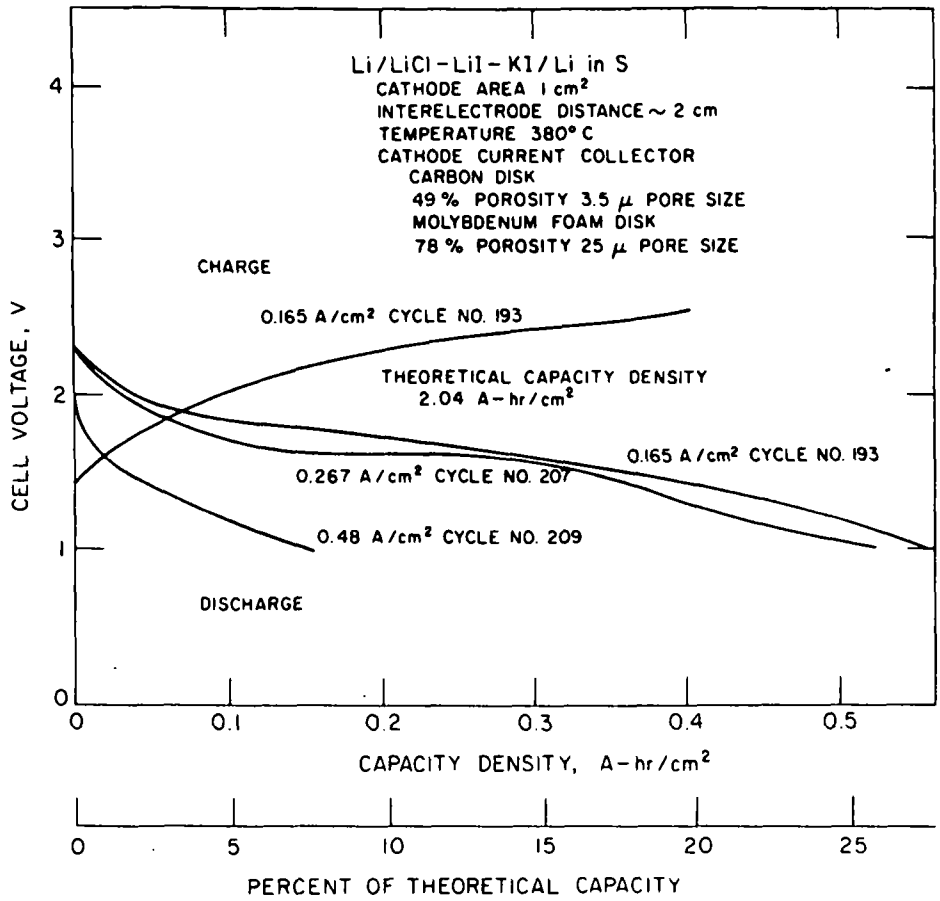

Fig. 11. Voltage-Capacity Density Curves for a Lithium/Sulfur Cell With an Enclosed Reservoir Cathode

The present reservoir-cathode design appears to increase the capacity density of the cell but does so at a reduced capacity per unit volume and a reduced sulfur utilization. Alternate design variations, especially with a larger-pore-size-graphite reservoir to promote product diffusion, will be attempted. This design would be even more attractive if cathode additives which increase the rate of product diffusion can be identified (see Section III. D).

A series of experiments to test the "mixed-cathode" design was conducted. The first cell contained a cathode composed of a mixture of 1-10 μm dia niobium fibers, carbon powder (Vulcan XC-72R Carbon Black), LiF-LiCl-KCl, and sulfur. The niobium fibers and LiF-LiCl-KCl were premixed by adding niobium fibers, which were obtained from a sheet of niobium felt (Brunswick Co., 98% porosity, 12-35 μm pore size), and LiF-LiCl-KCl to a Petri dish at 400°C. The resulting mixture was ground into a fine powder

(estimated at about 75 μm dia). This mixture was then added to a mixture of sulfur and carbon powder which had been prepared separately. The weight and volume percentages of each component are listed in Table III. The cathode housing was loaded with the mixture (0.4 vol % Nb - 5.1 vol % C - 48.5 vol % electrolyte - 46.0 vol % S) and sealed by a disk made of molybdenum foam (Spectra-Mat, Inc., 78.2% porosity, 67-μm pore size, 0.15 cm thick).

TABLE III. Physical Characteristics and Electrical Performance of Two Mixed-Cathode Cells

	Cell No.	
	67	68
Cathode		
Metal	Nb fibers	Nb Mesh
Weight, g	0.226	2.02
Vol %	0.40	4.4
Carbon		
Weight, g	0.51	0.8
Vol %	5.1	10.0
Electrolyte		
Weight, g	3.95	2.69
Vol %	48.5	43.5
Sulfur		
Weight, g	4.59	3.2
Vol %	46.0	42.1
Anode		
Lithium, g	2.11	1.85
Cathode Area, cm^2	2.55	2.55
Theoretical Capacity Density, A-hr/cm^2	3.0	2.1
Capacity Density,[a] A-hr/cm^2 (> 1-V cut off)	0.218	0.257
Capacity per Unit Vol. Cathode, A-hr/cm^3	0.114	0.172
Current Density, A/cm^2	0.1	0.1
Energy Density, W-hr/cm^2 (> 1-V cut off)	0.407	0.41
Percent of Theoretical Capacity	8.1	12.2
Average Voltage, V	1.78	1.58
Number of Cycles	82	3
Short-Term Cell Resistivity, ohm-cm	0.5	0.5

[a]Based on volume of sulfur charge, electrolyte, and current-collecting material (excluding housing and molybdenum sheath).

The electrical performance of the cell during 70 cycles and 230 hr of operation is shown in Fig. 12. During most of the cycles the capacity density was about 0.2 A-hr/cm^2 with a cut-off voltage of 1 V at current densities ranging from 0.1 to 0.3 A/cm^2. The low capacity densities during the first 24 cycles were due to a high resistance in the current terminal. When a new current terminal was installed, the performance improved.

The cut-off voltage for charge was gradually raised during operation. The initial cut-off voltage, 2.67 V, was raised to 2.75 V at the 47th charge to 2.95 V at the 53rd, and to 3.10 V at the 58th charge. The effect on the

cell performance is shown in Fig. 13. A significant energy gain at voltages above 2 V in the 59th discharge is noticeable. It is suspected that this energy gain was due to the possible formation of S_2Cl_2 at the sulfur electrode above 2.5 V.

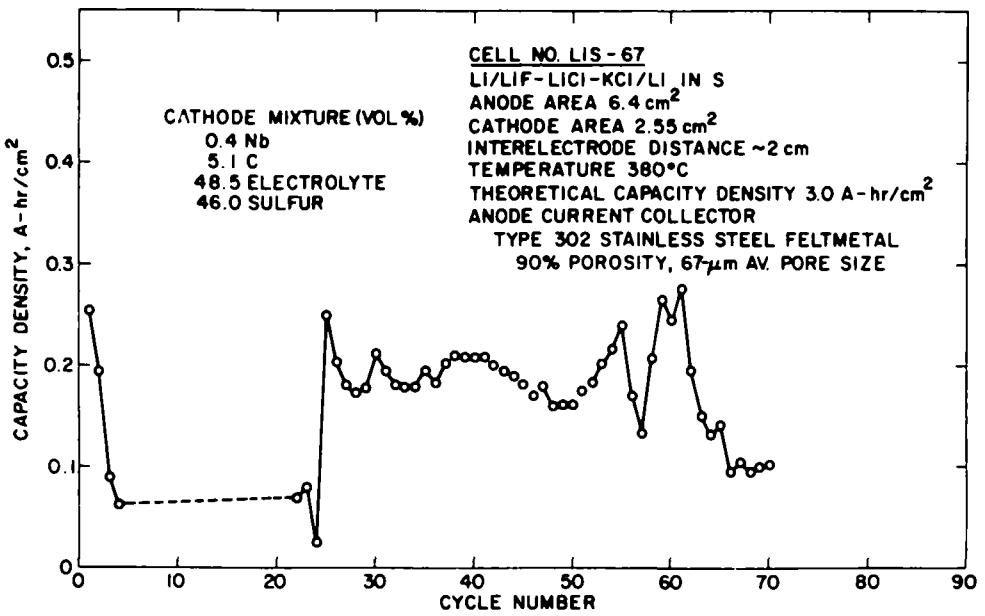

Fig. 12. Capacity Density as a Function of Cycle Number for a Lithium/Sulfur Cell With a Mixed Cathode

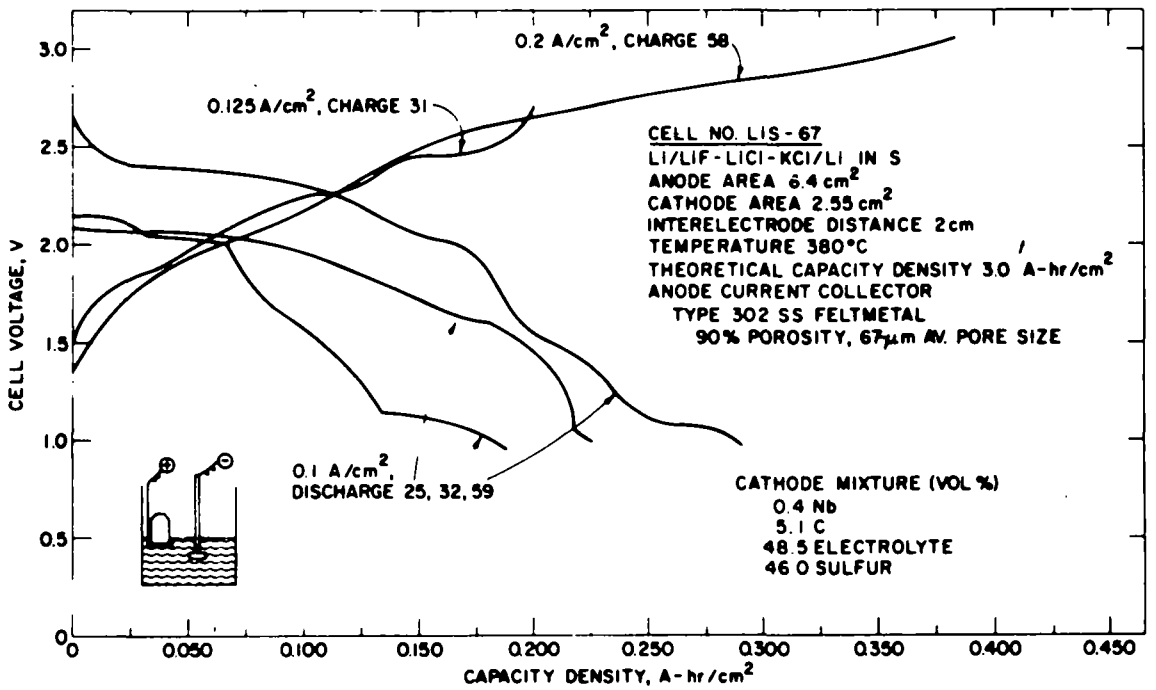

Fig. 13. Voltage-Capacity Density Curves for a Lithium/Sulfur Cell With a Mixed Cathode

A modification to the above cell was made by adding more carbon powder and using a niobium expanded-mesh coil in place of the niobium fibers. A sheet of niobium expanded mesh (Die Mesh Corp., 0.23-cm die size) was wound in a coil form, 1.8 cm dia. x 2.2 cm high. Alumina cloth strips (Zircar, Type ALK-15, 0.038 cm thick) presoaked with LiF-LiCl-KCl were inserted in the gaps of the niobium coil. The purpose of the alumina cloth was to insert a desired amount of the salt at desired locations in the cathode assembly. The cathode housing was loaded with the niobium coil and a premixed powder of sulfur and carbon and sealed with a molybdenum foam disk (Spectra-Mat, Inc., 78.2% porosity, ∿67-μm pore size, 0.15 cm thick). The composition of the mixture was 4.4 vol % Nb - 10.0 vol % C - 43.5 vol % electrolyte - 42.1 vol % sulfur. The electrical performance of the cell is shown in Fig. 14. Three cycles having capacity densities ranging from 0.44 to 0.26 A-hr/cm^2 with a cut-off voltage of 1 V at current densities from 0.1 to 0.4 A/cm^2 were obtained before indications of a malfunction were noted. An examination showed that the heater had burned out. Operation of the cell was terminted at this point.

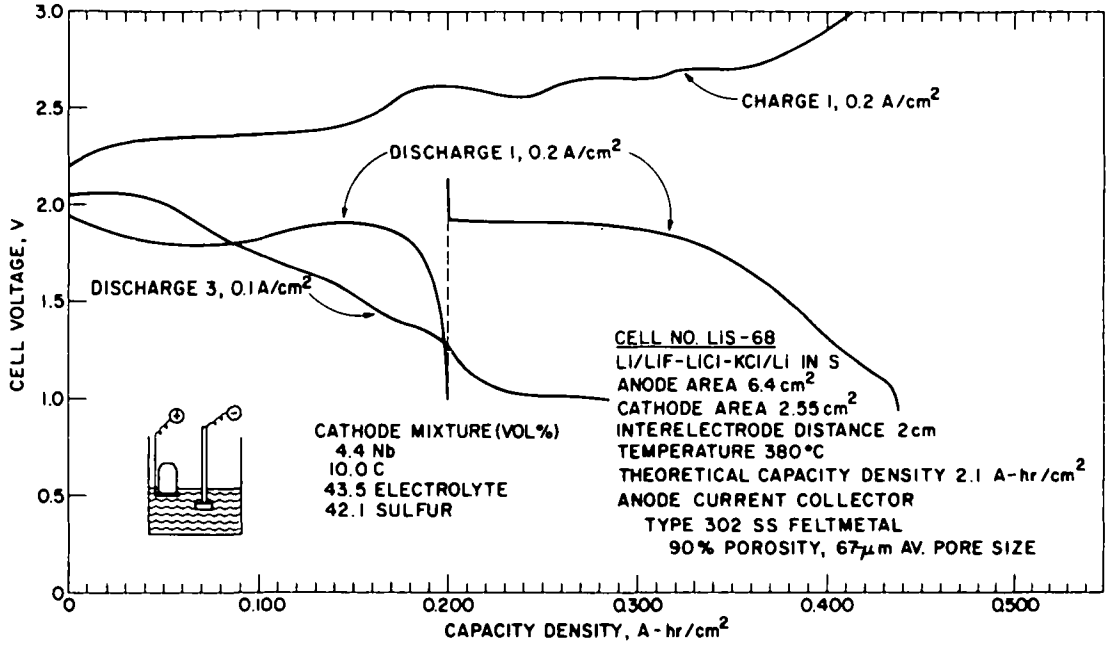

Fig. 14. Voltage-Capacity Density Curves for a Lithium/Sulfur Cell With a Mixed Cathode Containing a Niobium Expanded-Mesh Spiral Current Collector

From the experiments that were made with the mixed-cathode design, it appears that (1) the cell yields a consistent capacity density without loss; however, (2) more study is needed to achieve higher utilization of the sulfur in the cathode.

A sealed lithium/sulfur cell with an active electrode area of 5 cm^2 has been designed, fabricated, and operated three times. Figure 15 shows the construction of the cell. This cell was operated to determine if a lithium/sulfur cell could be operated in a "cathode-down" position, since most cells

have been operated "cathode-up" and reversal of the electrode positions might simplify cell design. Another objective was to identify problems associated with the design and operation of cells utilizing Grafoil as a sealing material. The performance characteristics of these cells are listed in Table IV. It appears that a lithium/sulfur cell may be operated with the anode uppermost. It also appears that a gasket seal of Grafoil that is effective in containing the molten-salt electrolyte can be designed. Post-test examination of the first two cells revealed that the anode had not been reabsorbing the lithium during cell recharge; in both cases beads of lithium were found in the salt. This phenomenon is under investigation (see Section III. E). In the third cell a layer of frozen electrolyte was formed over the molybdenum foam before the sulfur was added to the porous graphite. This technique should help to contain the sulfur during cell start up (i. e., before the salt becomes molten). Free sulfur could create a Li_2S film on the anode surface, and this film could inhibit lithium retention by the anode. A significant decrease in lithium beading in the third cell was observed.

C. Conclusion

In summary, lithium/sulfur cells that have been operated at ANL have shown performance characteristics commensurate with electric automobile requirements (capacity densities of about 0.4 A-hr/cm^2 at a current density of 0.4 A/cm^2) for several cycles and have also demonstrated lifetimes of over 800 cycles and 1100 hr at reduced capacity densities. No cell, however, has been capable of meeting both requirements simultaneously. Capacity per unit volume, sulfur utilization, and the retention of high performance

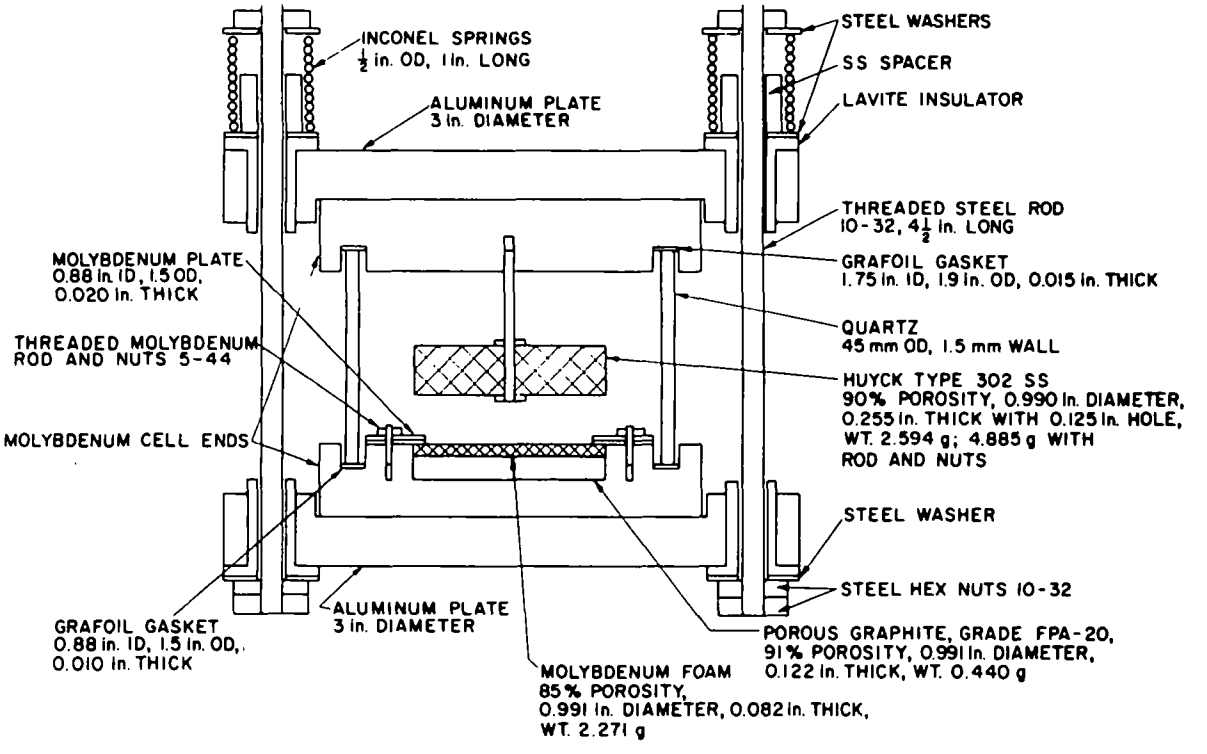

Fig. 15. Schematic Drawing of a Sealed Lithium/Sulfur Cell

TABLE IV. Construction and Performance Characteristics of a Sealed Lithium/Sulfur Cell

Cell Design
Anode Area, 5.0 cm^2; Cathode Area, 5.0 cm^2
Interelectrode Distance ∿1 cm
Temperature 380°C
Anode Current Collector:
Type 302 SS Feltmetal, 2.51 cm dia × 0.65 cm thick, 90% porosity, 67-μm pore size
Cathode Current Collector:
Porous graphite, 2.51 cm dia × 0.31 cm thick, 91% porosity, 50-μm pore size
Molybdenum foam sheath, 2.51 cm dia × 0.21 cm thick, 75% porosity, 25-μm pore size

	Theoretical Capacity		Cell Performance							
Cell No.	A-hr/ cm^2	A-hr/ cm^3	Open-Circuit Voltage	Cycle No.	Discharge Current Density, A/cm^2	Capacity Density, A-hr/cm^2	% of Theoretical Capacity	Average Discharge Voltage	Total No. of Cycles	Comments
1	0.478	0.956	2.35	1	0.25	0.136	29.8	1.6	11	Control circuit malfunction caused cell to overcharge to ∿4.8 V
			-	2	0.25	0.079	16.6	1.75		
			-	4	0.20	0.095	19.8	1.8		
			2.35	6	0.20	0.101	21.2	1.75		
			2.38	8	0.20	0.090	18.8	1.75		
			2.35	9	0.20	0.080	16.7	1.7		
2	0.501	1.00	2.30	1	0.20	0.109	21.8	-	11	Lithium beading caused short circuit
			2.29	2	0.20	0.074	14.8	-		
			2.34	3	0.10	0.102	20.3			
			2.27	5	0.20	0.068	13.6			
			2.18	9	0.20	0.066	13.2			
			2.13	11	0.20	0.032	6.4			
3	0.541	1.08	2.40	1	0.20	0.136	25.1	1.85	108	Electrolyte and sulfur leakage
			2.31	2	0.20	0.071	13.1	1.9		
			2.35	10	0.20	0.089	16.5	1.90		
			2.35	15	0.20	0.105	19.4	1.77		
			2.37	20	0.20	0.061	11.2	1.87		
			-	40	0.20	0.013	2.4	1.85		
			-	75	0.20	0.0046	0.9	1.80		

levels for extended cycle life require further improvement. The performance of the various cell designs is summarized in Table V, and the Appendix contains complete information on the cells operated during the year. The operation of long-life, high-performance cells remains the primary objective of the laboratory cell program. The cells operated to this time have been relatively small (<30 cm^2) and unsealed. Initial scale-up efforts are necessary to provide information on problem areas peculiar to the sealing, design, construction, and operation of larger cells. Finally, the assembly of cells into batteries will present new problem areas of cell matching, safety, reliability, long-term hermetic sealing, and temperature control.

The program until now has been a laboratory effort to demonstrate the technical feasibility of lithium/sulfur cells. A great deal of research and development remains to be done to reach the stage of a reliable battery.

TABLE V. Performance of Some Typical Lithium/Sulfur Cells

Cell No.	Electrolyte	Temp., °C	Structure Type	Depth, cm	Materials[a] & Thickness, mm	Area[b], cm^2	Theo. Capacity Density, A-hr/cm^2	Capacity Density >1 V, A-hr/cm^2	Current Density[c], A/cm^2	Average Cell Voltage[c], V	Cycle Life, cycles	Life, hr
30	LiBr-RbBr	395	Laminated	1.1	B,0.71;A,1.6	1.70	0.50	0.16	0.29	1.35	3	6
37	LiBr-RbBr	390	Laminated	1.1	A,1.6;C,0.45	0.96	2.06	0.52	0.52	1.50	3	6
44	LiBr-RbBr	395	Laminated	1.1	E,0.91;A,1.6	1.31	0.76	0.33	0.25	1.32	6	26
45	LiBr-RbBr	395	Comb	1.3	E,1.3;none	1.89	1.45	0.40	0.53	1.45	4	24
50	LiCl-KCl	390	Reservoir	0.56	E,0.63	1.00	1.48	0.28	0.30	1.90	6	8
55	LiCl-LiI-KI	380	Enclosed Laminated	2.1	E,1.5;G,3	2.53	0.33	0.17	0.20	1.82	>800	>1100
56	LiCl-LiI-KI	380	Enclosed Reservoir	1.3	F,3.0;G,4.0	1.00	2.04	0.52	0.27	1.64	>600	>700
68	LiCl-KCl-LiF	380	Mixed	1.4	-----;G,1.5	2.55	2.10	0.26	0.10	1.60	3	42

[a]The materials are given first for the sulfur-bearing, then for the electrolyte-bearing laminae. The meanings of the code letters are given below.
A = 302 SS, 80% porosity, 30μm pore size, Huyck Metals Co.
B = 304 SS, 85%, 40μm, Brunswick Corp.
C = 304 SS, 83%, 25μm, Brunswick Corp.
D = 347 SS, 90%, 67μm, Huyck Metals Co.
E = Grade AX graphite, 63%, 1.4μm, Poco Graphite Co.
F = FC-14 graphite, 49%, 3.5μm, Pure Carbon Co.
G = Mo foam, 78%, 25μm, Spectra-Mat, Inc.
H = Mo foam, 75%, 20μm, Spectra-Mat, Inc.
[b]The area given is the area facing the anode (the projected area).
[c]The average power density at the one-hour rate is the product of the average voltage and current density.

III. SUPPORTING LABORATORY INVESTIGATIONS

A. Phase Equilibrium Studies of Electrolyte-Containing Mixtures (J. P. Ackerman, B. S. Tani)

The electrolyte of an electrochemical cell must be in intimate contact with both the anode and the cathode. If material from either electrode should dissolve in the electrolyte, diffusion to the other electrode could produce several adverse effects such as chemical self-discharge, the formation of an insulating film on one of the electrodes, or dewetting of the electrode structure by the active material. Lithium does not dissolve in its salts to any significant extent;[7] but the solubility in the electrolytes of sulfur, Li_2S, Li_xS_y and other materials present in the cell cathode is essentially unknown. The purpose of these investigations is to evaluate a number of electrolytes with respect to their solvent power for cathode materials and to measure the variation of solubility with temperature. The information obtained will facilitate the choice of the electrolyte and of the operating temperature range for lithium/sulfur cells. The same type of experiment permits the investigation of the solubility of cathode materials containing various additives.

Mixtures of various amounts of electrolyte, sulfur, and lithium sulfide were heated in a specially constructed furnace and observed while at temperature through a viewing port. Visual determination of the number of phases indicated a general similarity of the Li_2S-S-electrolyte phase diagram to that of the system Li_2Se-Se-(LiBr-RbBr), which has been studied in some detail.[8] A typical Li_2S-S-electrolyte phase diagram at 360°C is shown in Fig. 16. There are apparently three liquid phases and one solid phase. These are

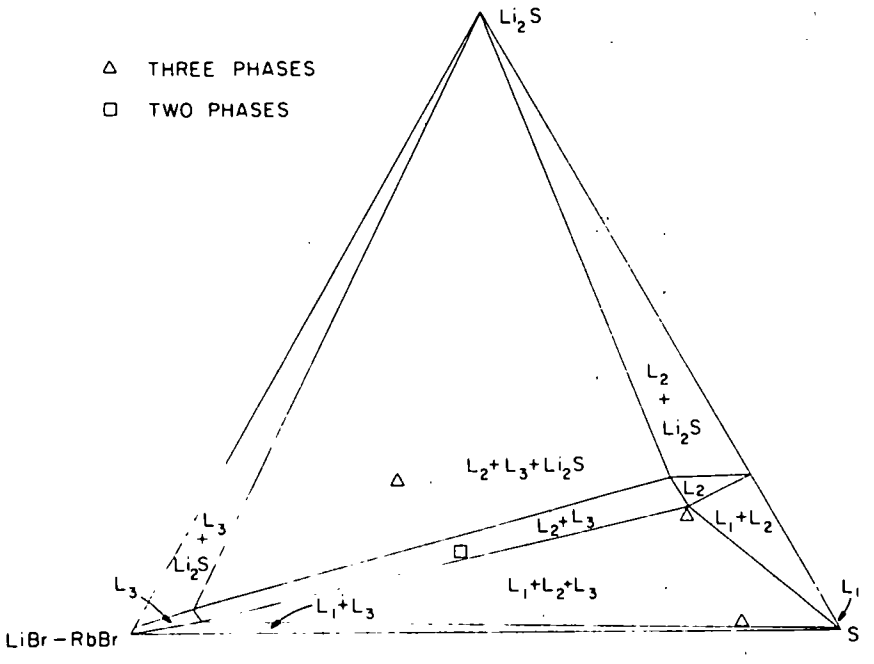

Fig. 16. Phase Diagram of the Pseudo-ternary System Li_2S-S-(LiBr-RbBr)

(1) The electrolyte-rich liquid phase, L_3. It is deep red at temperatures near 360°C when in equilibrium with the other components of the system, and yellow when quenched. This phase is more dense than any other phase in the system when the electrolyte contains bromide or iodide ions, and is less dense than the L_2 phase when the electrolyte contains fluoride and/or chloride ions only. The density of this phase is probably near the density of the pure electrolyte.

(2) A liquid phase, L_2, composed largely of Li_2S and sulfur with lesser amounts of electrolyte. It is black and opaque both at temperature and red in quenched samples, and has a density intermediate between those salts containing iodide or bromide and those which contain only chloride and fluoride, i.e., 2.28-2.95 g/cm^3 at 360°C. The L_2 field meets the Li_2S-S side of the pseudo-ternary phase diagram at the composition of the monotectic in the Li_2S-S binary system. This has been determined by P. T. Cunningham to be at 37 at. % lithium in sulfur.[9]

(3) A liquid phase, L_1, whose composition never differs greatly from pure sulfur. It is essentially insoluble in electrolyte and is the least dense of the phases present. It has a deep clear ruby color at temperatures near 360°C and is virtually indistinguishable from pure sulfur when quenched.

(4) The solid, Li_2S. It is essentially insoluble in electrolyte[10] and has been detected only in quenched samples by X-ray diffraction. Some typical compositions which were observed in the system Li_2S-S-(LiBr-RbBr) are shown in Table VI. For other electrolytes, observations were confined to samples having compositions in the fields of L_3 and $L_2 + L_3$.

TABLE VI. Phases Present at Selected Compositions in the System Li_2S-S-(LiBr-RbBr)

Sample	mol % Li_2S	mol % S	mol % LiBr-RbBr	Phases Observed
S-1	1.0	85.2	13.8	$L_1 + L_2 + L_3$
S-6	19.0	69.1	11.9	$L_1 + L_2 + L_3$
C-1	24.8	24.7	50.5	$L_2 + L_3 + Li_2S$
C-3	13.0	39.5	37.5	$L_2 + L_3$

The solubilities of Li_2S and of L_1 in L_3 are both very low. Thus, the remaining area of concern related to the solubility of sulfur-bearing species is the solubility of L_2 in L_3. Determination of this solubility should yield information of importance in the selection of the electrolyte which has the lowest solubility for sulfur-bearing species.

A straight line, drawn from the intersection of the L_2 field with the Li_2S-S side of the phase diagram to the pure electrolyte corner, passes through the L_2, L_3, and $L_2 + L_3$ fields. Intersection of this line with the boundary between the L_3 and $L_2 + L_3$ fields is a measure of the solubility of L_2 in L_3. This intersection is being determined at 360°C for LiBr-RbBr, LiCl-LiI-KI, and LiCl-KCl-CsCl and is being determined at 400°C for those electrolytes and the

higher-melting-point electrolytes LiF-LiCl-LiI, LiCl-KCl, and LiF-LiCl-KCl. The experimental procedure consists of encapsulation of mixtures of the desired compositions in quartz capsules, equilibration at temperature, centrifugation at 100-120 *g*, and quenching in liquid nitrogen. The quenched samples are microscopically examined to determine the number of phases present.

At first it was thought that the solubility of L_2 in L_3 could be determined by analyzing the L_3 phase for sulfur and Li_2S. Sulfide analysis was attempted by dissolving portions of the L_3 phase in water, and titrating with a $AgNO_3$ solution using a sulfide-specific electrode as an indicator. Samples submitted for total sulfur analysis by oxidation and Ba^{2+} precipitation, followed by turbidimetric or gravimetric determination of $BaSO_4$, showed that the sulfide ion determination did not provide the required accuracy. The experimental procedure was changed to one in which the limits of the L_2 field are determined by microscopic examination of quenched samples. Samples in which the sulfur-to-sulfide-ion ratio is maintained constant were mixed with varying amounts of electrolyte and equilibrated to determine the percentage of electrolyte present when the L_2 phase disappears. The samples were held in the centrifuge for 3-4 hr at a temperature 10-15°C above the desired temperature, cooled to the desired temperature, and equilibrated for another 3-4 hr. After liquid nitrogen quenching, the quartz capsules were broken just above the level of the contents, cast in Polylite,* sectioned by grinding parallel to the force field of the centrifuge, and examined microscopically. It is possible to estimate within approximately 1% the composition at which the L_2 phase disappears. The results to date are given in Table VII for 360 and 400°C. Where inequalities or ranges are given, the experimental data are not yet complete.

TABLE VII. Solubility of L_2 in L_3 for Various Electrolytes at 360 and 400°C

Electrolyte	Solubility, mol %[a]	
	360°C	400°C
LiBr-RbBr	92 ± 2	<70
LiCl-LiI-KI	94 ± 2	60-70
LiCl-KCl-CsCl	97 ± 1	>90
LiCl-KCl	–	>>90

[a]Mol percent electrolyte at which all L_2 is dissolved.

From these results it can be seen that generally those salts having small, difficultly-polarizable anions have a far less solvent power for L_2 than do the salts containing the large "soft" anions. At present LiCl-KCl and LiCl-KCl-CsCl electrolytes are clearly better for cell use from the point of view of solubility considerations. A similar electrolyte, LiF-LiCl-KCl, has not yet been investigated, but it is felt that, because of the presence of the small, hard fluoride ion, it may be somewhat better than those which have been examined already.

*A product of Reichold Chemicals.

B. Studies of Sulfur-Bearing Species in Molten Alkali Halides
(D. M. Gruen, A. J. Zielen)

The objective of this study is the characterization of sulfur-bearing species in fused alkali halide melts. Complex equilibria between species such as S_n, S^{2-}, and S_nS^{2-} undoubtedly occur and must be understood in order to optimize cell performance.

A variety of techniques, including electrochemical and spectrophotometric measurements, is being employed. The first major goal was the preparation of sulfur-free sulfide solutions in molten-salt electrolytes. It is essential to establish the properties of sulfide ion (and elemental sulfur) before the added complications of polysulfide species can be accommodated. Electrolytic reduction of a metal sulfide was selected as the preparative method. The "standard" sulfide solution so obtained could then be used in spectrophotometric studies and in evaluating the performance of sulfide-ion indicating electrodes.

A second major goal was the establishment of reliable analytical techniques for sulfide and sulfur, particularly direct determinations in the melt by electroanalytical methods. Precipitation titration with a coulometrically generated metal ion combined with a potentiometric end point was employed for in situ sulfide ion analysis. More conventional analytical procedures for sulfide and total sulfur in frozen eutectic samples are also under evaluation.

All experiments to date have been performed at 400 or 450°C in LiCl-KCl eutectic (59.5 mol % LiCl),* which had been treated with magnesium metal and filtered, treated with chlorine gas, purged with argon, and sealed in ampoules of 50 g under an argon atmosphere. A simplified sketch of the molten salt cell assembly is presented in Fig. 17. The cell top actually contained six standard-taper entry ports instead of the three shown. The extra ports were used for a thermocouple well, a tube with Rotaflo stopcock and ball joint for argon entry or vacuum, and a fourth (if desired) electrode compartment. The electrode and thermocouple-well positions were readily adjusted after easing the O-ring compression. Pyrex instead of quartz fritted ware was used in some of the earlier runs, but the results were poor because of severe attack by sulfide on Pyrex glass.

In a typical experiment, the apparatus was charged with frozen eutectic (50 g) and completely assembled in a nitrogen glove box. The sealed cell was then moved to the furnace, flushed with argon, and maintained under a positive argon pressure throughout the run. The eutectic was slowly melted and seeped into the fritted compartments with a period of 16-20 hr allowed for the cells to fill. The furnace was mounted with counter weights on vertical tracks so that it could be readily moved for visual inspection of the cell. Temperature control of the melt is estimated at ± 2°C.

Electrode and thermocouple potentials were measured to 0.1 and 0.01 mV, respectively, with Rubicon Portable Potentiometers. The constant-current source, built by the Electronics Division of Argonne National Laboratory, supplied dc current continuously variable from 1 to 100 mA and constant within

*Obtained from Anderson Physics Laboratories.

0.1%. Timing to 0.001 sec was provided by a Beckman Universal Eput and Timer with the start and stop triggers supplied by the voltage drop across a resistor in series with the constant-current source.

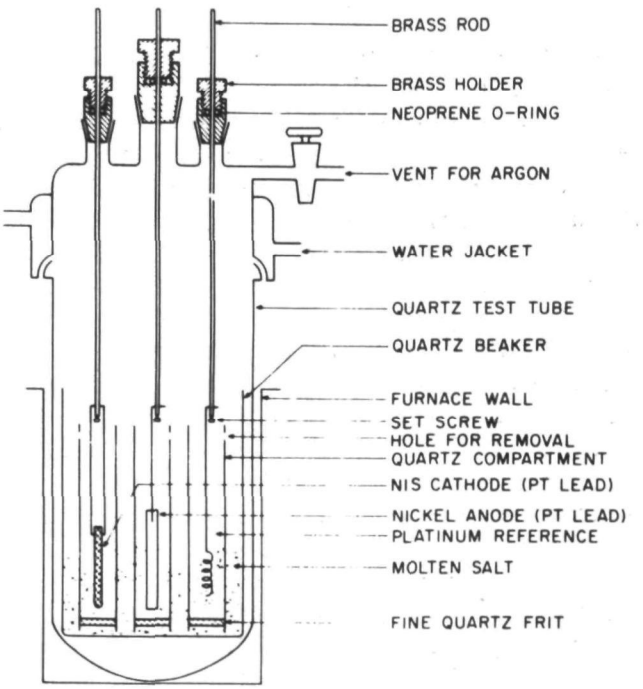

Fig. 17. Molten-Salt Cell Assembly for Sulfide-Ion Investigations

1. Electrodes

The reference electrode was a spiral of 30-mil platinum metal anodized at constant current for a measured length of time,[11] and the concentration of Pt(II) determined by the weight of salt in the compartment. The density values of the LiCl-KCl eutectic are 1.673 and 1.647 g/ml at 400 and 450°C, as interpolated from literature data.[2]

Silver sulfide cathodes were prepared by passing sulfur vapor in an argon stream over strips of heated silver foil. The result was a heavy coat of coarse crystalline needles, identified by X-ray and chemical analyses as pure monoclinic Ag_2S.

Nickel sulfide was prepared by sealing a 1:1 atomic weight ratio of powdered nickel and sulfur in an evacuated quartz tube and gradually heating in a vertical furnace for several hours until the temperature exceeded 1000°C (NiS melts at ∿980°C). The product was a golden ingot with a striking metallic appearance. The material, which was found to be an excellent conductor, was confirmed as NiS by chemical and X-ray analyses. Other nickel sulfide ingots were prepared by remelting portions of the original product, which is very brittle and can be crushed with a mortar and pestle. It was found that the addition of extra nickel metal produces an ingot, probably a mixture of NiS and Ni_3S_2, of improved strength and machinability.

Metal anodes, used as isolated counter electrodes and for in situ titrations, were prepared by spot-welding 5-mm strips of metal foil (Ni, Ag, or Pd) to 30-mil platinum lead wires.

2. Direct Sulfide Analysis in Molten Salt

Our first notable success was the in situ precipitation titration of S^{2-} with coulometrically generated Ni^{2+}, viz.

$$Ni + S^{2-} = NiS + 2e^- \qquad (1)$$

A typical titration curve is presented in Fig. 18; the equilibrium potential of the nickel electrode was determined after each anodization increment. Similar results were also obtained using a silver anode, but the end-point break was smaller and less sharp.

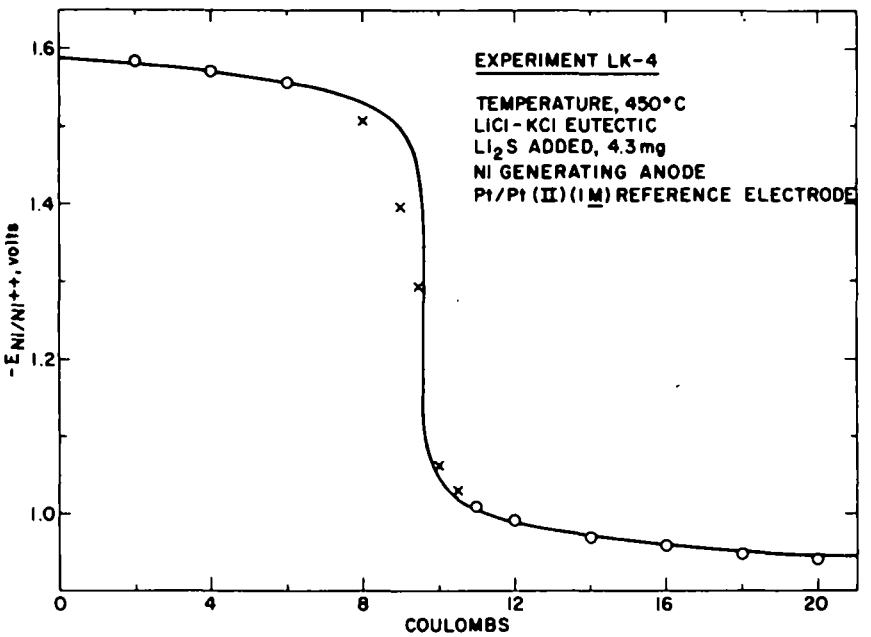

Fig. 18. Precipitation Titration Curve for S^{2-} With Generated Ni^{2+}; Experiment LK-4

If the potential of the nickel electrode is determined by the solubility equilibrium for NiS

$$NiS = Ni^{2+} + S^{2-}, \qquad K_{sp} = (Ni^{2+})(S^{2-}) \qquad (2)$$

$$E_{Ni/Ni^{2+}} = E^{\circ}_{Ni/Ni^{2+}} - (RT/2F) \ln (S^{2-})/K_{sp} \qquad (3)$$

Letting C equal the number of coulombs passed, A the initial concentration of S^{2-} in mol/liter, V the solution volume in liters, and dropping the subscripts of Eq. 3

$$E = E^{\circ} + (RT/2F) \ln [-A + C/(2FV) + \sqrt{(A - C/2FV)^2 + 4K_{sp}}]/2 \qquad (4)$$

The smooth curve of Fig. 18 was calculated from Eq. 4 after evaluating the adjustable parameters E°, K_{sp}, and A by a least-squares computer fit to the data. Since the emf measurements in the end-point region are always less accurate than the other data, these values ("X's" in Fig. 18) were used obtain A, and the remaining data established the E° and K_{sp} values.

Table VIII summarizes the Ni/Ni^{2+} formal potential and NiS solubility product values obtained by this technique. A value of -0.795 V at 450°C had been reported for E°.[11] The found (S^{2-}) values should correspond to the solubility limit of Li_2S in the eutectic except for experiment LK-4, where losses becauses of sulfide attack on the Pyrex glass cell may have resulted in an unsaturated solution. The percentage S^{2-} recovery entries will be discussed below.

TABLE VIII. Titration of S^{2-} in LiCl-KCl Eutectic with a Nickel Anode; Evaluation of Ni/Ni^{2+} Formal Potential and NiS Solubility Product

Experiment No.	°C	E°, volts[a]	K_{sp}, $(mol/liter)^2$	Found S^{2-}, mol/liter	% S^{2-} Recovery
LK-4	450	-0.809	1.8×10^{-13}	0.0122	53.0[b]
LK-11	400	-0.801	3.7×10^{-15}	0.0147	7.8[c]
LK-12	400	-0.790	2.1×10^{-15}	0.0118	94.3[d]

[a]Versus Pt/Pt^{2+} (1 *M*) reference electrode.
[b]Added as Li_2S (Foote Mineral Co.), Pyrex cell.
[c]Generated from Ag_2S cathode; no correction for S^{2-} removed with the generating electrode.
[d]Generated from NiS cathode; corrected for Li_2S precipitate found on generating electrode.

The Table VIII results present a consistent picture that confirms the successful in situ analysis for S^{2-} ion. A similar least-squares calculation was not made for the precipitation titration with a silver anode, but an estimate of 2×10^{-11} $(mol/liter)^3$ was made from the data for K_{sp} of Ag_2S at 450°C.

3. Electrochemical Generation of S^{2-}

The first attempts to generate sulfide ion employed Ag_2S cathodes:

$$Ag_2S + 2e^- = 2Ag + S^{2-} \qquad (5)$$

The procedure was to pass a constant current for a measured length of time and then to determine the electrode potential vs a Pt/Pt(II) reference. Usually 15-20 min were allowed for the potential to reach a (reasonably) steady value. Plots of electrode potential vs log (S^{2-}) or log (coulombs passed) were reasonably straight and reproducible but gave a Nernst slope for a one-electron reaction, possibly indicating the reaction

$$Ag_2S + e^- = Ag + AgS^- \qquad (6)$$

Check determinations made by similar semilogarithmic plots for the metal anode (Ag or Ni) used as the isolated counter electrode invariably gave excellent straight lines with standard deviations usually less than 1 mV and Nernst slopes within 1-3% of the theoretical values.

Another disturbing fact was that sulfide analyses made at the end of the generating run, either in situ as previously described or on the frozen eutectic, indicated very low yields of sulfide (cf. LK-11 in Table VIII). It was finally discovered that the missing sulfide was trapped or precipitated on the relatively large, irregular surface of the crystalline Ag_2S, and it was "lost" by the simple act of removing the generating electrode prior to the sulfide analysis.

Nickel sulfide was then tried as the generating cathode, i.e., the reverse of Eq. 1. The first attempt (Experiment LK-12) was very gratifying. Over the useful range of Li_2S solubility, the NiS electrode gave a Nernst response within 10% of the theoretical two-electron value, and the total sulfide found and generated values were in agreement (cf. Table VIII).

A mixed $NiS-Ni_3S_2$ cathode was used in the next experiment, LK-13. This run also featured a small nickel electrode in the cathode compartment with the intent of monitoring the sulfide ion concentration by means of the Ni/Ni^{2+} couple and Eq. 2. It was hoped that such a nonworking electrode would be better behaved than the generating cathode, and that is what occurred. The mixed-sulfide cathode gave very erratic potentials, probably indicative of mixed potential behavior. The nickel electrode data are presented in Fig. 19. The straight line is drawn with the theoretical slope; the horizontal break occurs due to Li_2S precipitation. Furthermore, if the observed Ni/Ni^{2+} potentials are combined with the LK-4 results of Table VIII to calculate log (S^{2-}) via Eq. 3, the results agree with the "coulombs-passed" values within a mean of 0.10 log unit. This is well within the error limits of Table VIII.

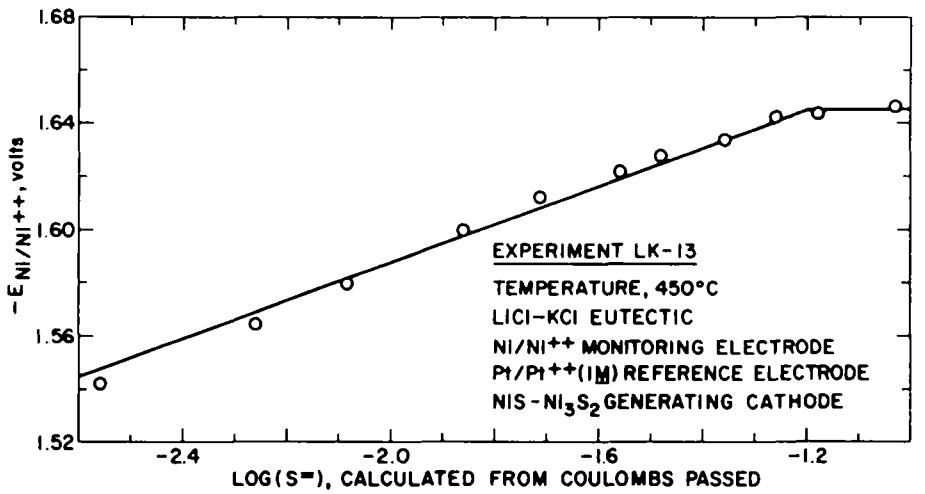

Fig. 19. The Potential of the Ni/Ni^{2+} Electrode as a Function of S^{2-} Concentration

Thus the electrochemical generation of S^{2-} in molten salt has been demonstrated satisfactorily. Future work will test the response of NiS as a nonworking, indicating electrode. A fully oxidized electrode of this type will be required in polysulfide solutions.

4. Spectrochemical Studies

A "standard" sulfide solution was generated with a nickel sulfide cathode, and the electrolyte was frozen. Remelted portions of this material with varying amounts of added sulfur are being examined spectrophotometrically. The results are too preliminary for discussion except to state that a definite polysulfide absorption has been observed that is reproducible and responds reversibly to temperature and mass action.

5. Analysis of Frozen Eutectic Samples

Analytical methods for sulfide and total sulfur in frozen eutectic are under evaluation. Sulfide ion determinations can be made conveniently by potentiometric titration with standard silver nitrate using an Orion silver/sulfide specific ion electrode as the end-point detector. Analyses made with a pure Na_2S stock solution in 1 *M* NaOH have given very satisfactory results (0.1% accuracy) if, as previously suggested,[12] the titration is made in 1 *M* NH_4OH + 0.1 *M* NaOH. Optimum performance is obtained if the Orion electrode is not inserted until near the end point. This minimizes coagulation of Ag_2S precipitate on the sensing membrane. The customary literature procedure of titrating in 1 *M* NaOH should be abandoned because of errors caused by Ag_2O coprecipitation.

The generally accepted best method for total sulfur is oxidation to sulfate with excess iodate in boiling 4 *M* NaOH solution and subsequent titration of the excess iodate with thiosulfate.[13] Thus for a polysulfide solution

$$(4 + 3n)\ IO_3^- + 3S_n^{2-} + 6nOH^- = (4 + 3n)I^- + 3(1 + n)SO_4^{2-} + 3nH_2O \qquad (7)$$

An independent sulfide ion determination must be combined with the iodate result to differentiate between S and S^{2-}. Problems arise in the iodate titration because sulfur is formed as an intermediate product and further oxidation is slow. Thus low results can be obtained because of incomplete oxidation and/or loss of sulfur by steam distillation. Using our standard Na_2S solution, values ranging from 68 to 97.8% of the calculated sulfide have been observed, depending upon the excess of iodate used and the boiling time. However, it is anticipated that, with the proper conditions, accurate results will be obtained.

C. Solid-Electrolyte Studies
(T. W. Latimer, J. N. Mundy)

The majority of solid materials exhibiting ionic conductivity have conductivities of less than 10^{-2} ohm^{-1} cm^{-1} at temperatures which have been used for lithium/sulfur cells (375-400°C). Molten-salt electrolytes in the same temperature range have conductivities of 1 to 10 ohm^{-1} cm^{-1}. Because solid electrolytes offer some design advantages, and offer the possibility of avoiding cathode material solubility in the electrolyte, an exploratory investigation is being undertaken in search of solid electrolytes with high lithium-ion conductivity.

In solid materials, ions move through the interlaced cation and anion network by means of defects in the network. These defects, such as ions on interstitial sites or vacant ion sites in the network, can be generated thermally or be present because of charge-balance impurities in the material. In normal crystals the number of defects present is relatively small, and consequently their ionic conductivity is small. There are, however, a number of solid compounds which have ionic conductivities greater than 0.1 ohm^{-1} cm^{-1}. These compounds show a much lower temperature dependence of conductivity than that found for normal crystals.

There appear to be three broad classes of compounds with high ionic conductivity. These are (1) the silver halides and a number of ternary compounds of silver halide with an alkali metal, (2) Li_2SO_4, Li_2WO_4, and the mixtures $(Li, Na)_2SO_4$ and $(Li, Ag)_2SO_4$, and (3) the ceramics based on β-alumina ($M_4Al_{22}O_{17}$, where M_4 can be alkali metal or silver). The first class of materials has essentially a rigid crystalline arrangement of anions with a large number of interstitial sites on which the cations are distributed in a disordered fashion. There are always far more sites than cations. The situation is similar in Li_2SO_4, where in each cell the two lithium ions have three cation sites. The β-alumina lattice has a hexagonal layer structure. Every fifth layer of oxygen is no longer a close-packed layer but contains only one quarter of the usual number of oxygen ions. In this layer alkali metal ions can be present on both oxygen and interstitial ion sites.

In all these classes of material there are always more cation sites available than the number or cations present, and this is the basic reason for the high conductivity. The β-alumina is slightly different from the other materials in that the cation disorder is only present in well-defined layers and not throughout the entire structure. While this limits the overall ionic conductivity, measurements have shown that this should not prove a limiting factor in the use of this material as a solid electrolyte in high-temperature batteries.

Both Li_2SO_4 and Li_2WO_4 have cation-disordered structures above 450 to 500°C. This temperature is too high for the lithium/sulfur battery, and in any case there would be compatibility problems using Li_2SO_4. On the basis of our survey of cation-disordered structures, we decided that the greater possibility of finding a high-lithium-ion conducting material lay in materials possessing the β-alumina layered structure. We believe that there should be lithium compounds analogous to the sodium compounds possessing the β- and β"-type phases. The following sections describe the methods we have employed to synthesize these structures and to determine whether the materials possess a high conductivity.

1. Li_2O-MgO-Al_2O_3 System

This system was investigated because of the possibility of obtaining lithium β- or β"-aluminas by conventional ceramic fabrication techniques. Eight compositions in the Al_2O_3 corner of the phase diagram were chosen for investigation and are given in Table IX.

TABLE IX. Starting Compositions (in wt %) of Li_2O-MgO-Al_2O_3 Specimens

No.	Li_2O	MgO	Al_2O_3
1	5.54	-	94.46
2	5.15	6.95	87.90
3	2.50	2.50	95.00
4	2.50	5.00	92.50
5	3.75	3.75	92.50
6	5.00	2.50	92.50
7	5.00	5.00	90.00
8	6.25	3.75	90.00

The raw materials were Li_2CO_3, MgO, and Al_2O_3 (Alcoa Type A-15). After calcining in air at 685°C for 1 hr, the specimens were fired at 1700 and 1800°C for 1 hr in helium. Weight losses at the two firing temperatures and densities at 1800°C are given in Table X. The weight losses at the firing temperatures are attributed to the vaporization of Li_2O.

TABLE X. Weight Loss and Density of Li_2O-MgO-Al_2O_3 Compositions Fired at 1700 and 1800°C

	1700°C	1800°C	
No.	Wt Loss, %	Wt Loss, %	Density, g/cm^3
1	0.72	1.42	2.92
2	1.02	2.39	3.11
3	0.38	0.34	2.86
4	0.40	0.46	2.85
5	0.44	0.75	2.86
6	0.67	1.31	3.03
7	1.02	1.59	3.18
8	1.90	-	-

These weight losses were considerably less than those found with similar Na_2O-MgO-Al_2O_3 compositions. The conductivities of all the specimens were of the order of 2×10^{-8} ohm^{-1} cm^{-1} at 400°C. The low conductivities and low weight losses of these compositions indicate no tendency to form the hexagonal β"-alumina structure. The compound $Li_2O \cdot 5\ Al_2O_3$ (Composition 1) belongs to the cubic crystal system.[14]

The use of Alcoa Type A-16 alumina (crystallite size $\leq$1 μm) instead of Type A-15 alumina (crystallite size = 2.5 μm) increased the fired density of Composition 1 by 15% and was used in all subsequent studies using alumina as a raw material.

2. Li_2O-La_2O_3-Al_2O_3 System

This system was thought to be of interest because of the occurrence of the compound $La_2O_3 \cdot 11\ Al_2O_3$ having the β-alumina structure without alkali ions.[15] A preliminary study of six compositions in the Li_2O-La_2O_3-Al_2O_3 system

in the area of $La_2O_3 \cdot 11\ Al_2O_3$ was begun in order to determine the extent of the phase field containing the β-alumina structure. The starting compositions are given in Table XI.

TABLE XI. Starting Compositions (in wt %) of Li_2O-La_2O_3-Al_2O_3 Specimens

No.	Li_2O	La_2O_3	Al_2O_3
L-1	-	22.51	77.49
L-2	2.00	22.06	75.94
L-3	4.00	21.61	74.39
L-4	2.36	17.15	80.49
L-5	4.65	16.00	79.35
L-6	4.88	12.00	83.12

The raw materials for these compositions were Li_2CO_3, La_2O_3, and Al_2O_3 (Alcoa Type A-16). The compositions containing 4 wt % or more Li_2O were overfired at 1650°C. The weight losses and densities of the samples fired at 1500, 1650, and 1700°C are given in Table XII.

TABLE XII. Weight Losses and Densities of Li_2O-La_2O_3-Al_2O_3 Compositions Fired at 1500, 1650, and 1700°C

	Weight Loss, %			Density, g/cm^3		
No.	1500°C	1650°C	1700°C	1500°C	1650°C	1700°C
L-1	1.46	14.2	1.63	3.10	3.44	3.94
L-2	3.12	3.72	3.84	3.15	3.85	3.96
L-3	3.14	OF[a]	-	3.49	OF	-
L-4	2.48	3.02	3.10	3.10	3.89	3.99
L-5	2.49	OF	-	3.25	OF	-
L-6	1.99	OF	-	3.27	OF	-

[a]Overfired.

Conductivity measurements of these samples indicated that no high-conductivity phases were present. However, the weight losses may have influenced the crystal structure, and the firings will be repeated in an alkaline atmosphere, similar to the method used in firing sodium β-alumina.

3. Sodium β- and β"-Alumina

Since the direct synthesis of lithium β- or β"-alumina structures does not appear to be very promising, the investigation of a method for their production from sodium β-alumina by ion exchange was begun. The first source of sodium β-alumina was Monofrax H,* a commercial refractory product, containing 5.7 wt % Na_2O. Approximate weight losses on firing Monofrax H were measured (in vacuum) on a single 1-in.-dia specimen by means of a thermogravimetric balance. The weight-loss rates were 4.8 mg/hr at 1400°C, 11 mg/hr at 1500°C, 58 mg/hr at 1600°C, and 120 mg/hr at 1700°C.

*Product of the Carborundum Co., Falconer, N.Y.

Three compositions (S-4, S-5, and S-6) were prepared after milling -12 mesh Monofrax H for 14 hr. Composition S-4 was Monofrax H; Compositions S-5 and S-6 were Monofrax H with additions of 1.78 wt % H_3BO_3 and 4.56 wt % Na_2CO_3, respectively. Based on the thermogravimetric data, a fast firing in helium consisting of a 30-min soak at 1400°C, an increase to 1675°C in 15 min, and a 5-min soak at 1675°C was tried. Other specimens were packed in -20 mesh Monofrax H and fired in helium for 1 hr at 1700°C. Table XIII gives the fired densities obtained by these methods; neither yielded specimens of sufficiently high density.

TABLE XIII. Fired Densities of Monofrax H Specimens

No.	Fast Fire to 1675°C, g/cm^3	1700°C Packed in Monofrax H, g/cm^3
S-4	2.66	2.81
S-5	2.57	2.68
S-6	2.75	2.69

The use of Monofrax H as a starting raw material was discontinued upon receiving 100-325 mesh β-alumina (sodium content = 7.3 wt %) from Alcoa. This material was ground for 16 hr with sampling at 4-hr intervals to determine the effect of grinding time on density. The specimens were fired at 300°C/hr to 1700°C in helium (1-hr soak). Table XIV shows the unfired and fired densities as a function of milling time.

TABLE XIV. Effect of Milling Time on Unfired and Fired Densities of Alcoa β-alumina

Milling Time, hr	Unfired Density, g/cm^3	Fired Density, g/cm^3
4	2.15	2.78
8	2.25	3.00
12	2.27	3.04
16	2.28	3.05

An attempt to fire the specimens at 550°C/hr resulted in specimens having densities of under 3.0 g/cm^3. A slightly higher firing temperature is expected to increase the density to 3.15-3.20 g/cm^3 for specimens to be used for lithium ion-exchange studies.

Two compositions in the Na_2O-MgO-Al_2O_3 systems were chosen for preliminary study of sodium β"-alumina. These were S-2 (8 wt % Na_2O, 3 wt % MgO, 89 wt % Al_2O_3) and S-3 (10 wt % Na_2O, 4 wt % MgO, 86 wt % Al_2O_3). Firing these compositions in helium at 1800°C after prefiring at 700°C resulted in high weight losses of 4.8-7.2 wt % for S-2 and 7.8-10.6 wt % for S-3. The conductivity of S-3 was 3×10^{-3} ohm^{-1} cm^{-1} at 400°C despite the large Na_2O loss. Firing in an alkaline atmosphere (packed in Monofrax H) resulted in lower Na_2O losses, but expansion caused by the density change involved in the formation of the β"-alumina structure cracked the specimens. The effects of prereaction temperatures and times (before forming) on the fired products are being investigated.

4. Conductivity

Measurements were made of the ionic conductivity of each sample. The results were used to determine whether any high-conductivity phase was present in the sample. This method of "screening" samples proved to be a relatively quick and reliable procedure.

The measurements were made with an ac bridge (Electro Scientific Industries, Model 291-A), operating at a frequency of 1000 Hz, and an oscilloscope (Tektronix Model 515A) to improve the sensitivity. A two-probe cell was used because of the simplicity of sample changing. The problems associated with two-probe cells did not present any difficulties with the measurements. The aluminate disks were coated with graphite on each flat surface and mounted between platinum electrodes. The conductivity of each sample was measured in a flowing stream of argon (purity, 99.999%). To confirm that the ac bridge was operating correctly, the conductivity of a sample of NaCl was measured. The results agreed with previous data on NaCl.

Hsueh and Bennion[16] found that the hygroscopic nature of β-alumina made their conductivity measurements strongly dependent on prior heat treatment. None of the lithium-containing samples investigated appeared to be hygroscopic. It is possibly not surprising that when the "layered" β-alumina structure is formed, the material becomes hygroscopic. To eliminate the possibility of this effect on our conductivity measurements, we have followed Hsueh and Bennion's procedure of heating the samples to 900°C in an argon atmosphere and holding at that temperature for 1 hr. Conductivity measurements were then made as the sample was slowly cooled from 900 to 350°C. From the data obtained, plots were made of log conductivity versus 1/T. The results of all the measurements are shown in Fig. 20. It was found that the plots were linear for all the lithium-containing samples. The data for the individual samples are not shown in Fig. 20; however, each plot lay within the shaded area appropriate to the composition series. The activation energies for all the lithium-containing samples were between 17 and 21 kcal/mol.

It can be seen in Fig. 20 that the conductivities of all the samples in the two lithium series have similar activation energies to those of LiCl and NaCl in their extrinsic conductivity range (lower slopes). It appears likely that the conductivity of the lithium-containing samples occurs by the same processes that are responsible for the conductivity of the alkali halides. In the extrinsic range of conductivity, the defects responsible for the conductivity occur because of impurities which are present in the material. The greater the amount of impurity, the higher the conductivity. Unfortunately, impurity solubilities limit the amount of conductivity gain that can be achieved. The range of values represented in each shaded area of Fig. 20 gives an indication of the changes that were obtained by varying the compositions of the samples in any one series.

The samples of sodium aluminates (S-3 and Monofrax H) show a very different variation of conductivity with temperature. The plots are curved and at about 400°C have an activation energy of approximately 5 kcal/mol. This value of the activation energy is similar to that found by Imai and Harada[17] in their investigation of the effects of divalent impurities on the conductivity of β-alumina. A low value for the activation energy is to be

expected in a "layer" structure like β-alumina. In normal ionic conductors, the activation energy is higher because it includes the energy to form the defect responsible for the conduction and also the energy to move an ion by means of that defect. In a cation-disordered structure such as β-alumina, there is a large fraction of vacant cation sites always present in the network, and the energy required to move the cations is small.

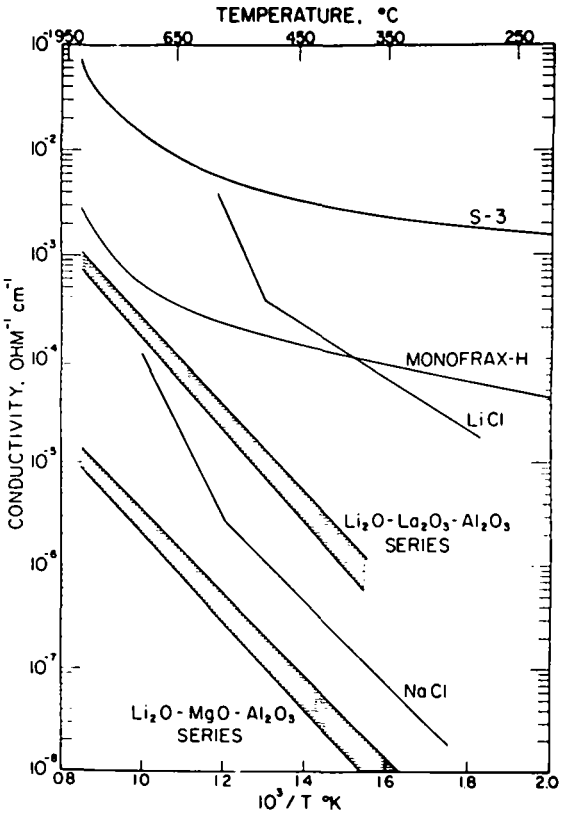

Fig. 20. Ionic Conductivity of Aluminate Samples

While the activation energies for the ionic conductivities of our samples of sodium β-aluminates are the same as that found by Imai and Harada, the absolute values of the conductivity are considerably lower. This is almost certainly due to the small amount of high-conducting phase present in our samples. Only a small amount of the β-alumina phase was formed due to large Na_2O losses during the firing of the samples. The improved procedure for sample firing should minimize these losses and result in compacts having ionic conductivities of the order of 10^{-1} ohm^{-1} cm^{-1} at 400°C.

D. Cathode Material Studies
(R. K. Steunenberg, R. M. Yonco)

Small-scale cell tests have shown that elemental sulfur alone can be used as the active cathode material in lithium/sulfur cells. However, the use of additives to increase the electronic conductivity and decrease the vapor pressure of the sulfur may result in improved electrical performance of the cells, and possibly permit a simpler, lighter-weight cathode current-collector design. Iron, thallium, and other materials have been under consideration as potential sulfur additives.

The solubility of iron in liquid sulfur at 400°C is reported to be about 5 at. %.[18] Several unsuccessful attempts were made to prepare a 4 at. % solution of iron in sulfur by heating FeS in liquid sulfur at temperatures up to about 450°C. Thermal-analysis results and visual observation indicated that the FeS had not dissolved completely, even after several days at temperatures around 400°C. One sample of FeS in sulfur was held for several days at 450°C and filtered through a fine Pyrex frit. The electrical conductivity of the filtrate was $\leq 10^{-7}$ ohm^{-1} cm^{-1} at 127 and 377°C. This sample was then ignited in air. The weight of the residue was negligible (<0.01 wt %), which, together with the conductivity data, indicates that the sulfur contained little or no iron. (The conductivity of high-purity sulfur at 377°C is $\sim 10^{-9}$ ohm^{-1} cm^{-1}.) These results may be attributed either to a slow dissolution rate of iron sulfides in sulfur, which is consistent with observations reported in the literature,[19] or to an error in the published phase diagram.[18] In either case, iron does not appear to be a promising additive to sulfur cathodes in lithium/sulfur cells and no further studies are planned on the iron-sulfur system.

Sulfur-thallium mixtures are reported to have a high electrical conductivity (~1 ohm^{-1} cm^{-1}) at 400°C.[20] These data, however, were obtained at relatively high thallium concentrations (>37.5 at. %), which would be undesirable in a lithium/sulfur cell because of the high atomic weight of thallium (204.37 g/g-atom). Therefore, the electrical conductivities of sulfur containing much lower concentrations of thallium are of interest as a possible cathode material. Because the thallium-sulfur system is reported to have a liquid miscibility gap in the sulfur-rich region of the phase diagram and the phase boundaries of the gap appeared to be poorly known,[21] a brief investigation was undertaken to define the compositions of the two liquid phases. In the first experiment, a sulfur-20 at. % thallium mixture was prepared by heating the elements together in a sealed quartz tube. The existence of the miscibility gap was confirmed by the formation of two liquid layers.

In subsequent experiments, the boundaries of the miscibility gap were determined over the temperature range 350 to 444°C. Quartz ampoules containing approximately 20 at. % thallium in sulfur were equilibrated for periods of 15 to 25 days at temperatures of 350, 410, and 444°C and then quenched. Samples of the upper and lower phases were analyzed for thallium by wet chemical methods. The results were as follows:

Equilibration temperature, °C	350	410	444
Thallium concentration, at. %			
Upper phase	<0.02	<0.08	0.09
Lower phase	26.5	26.0	26.9

These results indicate that the solubility of thallium in sulfur is considerably lower than that reported in the literature and that the thallium content of the higher-density phase is slightly less than the literature value.

The electrical conductivities of the two liquid phases were measured, using a Pyrex "U-tube" conductivity cell with molybdenum electrodes. The conductivity results are presented in Table XV. The fact that the conductivity of the sulfur-rich phase is very low suggests that small concentrations of thallium do not have a significant doping effect on the sulfur. The relatively high conductivity of the thallium-rich phase may prove beneficial

to a lithium/sulfur cell containing thallium as a cathode additive if a sufficiently small amount of thallium can be used.

TABLE XV. Electrical Conductivities of the Two Immiscible Liquid Phases in the Sulfur-Rich Region of the Thallium-Sulfur Phase Diagram

Conductivity Cell

Material:	Pyrex
Shape:	U-tube
Electrodes:	molybdenum
Cell Constant:	27.4 cm^{-1}

Upper (Sulfur-Rich) Phase

Frequency, kHz	Specific Conductivity, ohm^{-1} cm^{-1}	
	150°C	345°C
0 (dc)	9.5×10^{-9}	1.4×10^{-9}
0.1	2.2×10^{-9}	2.0×10^{-9}
1.0	1.6×10^{-8}	2.6×10^{-7}
10.0	5.5×10^{-7}	5.6×10^{-7}

Lower (Thallium-Rich) Phase

Frequency, kHz	Specific Conductivity, ohm^{-1} cm^{-1}	
	142°C	367°C
0 (dc)	1.57×10^{-2}	3.8×10^{-1}
0.1	1.59×10^{-2}	4.4×10^{-1}
1.0	1.59×10^{-2}	4.4×10^{-1}
10.0	1.60×10^{-2}	4.4×10^{-1}

In addition to the above studies, samples of sulfur containing a proprietary additive that is claimed to raise its conductivity to about 10^{-1} ohm^{-1} cm^{-1} at 130°C were obtained from the Freeport Sulphur Company, Belle Chasse, La. (The conductivity of high-purity sulfur at 130°C is 10^{-12} ohm^{-1} cm^{-1} or less.[22]) Preliminary tests with a volt-ohmmeter showed this material to be conductive both when molten and at room temperature after it had solidified. Subsequent conductivity measurements were made, using a Pyrex cell with molybdenum electrodes. The following results were obtained:

Frequency, kHz	Specific Conductivity, $ohm^{-1}\ cm^{-1}$	
	136°C	158°C
0.1	1.23×10^{-3}	1.43×10^{-3}
1.0	1.23×10^{-3}	1.43×10^{-3}
10.0	1.23×10^{-3}	1.42×10^{-3}
dc	1.16×10^{-3}	

These results show no dependence of the conductivity upon frequency in the ac measurements, and the ac and dc data are in reasonable agreement. In the dc measurements, the system exhibited Ohm's law behavior up to the maximum potential that was applied (5 V). The conductivity appears to increase somewhat with increasing temperature. It was not possible to obtain consistent conductivity data at higher temperatures because of a tendency of the material to form gas bubbles in the cell.

The results of the above studies indicate that iron is unlikely to be a useful additive to the cathodes of lithium/sulfur cells. Thallium may prove to be somewhat beneficial, but its toxicity is a potential disadvantage. The proprietary "high-conductivity" sulfur supplied by the Freeport Sulphur Company appears to be unsuitable for use in lithium/sulfur cells because of its tendency to segregate and to release gases. There are other potential additives, however, which are believed to merit investigation, and further work is planned in this area.

E. Mass-Transport Studies

(B. A. Feay)

Work in this area has been concentrated on two problems: (1) increasing the cycle life of the lithium anode and (2) increasing the capacity density of the sulfur cathode. Considerable progress has been made in the work on the lithium electrode. It appears that the problem is understood and is amenable to solution. The work on the sulfur electrode has been hindered by the difficulty in developing a suitable test cell. However, recent results are encouraging.

To study the lithium electrode, the cell shown in Fig. 21 was designed to allow the simple operation of lithium electrodes of various designs in molten-salt electrolytes of different compositions. The lithium electrode shown in the figure is typical of the anodes presently used in lithium/sulfur cells. It consists of lithium soaked into Type 302 stainless steel Feltmetal (90% porosity, 67-μm pore size). The lithium was added to the Feltmetal in a furnace well at 650°C. The counter electrode is a disk of aluminum. When the cell is discharged, lithium is transferred from the Feltmetal to the aluminum, creating a Li-Al alloy. When the cell is charged, lithium is transferred from the aluminum back to the Feltmetal. The aluminum counter electrode was chosen because of the stable voltage and good cycling capability of the Li-Al alloy, which allows an evaluation of the lithium electrode alone.

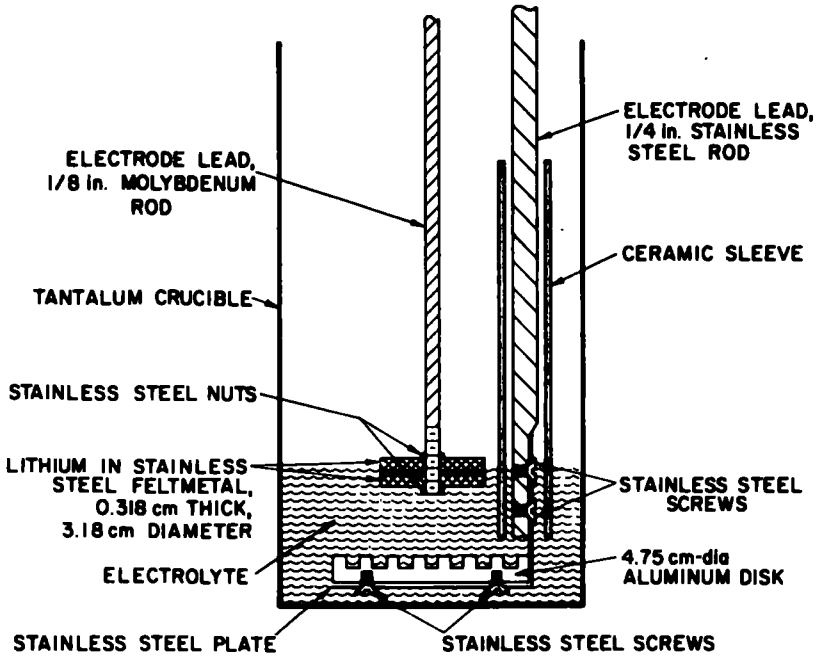

Fig. 21. Schematic Diagram of the Lithium Electrode Test Cell

The cell was operated in the furnace well of a helium-atmosphere box and was heated to temperatures between 380 and 425°C. The cell was cycled continuously by charging and discharging between maximum and minimum cutoff voltages. A voltage-time trace for a typical cycle at a current density of 0.25 A/cm^2 (2.0 A) is shown in Fig. 22. As the cell was discharged, the voltage decreased gradually, and then dropped rapidly to the cutoff voltage of 0.05 V when the lithium became depleted in the Feltmetal. As the cell was charged, the voltage increased gradually, and then rose rapidly to the cutoff voltage of 0.55 V when the lithium became depleted in the aluminum. During this cycle, the capacity density was 0.8 A-hr/cm^2 (based on the Feltmetal electrode).

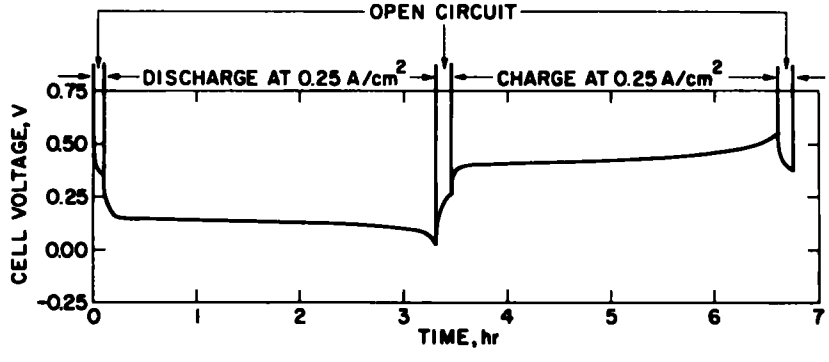

Fig. 22. Typical Voltage-Time Behavior of a Li/LiCl-KCl/Li-Al Cell at 425°C and at a Current Density of 0.25 A/cm^2

The performance of the four cells that have been run is summarized in Table XVI. The maximum capacity density is a measure of the amount of lithium

the Feltmetal could hold if the lithium were available. The observed capacity density is based on the amount of available lithium transferred during a cycle. The capacity density based on lithium added compared with the observed capacity density is a measure of the unavailable lithium. Most of this unavailable lithium is probably tied up in remote regions of the lithium-aluminum electrode.

TABLE XVI. Summary of Lithium Electrode Cell Tests

Lithium Electrode: Lithium in Huyck Type 302 stainless steel Feltmetal (90% porosity, 67-μm pore size)
Counter Electrode: Lithium in Aluminum
Interelectrode Distance: 1 cm

	Cell Number			
	1	2	3	4
Lithium electrode dimensions, cm	Two disks, 3.18 dia × 0.318	One disk, 2.54 dia × 0.318	One disk, 2.54 dia × 0.318	One disk, 2.86 dia × 0.318
Projected area, cm^2	8.0	5.0	5.0	6.4
Counter electrode dimensions, cm	Aluminum disk 4.75 × 0.635 thick, with four concentric grooves (0.318 × 0.318) cut in surface			Aluminum disk 5.1 dia × 0.318 thick
Projected area, cm^2	17.8	17.8	17.8	20.3
Electrolyte, mol %	LiCl 58.5 KCl 41.5	LiCl 8.5 LiI 59.0 KI 32.5	LiCl 8.5 LiI 59.0 KI 32.5	LiF 3.5 LiCl 56.0 KCl 40.5
Position of lithium electrode	At surface of electrolyte			Top surface 0.32 cm below electrolyte surface
Insulator	Al_2O_3	Al_2O_3	Al_2O_3	BeO
Temperature, °C	425	390	390	395
Hours of operation	100	4	2	675
Number of cycles[a]	10	2	1	202
Capacity density, A-hr/cm^2				
Maximum[b]	1.18	0.59	0.59	0.59
Based on total lithium	1.11	1.11	1.11	1.11
Observed	0.8 at 0.25 A/cm^2	0.25 at 0.25 A/cm^2	-	0.51 at 0.125 A/cm^2, 0.375 at 0.25 A/cm^2
Remarks	Failure by lithium beading on Feltmetal during 10th cycle recharge	Lithium beading on first recharge	Lithium beading on inserting lithium electrode	10 g of LiCl-LiI-KI added at cycle No. 139 (480 hr); instant bubbling, lithium beading, deterioration in cell performance

[a]Above a current density of 0.125 A/cm^2.
[b]Based on quantity of lithium required to fill void volume of the Feltmetal.

During the operation of the first three cells, a problem occurred which appears to be a major factor that limits the cycle life of the present lithium electrodes. While the cell was charging, the returning lithium failed to soak into the Feltmetal. Instead, it formed beads on the surface of the Feltmetal which escaped from the electrode by floating to the surface of the electrolyte.

Cell No. 4, which had a LiF-LiCl-KCl eutectic electrolyte, performed very well for 480 hr and 138 cycles. The electrolyte remained clear and colorless and there was no evidence of lithium beading on the stainless steel Feltmetal. During the first few days of operation, the capacity density decreased gradually, probably because lithium migrated to remote regions of the aluminum disk and became inaccessible. When more lithium was added to the Feltmetal, the lithium soaked in immediately, and the capacity density increased. After the first few days, the capacity density stabilized. At a current density of 0.125 A/cm^2 the capacity density was 0.51 A-hr/cm^2, and at 0.25 A/cm^2 the capacity density was 0.375 A-hr/cm^2

On Cycle No. 139, after 480 hr of operation with no noticeable deterioration in performance , 10 g of LiCl-LiI-KI eutectic was added to the electrolyte. Immediate bubbling occurred around the electrodes, the electrolyte became clouded, there was some lithium beading, and the capacity density decreased. The electrolyte gradually cleared, and the capacity density stabilized. At 0.125 A/cm^2 the capacity density was 0.44 A-hr/cm^2, and at 0.25 A/cm^2 the capacity density was 0.125 A-hr/cm^2. The lithium beading continued and became more and more pronounced. After 460 hr of operation, the lithium electrode was removed and inspected. Most of the lithium appeared to be on the surface of the Feltmetal. The electrode was replaced and a small piece of lithium was added. The lithium did not soak into the Feltmetal, and the capacity density did not increase. On Cycle No. 202, after 675 hr of operation, the cell was shut down and disassembled.

The significant differences between the fourth cell and the three previous cells were

(1) LiF-LiCl-KCl eutectic was used as the electrolyte;
(2) beryllium oxide was used instead of Al_2O_3 for ceramic sleeve;
(3) the lithium-soaked Feltmetal was completely immersed in the electrolyte instead of being partially exposed to the box atmosphere.

Under these operating conditions, the present lithium anode design appears capable of good cycle life. The addition of the LiCl-LiI-KI had an obvious deleterious effect. A probable cause was moisture in the iodide salt. If iodide-containing electrolytes are to be used, it appears that they must be of much higher purity. It may be that iodide has such a strong tendency to pick up moisture that it cannot be used. It is also possible that iodide ion has a significant effect on the ability of the electrolyte to displace lithium from the Feltmetal.

The second problem under study is increasing the capacity density of the sulfur cathode. An attempt was made to develop a cell which would run in a quartz housing. This housing would have allowed visual observation of the cell during operation. However, the failure of several cells indicated that quartz was too susceptible to lithium attack, even when Li-Al alloy was used in place of pure lithium for the anode.

From the experience gained with the quartz cell housing and from cells developed for other tasks, the cell shown in Fig. 23 was designed and constructed. Preliminary tests with this cell indicate it will be an excellent cell for studying sulfur cathodes. It is sealed and is easy to assemble and disassemble. It is easy to use various cathode materials, and the cathode design can be changed without changing other parts of the cell. The first series of tests to be run with this cell will be to study the effect of different carbon and graphite materials, used as cathode current collectors, on cell performance.

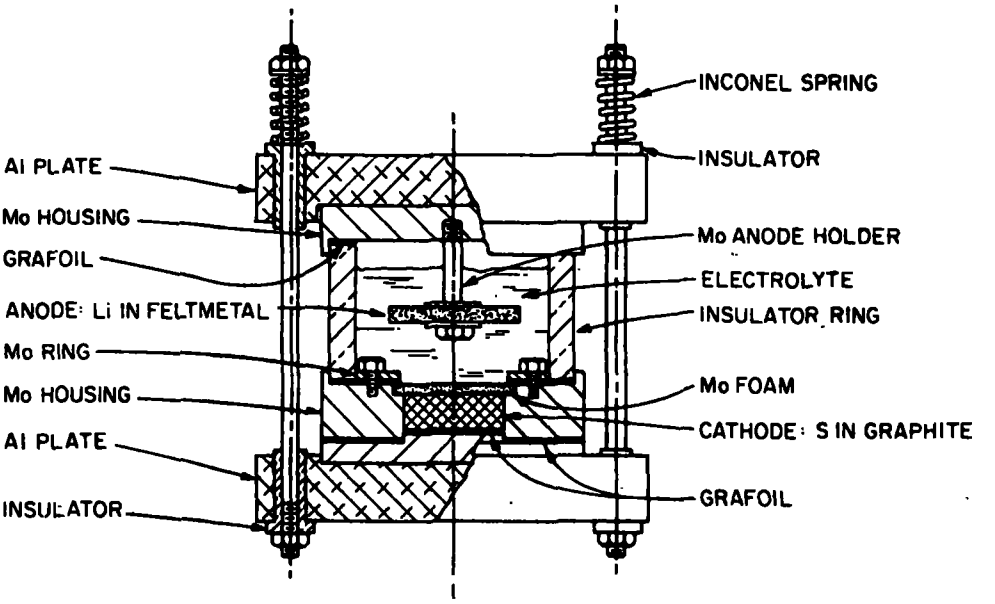

Fig. 23. Lithium/Sulfur Test Cell

IV. MATERIALS TESTING AND FABRICATION

The corrosion resistance of various materials to simulated cell environments is being studied to identify materials with potential usefulness for cell applications. Two distinctly different classes of materials resistant to cell conditions are required. First, corrosion-resistant materials possessing good electrical conductivity are required to serve as current collectors and cell housings. Secondly, a corrosion-resistant, electrically insulating material is required to prevent short-circuit contacts within the cell. The materials chosen for the cell cathode must be resistant to attack by sulfur, lithium-sulfur mixtures, and electrolyte at 375°C for thousands of hours. The anode housing and current collector must withstand exposure to molten lithium and the electrolyte under the same time and temperature conditions. Electrical insulators may require resistance to all of the cell constituents. Still other materials may be needed for hermetic sealing of cells, electrical feedthroughs, thermal insulation, and exterior housings. The performance of these various materials can be evaluated fully only through their use in operating cells and batteries. This type of materials testing, however, is expensive and time-consuming, and many candidate materials can be eliminated from consideration by relatively simple corrosion tests.

In addition to corrosion testing, scaling-up the lithium/sulfur cells from the successful laboratory sizes to larger sizes has indicated a need for materials and materials-processing development. Two types of materials that are undergoing such development are (1) corrosion-resistant, high-surface-area, open-structure, cathode current collectors and (2) corrosion-resistant ceramic insulators and electrical feedthroughs. The bulk of the work was concentrated on the development of corrosion-resistant ceramic insulators because of a more immediate need.

A. Experimental Procedure

Corrosion tests in a 20 at. % lithium-80 at. % sulfur mixture were normally conducted as dynamic isothermal tests. In these experiments, the samples (about 0.32 × 0.32 × 2.5 cm) were loaded into quartz capsules (about 2.5 cm dia, 6.25 cm long) with the appropriate amount of lithium-sulfur mixture. The capsules were sealed and held at temperature (usually 375°C) for 200 to 600 hr. The samples were held in a rocking furnace which rotated 180° every few minutes. This type of furnace was used to insure relatively uniform contact between the surface of the specimen and the lithium-sulfur mixture.

After the sample was removed from the furnace the adhering lithium-sulfur mixture was removed with water or CS_2. The weight loss or gain of the specimen was measured. The weight loss was converted to an annual corrosion rate which is reported in millimeters per year penetration; extrapolation is based on an assumed linear rate. For samples gaining weight because of film formation, extrapolation is based on an assumed parabolic rate. The exposed samples were examined metallographically to determine corrosion effects not apparent from simple weight-change considerations. All metal samples were also tested for electrical conductivity after exposure, since some sulfide films tend to be electrically insulating.

The samples were tested in mixtures of lithium and sulfur rather than in pure sulfur because preliminary investigations indicated that materials resistant to sulfur alone are not necessarily resistant to a lithium-sulfur mixture. For example, stainless steel is commonly protected from corrosion because of the presence of a surface oxide film. Oxidized Type 304 stainless steel is not severely attacked by sulfur at 375°C because of this oxide film. Lithium-sulfur mixtures, however, appear to attack the oxide film and thereby permit reaction of the stainless steel with sulfur. Therefore, corrosion tests were performed with mixtures of 20 at. % lithium-80 at. % sulfur. This composition was chosen as representative of the conditions in the cathode compartment of a partially discharged cell.

Corrosion tests in molten lithium were normally performed as static isothermal tests in which the specimen was immersed in molten lithium (helium atmosphere) for 100-1000 hr at 375°C. Upon termination of the experiment, the molten lithium was removed with methyl alcohol and the specimens were analyzed as indicated above.

B. Metallic Components Studies
(M. L. Kyle, J. R. Pavlik)

Corrosion rates of the more corrosion-resistant electrically conducting materials that were obtained in short-term and long-term screening tests in 20 at. % lithium-80 at. % sulfur at 375°C are presented in Fig. 24. Among the materials that were tested, molybdenum and chromium had low corrosion rates in both short-term tests of 100-300 hr and long-term tests of about 600 hr. Molybdenum, in particular, has been used in many of the experimental cells for periods up to several hundred hours and has shown good corrosion resistance under these conditions.

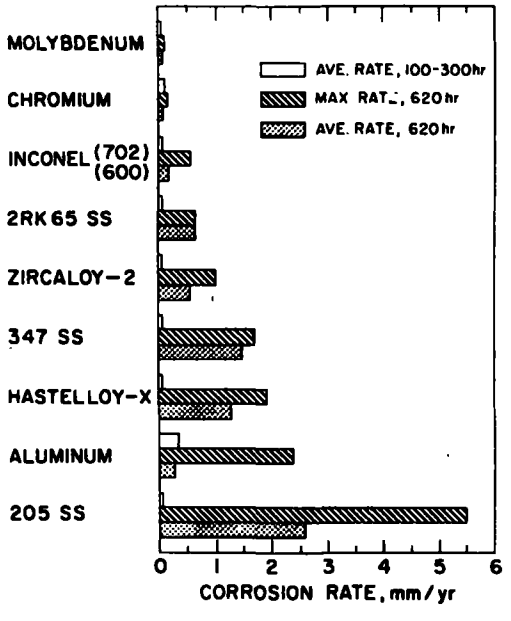

Fig. 24. Corrosion Rates of Metals Exposed to 20 at. % Li-S Mixtures at 375°C

The austenitic stainless steels, such as Types 2RK65, 347, and 205 (15 wt % Mn), had low corrosion rates in short-term tests, but much higher rates in the longer tests. The nickel-base alloys, such as Inconels 702 and 600 and Hastelloy X, as well as Zircaloy-2, showed similar behavior. The reason for the higher corrosion rates in the long-term tests is not fully understood, but it may be related to intergranular attack or to the temporary existence of a protective film.

The corrosion rate of aluminum by 20 at. % lithium-80 at. % sulfur mixtures has proved to be highly variable, with rates ranging from 0.01 to 2.4 mm/yr in 600-hr tests. It is suspected that these variations are associated with the nature of a surface film that is formed during the exposure. Not shown in Fig. 24 are the corrosion rates for tantalum, iron, titanium, nickel, and beryllium. All of these metals showed poor corrosion resistance to lithium-sulfur mixtures and have been excluded from consideration for use in the cathode of lithium/sulfur cells.

The metallic conductors used in lithium/sulfur cells should be both lightweight and low cost if batteries of these cells are to have a specific energy of at least 220 W-hr/kg. Two materials, aluminum and chromium, are of particular interest in the current materials program since they meet the weight and cost requirements. Molybdenum, on the other hand, is a high-density, relatively high-cost product. It is usable in laboratory and scaled-up cells, but its eventual replacement by a lighter, lower-cost material is desirable. Much of the current materials program is concentrated upon methods of using aluminum and chromium as cell components.

Three aluminum alloys (A-288, 5050, and 3004) and a ferritic chromium steel (E-Brite 26-1) were tested for corrosion resistance to the molten LiCl-KCl eutectic at 375°C for 113 hr and to 20 at. % lithium-80 at. % sulfur at 375°C for 480 hr. The aluminum alloys selected were those which are reported to be more resistant to chloride-ion attack.[23] The ferritic stainless steel is high in chromium content, and since chromium performed well in the corrosion tests, it was hoped that an alloy high in chromium would exhibit similar characteristics. The results of these tests are presented in Table XVII.

The electrolyte tests showed aluminum to be attacked at a rate of several tenths of a millimeter per year (six-sample average, 0.67 mm/yr). The attack was not uniform and most samples were noticeably pitted. This corrosion rate is too high for practical cell application. The ferritic stainless steel with the high chromium content showed excellent corrosion resistance. The sample surface was shiny before and after test and no sign of attack was evident.

When these materials were retested in the cathode material, different results were obtained. The three aluminum alloys, which had been attacked by the electrolyte, had a slight gray-to-yellow coloration and were electrically conductive. Except for some surface roughening, the samples were almost unaffected. The ferritic stainless steel, which was unaffected by the electrolyte, was severely attacked in the lithium-sulfur mixture by a mechanism which appeared to be dissolution.

TABLE XVII. Corrosion of Aluminum and Ferritic Stainless Steel in LiCl-KCl Electrolyte and 20 at. % Li-S Mixtures at 375°C

Material	Observed Corrosion Rate, mm/yr	
	113-hr Exposure to LiCl-KCl	480-hr Exposure to 20 at. % Li-S
A-288 Al[a]	0.65, 0.78	0.000, 0.013
5050 Al[b]	0.20, 1.3	0.048
3004 Al[c]	0.47, 0.66	0.031
E-Brite 26-1[d]	3.0×10^{-4}, 2.4×10^{-3}	0.46

[a]Composition (wt %): 1 Ni, 0.5 Fe, 0.1 Ti, balance Al.
[b]Composition (wt %): 1.4 Mg, balance Al.
[c]Composition (wt %): 1.2 Mn, 1.0 Mg, balance Al.
[d]Composition (wt %): 0.005 C, 0.25 Si, 26 Cr, 1.0 Mo, balance Fe; product of Airco Vacuum Metals, Berkeley, California.

The above results are taken to indicate that the corrosion resistance of aluminum will depend to a large extent upon the presence of a surface film to render the material inert to the electrolyte. The emphasis now will shift to the identity and method of formation of an inert surface film. The initial attempts will be with cathode, nitride, and sulfide films. High-chromium-content steels will be included in tests. Corrosion tests have been screening tests to determine the ability of various materials to withstand chemical and thermal effects in cells for times up to 1000 hr. These tests are not definitive, however, since electrical and mass-transfer effects in an operating cell cannot be readily simulated. The definitive materials tests must be performed in an operating cell; this phase of the program has been undertaken.

The design of a chromium-plated cell is shown in Fig. 25. The cell

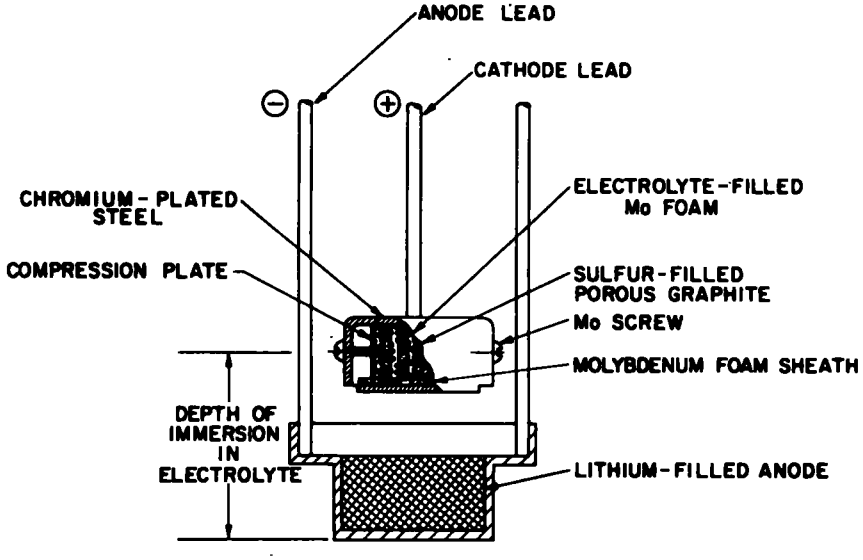

Fig. 25. Schematic Diagram of a Chromium-Plated Cell

is of a laminated-cathode design using a molybdenum foam (Spectra-Mat, Inc., 78.2% porosity, 25-μm av. pore size, 0.19 cm thick × 1.1 cm × 1.2 cm) sheath filled with electrolyte and porous graphite (Poco Graphite, Inc., 63% porosity, 1.4-μm av. pore size, 0.15 cm thick × 1.1 cm × 1.2 cm) filled with sulfur. The cell was fabricated of Type 304 stainless steel which was chromium-plated by conventional aqueous electroplating techniques.

The initial operation of the cell, using the LiBr-RbBr electrolyte and a stainless steel anode current collector, consisted of about 95 hr at 375°C and 20 charge-discharge cycles at current densities from 0.06 to 0.15 A/cm^2. Cell operation was terminated because of a short circuit caused by molten lithium floating on the electrolyte surface. Inspection of the cell showed that nearly all the chromium plating exposed to the electrolyte had been darkened or removed.

The cell performed smoothly during the experiment before the short circuit caused termination. The first discharge was made at a current density of 0.15 A/cm^2, and the cell delivered a capacity density of 0.14 A-hr/cm^2 (27% sulfur utilization to a final product of Li_2S above a 1-V cutoff). By the third discharge (at a current density of 0.13 A/cm^2), the capacity density had decreased to 0.05 A-hr/cm^2 (8.5% sulfur utilization) and remained at or near this value through the twentieth discharge. The discharge curves are shown in Fig. 26. Table XVIII presents the discharge data for the 20 cycles.

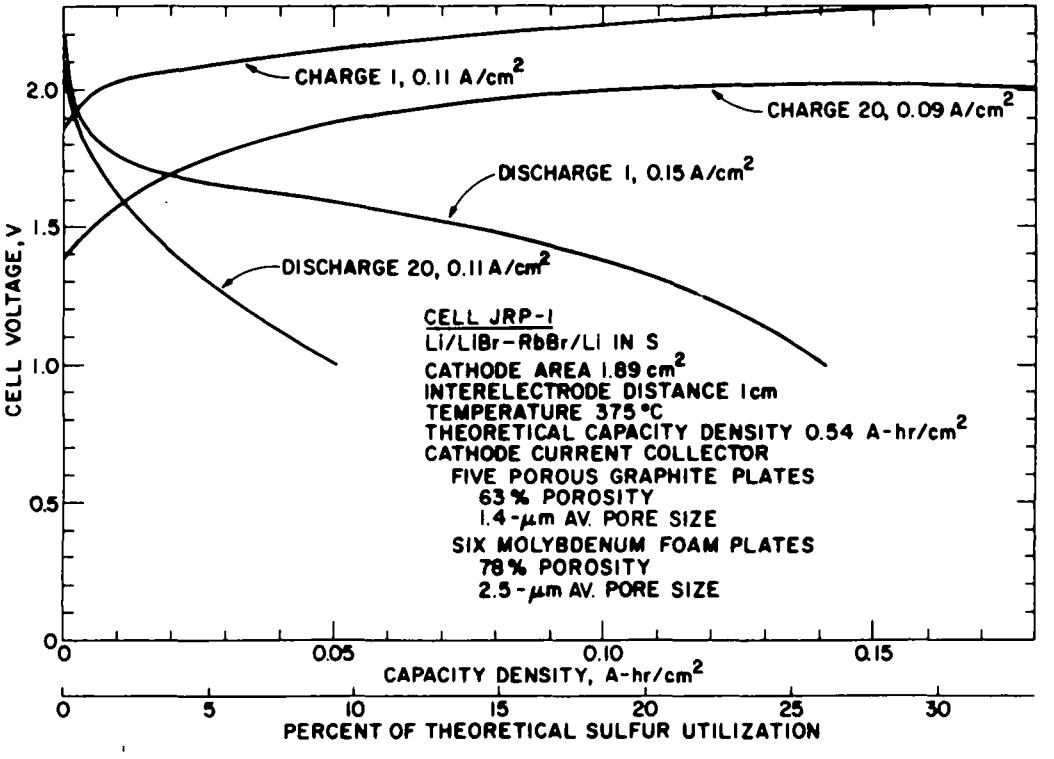

Fig. 26. Voltage-Capacity Density Curves for a Chromium-Plated Li/S Cell With LiBr-RbBr Electrolyte

TABLE XVIII. Performance of a Chromium-Plated Li/S Cell

Temperature: 375°C
Electrolyte: LiBr-RbBr
Anode: Lithium contained in Huyck Feltmetal, Type 302 SS, 90% porosity, 67-μm av. pore size
Cathode: Electrolyte elements (6)
Molybdenum foam, Spectra-Mat, Inc., 78% porosity, 25-μm av. pore size, 0.19 cm thick
Sulfur elements (5)
Porous graphite, Poco Graphite, Inc., 63% porosity, 1.4-μm av. pore size, 0.15 cm thick

Discharge No.	Current Density, A/cm^2	Capacity Density, > 1 Volt, $A\text{-}hr/cm^2$	Sulfur Utilization, %
1	0.15	0.141	27
2	0.13	0.100	18
3	0.13	0.047	8.5
4	0.11	0.037	6.8
5	0.11	0.075	14
6	0.11	0.070	13
7	0.11	0.053	9.7
8	0.11	0.053	9.7
9	0.12	0.068	12
10	0.12	0.047	8.5
11	0.06	0.081	15
12	0.11	0.062	11
13	0.11	0.060	11
14	0.11	0.062	11
15	0.11	0.056	10
16	0.11	0.051	9.4
17	0.11	0.053	9.7
18	0.11	0.055	10
19	0.11	0.051	9.4
20	0.11	0.048	8.7

The cell was operated a second time with two modifications: (1) the electrolyte was changed from LiBr-RbBr to LiF-LiCl-KCl in order to obtain better wetting of the molybdenum foam, and (2) the anode current collector was changed from Type 302 stainless steel (Huyck Metals Co., 90% porosity, 67-μm pore size) to nickel (Huyck Metals Co., 85% porosity, 85-μm pore size) to test nickel as an anode current collector and determine its wetting properties in cell applications.

The cell operated for only a single discharge cycle, which is displayed in Fig. 27. The discharge at 0.14 A/cm^2 produced a capacity density of 0.17 $A\text{-}hr/cm^2$ with 41% sulfur utilization (based on a 2 Li + S → Li_2S overall cell reaction). Most of this capacity was obtained at a terminal voltage >1.5 V. These results were considered very encouraging, but when the cell was recharged, the lithium did not return to the Feltmetal, but floated to the electrolyte surface. After repeated attempts to recharge the cell, its operation was terminated.

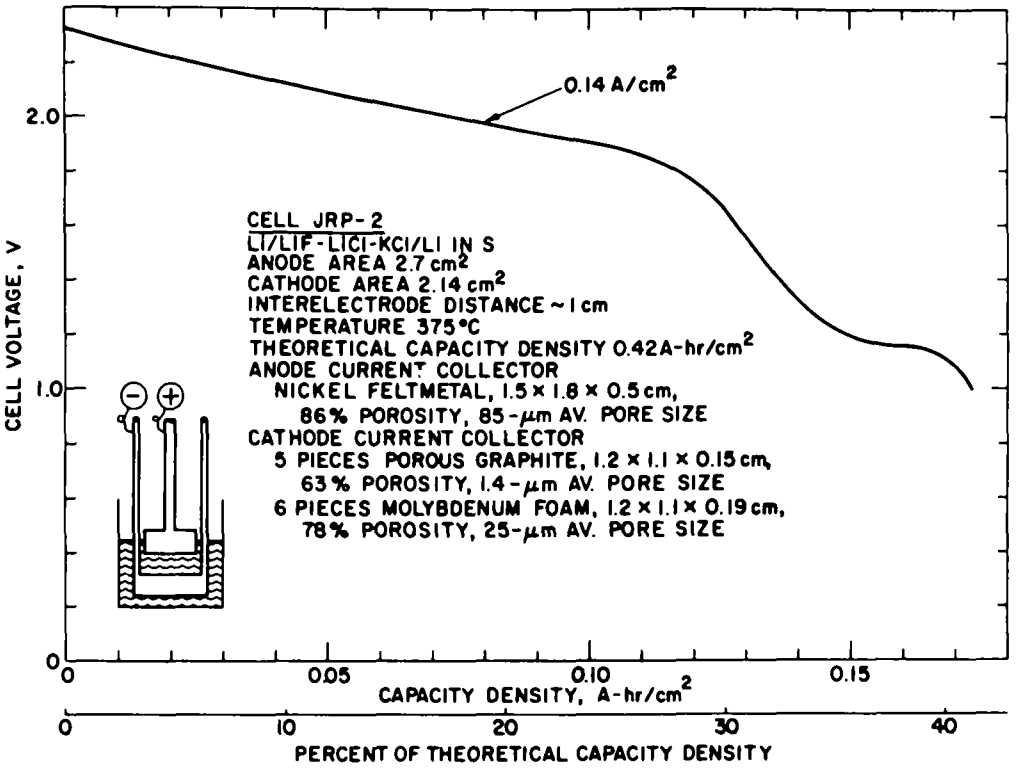

Fig. 27. Voltage-Capacity Density Curves for a Chromium-Plated Li/S Cell With LiF-LiCl-KCl Electrolyte

The anode Feltmetal was nickel, rather than Type 302 stainless steel used in most cells, and had a characteristic pore size of 85 rather than 67 μm. Whether the nickel, the larger pore size, or neither of these caused the cell failure is not known. The conclusion that nickel is an unacceptable anode current collector should not be drawn on the basis of this single test. Other cells using nickel Feltmetal will be operated.

The chromium-plated cell was destructively examined after the second cell test. Metallographic examination indicated that the chromium coating on the cathode housing was almost completely destroyed, while that on the anode housing was present but badly cracked. Analysis of parts remote from the active electrode surfaces showed the presence of an integral, well-bonded coating. It is concluded that the chromium-plating operation, performed by aqueous techniques, was done well. The coating apparently cracked from thermal stresses during operation, and in those areas of the cell (i.e., the cathode) where the base metal was not resistant to the corrosive environment, base-metal attack caused coating failure. In other areas (i.e., the anode) where the base metal was resistant, the coating remained in place. These results indicate that chromium plating should be explored further with added emphasis on cell design, plating temperature, and plating process, all of which are capable of reducing the thermal stresses that probably caused the plating to fail.

C. Seals and Insulating Component Studies
(M. L. Kyle, J. R. Pavlik)

Lithium/sulfur cells will probably require an electrical insulator resistant to lithium and electrolytes and, perhaps, to cathode mixtures. Currently BeO and BN are the only insulators which have demonstrated any appreciable lifetime in cell service, and BN is not thought to be usable in long-lived cells because of a corrosion mechanism which produces an electrically conducting film on the insulator surface. Although BeO has operated very well in cell service, alternative insulators are still being sought because of the cost and health hazard associated with BeO.

The results of 300-hr tests to determine the corrosion resistance of several potential electrical insulators to molten lithium at 375°C are shown in Table XIX. The tests indicated that γ-$LiAlO_2$, high-purity Al_2O_3, $Li_2O \cdot 5Al_2O_3$, $Li_2O \cdot MgO$ spinel structures, and $B_{12}O_2$ are not resistant to molten lithium. These materials have been eliminated from further consideration as lithium/sulfur cell insulators.

Three insulators, Y_2O_3, $Y_3Al_5O_{12}$, and the $MgO \cdot Al_2O_3$ spinel, were translucent before testing and darkened during testing but otherwise resisted attack very well. The observed corrosion rates of <0.06 mm/yr compare favorably with those of BeO and other insulators tested to date. It is interesting to note that these insulators were fabricated by hot-pressing. Hot-pressed BeO also appears to be superior in corrosion resistance to BeO fabricated by other techniques.

The corrosion resistance of lithium aluminate ($LiAlO_2$) also appears to be strongly affected by its method of preparation. Specimens of α-$LiAlO_2$ prepared by Foote Mineral and material compacted by McGraw-Edison from ANL-produced α-$LiAlO_2$ were both destroyed in testing. Other compacts prepared at ANL by pressing and sintering high-purity α-$LiAlO_2$ at 1600°C (γ-$LiAlO_2$ after sintering) were more corrosion resistant with observed corrosion rates of 0.12, 0.29, and 0.50 mm/yr in molten lithium at 375°C. The latter two samples were retested in LiF-LiCl-KCl mixtures at 375°C to simulate the presence of cell electrolyte and showed corrosion rates of 0.98 and 0.29 mm/yr. The corrosion resistance of the various insulators tested in lithium is shown in Fig. 28.

It is concluded that the purity of the material and the method of fabrication are important variables affecting the corrosion resistance of electrical insulators to molten lithium. Work at ANL will concentrate on procedures for preparing $LiAlO_2$- and Y_2O_3-based ceramic insulating materials and on preliminary testing of other potential insulators, particularly nitrides, while external sources of high-purity AlN, Y_2O_3, and BeO will be sought to begin evaluating some of these insulators in actual cell operation.

Grafoil,* a flexible graphite material containing no resins or fillers, is being evaluated as a sealing material. This material has been used in several lithium/sulfur cells and appears to provide a good seal. Grafoil

*A product of Union Carbide Corporation.

will be evaluated more extensively. It is expected that it is corrosion resistant to both sulfur and the molten-salt electrolyte but not to molten lithium.

TABLE XIX. Corrosion Rates of Electrical Insulators in Molten Lithium

Temperature: 375°C
Exposure Time: 300 hr

Sample Number	Starting Material	Source	Observed Corrosion Rate, mm/yr	Remarks
Li-281	γ-$LiAlO_2$	Foote Mineral	1.9	Severe attack
Li-282	γ-$LiAlO_2$	Foote Mineral	>3	Sample destroyed
Li-283	Al_2O_3 (Coram)	Corning Glass	>3	Sample destroyed
Li-284	Al_2O_3 (Lucalox)	General Electric	>3	Sample destroyed
Li-285	α-$LiAlO_2$	McGraw-Edison	>24	Sample destroyed
Li-286	$Li_2O \cdot 5Al_2O_3$	ANL	>26	Sample destroyed
Li-287	$Li_2O \cdot MgO$	ANL	6.0	Severe attack
Li-288	α-$LiAlO_2$	ANL	0.29[a]	Sample intact, little dimensional change
Li-292	α-$LiAlO_2$	ANL	0.98[b]	Retest of Sample Li-288 with salt present; sample friable after test
Li-289	α-$LiAlO_2$	ANL	0.50[a]	Sample intact; little dimensional change; some areas green-brown
Li-293	α-$LiAlO_2$	ANL	0.29[b]	Retest of Sample Li-289 with salt present; sample friable after test
Li-290	α-$LiAlO_2$	ANL	0.12	Sample intact
Li-291	Y_2O_3	ANL	>20	Sample destroyed
Li-303	$B_{12}O_2$	U. of Ill.[c]	High	Destroyed
Li-304	$Y_3Al_5O_{12}$	AMMRC[d]	1.6×10^{-2}	Mottled gray surface
Li-306	Y_2O_3	AMMRC	1.6×10^{-2}	Dull black surface film
Li-307	$Li_2O \cdot 5Al_2O_3$	AMMRC	0.97	Glaze destroyed; sample friable
Li-305	$MgO \cdot Al_2O_3$	AMMRC	5.9×10^{-2}	No longer translucent, gray surface

[a]Corrosion rate based on observed weight change. Samples did not change dimensions.
[b]Exposed to Li-KCl-LiCl mixture.
[c]Prepared by Professor Nelson of the University of Illinois.
[d]Obtained from Mr. G. E. Gazza of the Army Materials and Mechanics Research Center.

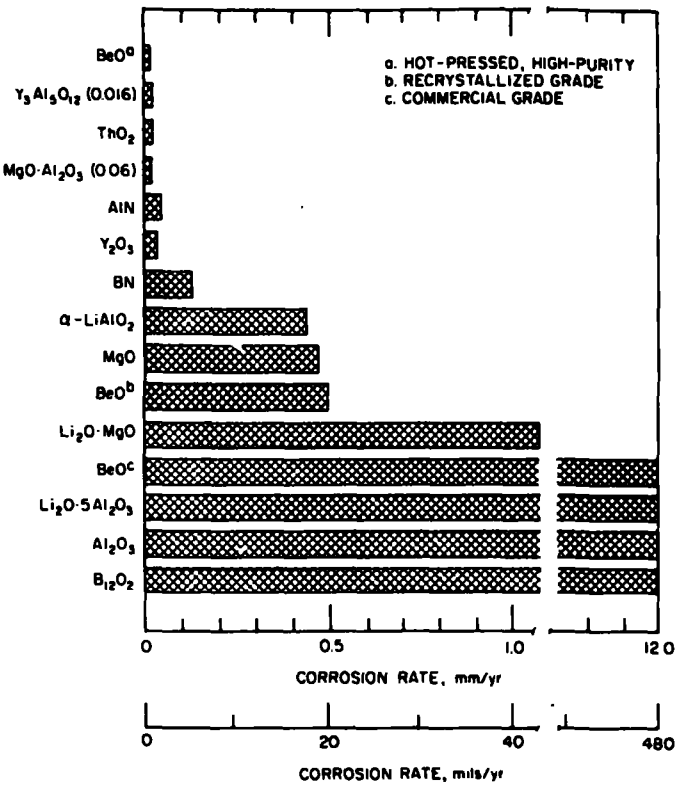

Fig. 28. Corrosion Rates of Electrical Insulators in Molten Lithium at 375°C

D. Development and Fabrication of Ceramic Insulators (D. E. Walker)

Boron nitride has been used as the cell insulator because it had shown good short-term corrosion resistance to lithium, sulfur, selenium, and the LiF-LiCl-KCl electrolyte and because it was readily available and machineable into the required shapes. In service, these insulators had lifetimes of 200 hr or less because of the formation of a conducting film on the insulator surface when dissolved lithium was present in the electrolyte.

The corrosion tests of various other ceramics discussed above indicated acceptable corrosion resistance for materials such as BeO, Y_2O_3, and $LiAlO_2$. However, these materials are not readily available in the required shapes, and the commercial materials were not uniform, showing varying degrees of corrosion resistance from one lot to another.

It was believed that impurities in the grain boundaries as well as low-density bodies with interconnected porosity were major reasons for poor corrosion resistance. Therefore, the approach selected was one that would produce a high-density body without the use of sintering additives. High density was to be obtained by sintering at a temperature as close to the melting point as possible.

The ceramic materials studied were $LiAlO_2$, Y_2O_3, and 90 wt % Y_2O_3-10 wt % Eu_2O_3. The bulk of the work was concentrated on $LiAlO_2$.

1. Lithium Aluminate

The $LiAlO_2$ powders used in this work derived from two basic batches. One batch was made by calcining a mixture of Al_2O_3 and Li_2CO_3 at about 700°C to form $LiAlO_2$ by the reaction:

$$Al_2O_3 + Li_2CO_3 \xrightarrow{\Delta} 2LiAlO_2 + CO_2\uparrow$$

This powder contained excess Li_2CO_3, which was not considered troublesome for high-temperature sintering processes because it was expected to decompose and volatilize during sintering. The bulk of this material (JK-2) was washed to remove the excess Li_2CO_3 and vacuum dried. The second material was a commercial product from Foote Mineral Company. This material was dry ball-milled in alumina equipment before use to reduce the particle size for better handling characteristics. The powders were characterized as indicated in Table XX.

TABLE XX. Characteristics of $LiAlO_2$ Powders

$LiAlO_2$ Source	Surface Area, m^2/g	Density,[a] g/cm^3	Average Particle Size, μm	Structure[b]	Remarks
CEN-1	--	--	--	--	Used as received
CEN JK-2	17.15	2.73	25% <44	γ-$LiAlO_2$[b] α-$LiAlO_2$	Washed and vacuum dried
Foote Mineral	3.18	2.79	77.4	γ-$LiAlO_2$[b] α-$LiAlO_2$	As-received
Foote Mineral	7.33	2.82	66.1	--	Ball-milled 34 hr

[a]Powder density determined by an air pycnometer and is higher than the handbook value of 2.55 g/cm^3 at 25°C.
[b]Indicates the major constituent.

2. Lithium-Aluminate Sintering Studies

Wafers (approximately 2.5 cm dia, 0.2 cm thick) were used to develop the best sintering conditions for the $LiAlO_2$ ceramic bodies. These wafers were cold-pressed in a steel die at pressures from 6.3×10^6 to 9.1×10^6 kg/m^2. The melting point for the 1:1 Li_2O-Al_2O_3 compound has been reported[24] as 1700 ± 15°C. A eutectic exists at 45 mol % Li_2O with a melting point of 1670 ± 15°C. These values are in agreement with our work. The as-received $LiAlO_2$ containing excess Li_2CO_3 could be sintered at 1675°C without melting, while the washed batch, JK-2, melted at this temperature. It was apparent that the higher-melting $LiAlO_2$ was stable at the 50 mol % composition during sintering because of the presence of Li_2O from decomposition of the excess Li_2CO_3. This Li_2O compensated for the usual Li_2O volatilization loss from the compound at elevated temperatures. The washed $LiAlO_2$ did not have an excess of Li_2CO_3 present, and the normal loss of Li_2O during sintering moved the composition towards the eutectic mixture and the lower melting temperature.

Small amounts of an organic binder and lubricant had to be added to the powders in order to produce a pressed body with sufficient strength to withstand removal from the die and necessary handling prior to sintering. Benzene solutions of stearic acid + polyvinyl alcohol, stearic acid + carbowax, stearic acid + acroloyd, and a commercial binder, Mobilcer-R (produced by Socony Mobile Oil Company), were evaluated. The Mobilcer-R binder is a water emulsion of microcrystalline wax. These binders were incorporated into the $LiAlO_2$ powder by mixing a slurry of powder and binder emulsion. The benzene solutions were added at the rate of 2 cm^3 solution per gram of powder. The water emulsion was added to the powder in the amount of 1 cm^3 per gram of powder. After the blended mix dried, the powder cake was crushed and sieved through a No. 20 sieve (U. S. sieve series). The best results were obtained with Mobilcer-R added in the amount of 3-5 wt % wax.

Sintering was accomplished in two steps. The first, in air, consisted of heating the pressed samples slowly to 300°C, holding at this temperature until the organic addition had been driven off, and then continuing to heat to 700°C. The higher temperature completed the organic removal step by oxidizing the residual carbon to CO_2, which diffused easily out of the low-density green compacts. The sintering step was accomplished in a helium atmosphere in a high-temperature, resistance-heated, tungsten, cold-wall furnace. The sintering temperature was originally set at 1675°C but was lowered to 1600°C to avoid melting the samples.

The disks produced during this study ranged in density from 1.84 to 2.50 g/cm^3 or from 72 to 98% of the theoretical density of 2.55 g/cm^3. Table XXI lists the characteristics of the $LiAlO_2$ ceramic bodies produced.

Very little work was done on producing Y_2O_3 ceramic bodies for insulators because the $LiAlO_2$ ceramics appeared to be satisfactory. However, the same criterion of high density for corrosion resistance was applied and several samples were made. Yttrium oxide powder of 99.99% purity from Consolidated Astronautics, Inc., was pressed in a 2.5-cm steel die. These wafers were sintered in helium at 2175°C. The samples attained a moderate density of 89% of the theoretical 5.03 g/cm^3. A second group of samples was made from a mixture of 90 wt % Y_2O_3-10 wt % Eu_2O_3. This mixture was prepared with the intention of utilizing the lower melting temperature of the Eu_2O_3 (2050°C) to provide liquid-phase sintering, which generally promotes the formation of high-density bodies. It was expected that the resulting ceramic would be a single-phase solid solution and as corrosion resistant in the cell environment as the Y_2O_3. Six 2.5-cm dia disks were pressed and sintered at 2200°C in helium. The results were inconclusive because trouble with the furnace controls caused rapid cooling from 1400°C. The wafers were badly cracked. Evaluation of one sample indicated a density of 4.99 g/cm^3, which is 94.7% of the calculated theoretical density for this mixture. The sintered material appeared grey-brown in color and was translucent.

3. Cell Insulator Production

One type of insulator being considered for the lithium/sulfur cells is a ceramic ring 73.6 mm OD × 64.6 mm ID × 0.79 mm thick. Procedures were developed to press and sinter this ring to the required diameter. The thickness was obtained by grinding the sintered ring to size.

TABLE XXI. Characteristics of Sintered $LiAlO_2$ Ceramic Bodies

Sample No.	Material Source	Sintering Weight Loss, %	Sintered Density, g/cm^3	Percent Theoretical Density, %	Sintering Temp. °C	Remarks
Al- 1	CEN-1	3.8	2.43	95	1675	No organic additions; no pre-firing in air.
- 2	CEN-1	3.6	2.48	97	1675	
- 3	CEN-1	3.6	2.43	95	1675	
- 4	CEN-1	3.7	2.43	95	1675	
Al- 9	CEN-1	1.5	2.49	97.6	1675	Organic binder, air-fired to 700°C
-10	CEN-1	1.8	2.50	98.0	1675	
Al-11	CEN JK-2	0.76	2.21	86.6	1630	Organic binder, air-fired to 700°C
-12	CEN JK-2	1.33	2.00	78.4	1630	
-13	CEN JK-2	1.98	2.20	86.3	1630	
-14	CEN JK-2	0.78	2.21	86.6	1630	
AL-28	Foote	1.77	1.84	72.16	1600	Organic binder, air-fired to 700°C
-29	Mineral,	1.57	1.85	72.55	1600	
-30	as-received	1.50	1.85	72.55	1600	
AL-34	Foote	1.60	2.33	91.37	1600	Organic binder, air-fired to 700°C
-35	Mineral,	1.18	2.34	91.76	1600	
-36	ball-milled 10 hr	1.21	2.36	92.55	1600	

The rings were pressed from powder in an isostatic press using a rubber die, such as that shown in Fig. 29. A pressed ring is shown in place in the die. The metal part on the right is the plug that seals the rubber die cavity from the working liquid in the isostatic press. In use, dry powder containing binder is poured into the ring-shaped portion of the die cavity and leveled with the surface. The metal plug is pressed into the die cavity until it bottoms against the powder-filled ring. This assembly is then placed into a steel support and lowered into the fluid in the isostatic press chamber. The press chamber is closed and the fluid is pressurized to the desired level. The pressure release rate is automatically controlled by means of a micrometer adjustment on the pressure-relief valve. After isostatic pressing, the working fluid is washed off the rubber die assembly and the metal plug is removed. The pressed ring is then removed. Figure 30 shows a group of five pressed rings after the 700°C binder removal step. The sintering procedure was the same as that used for the development samples. After burning out the binder, the rings were placed in a tungsten, resistance-heated, cold-wall furnace and heated to 1600°C in a helium atmosphere. The heating and cooling schedule was automatically controlled by means of a Data-Trak control unit to provide an 8 1/2-hr heat-up to 1600°C, 1/2 hr at temperature, and a 9-hr cool down.

A total of 46 rings have been pressed and sintered during this development. Twelve of the rings have been ground to produce flat, parallel faces and the desired thickness. One of the 12 rings broke during grinding, and another had a visible crack.

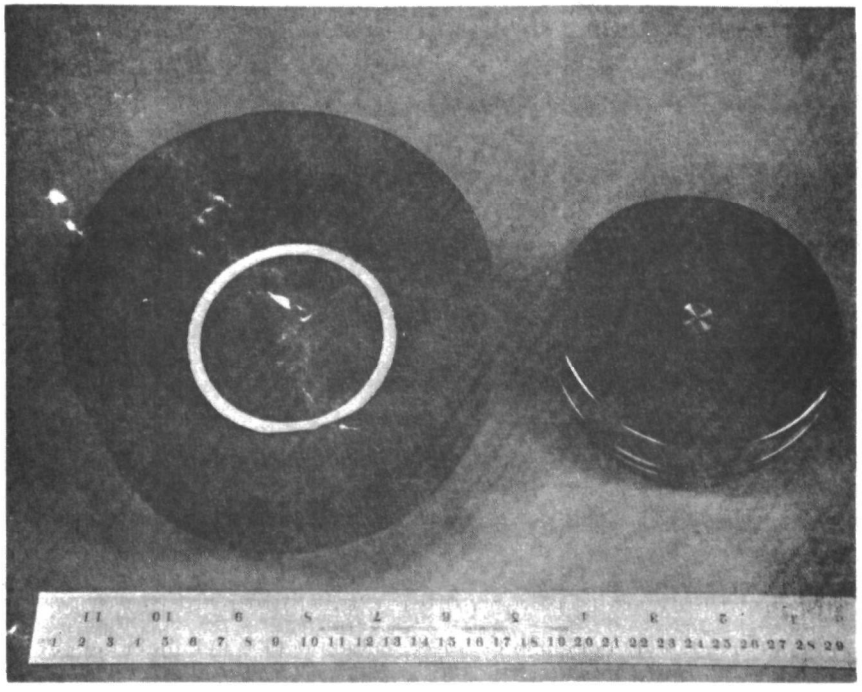

Fig. 29. Photograph of a Rubber Die and Sealing Plug

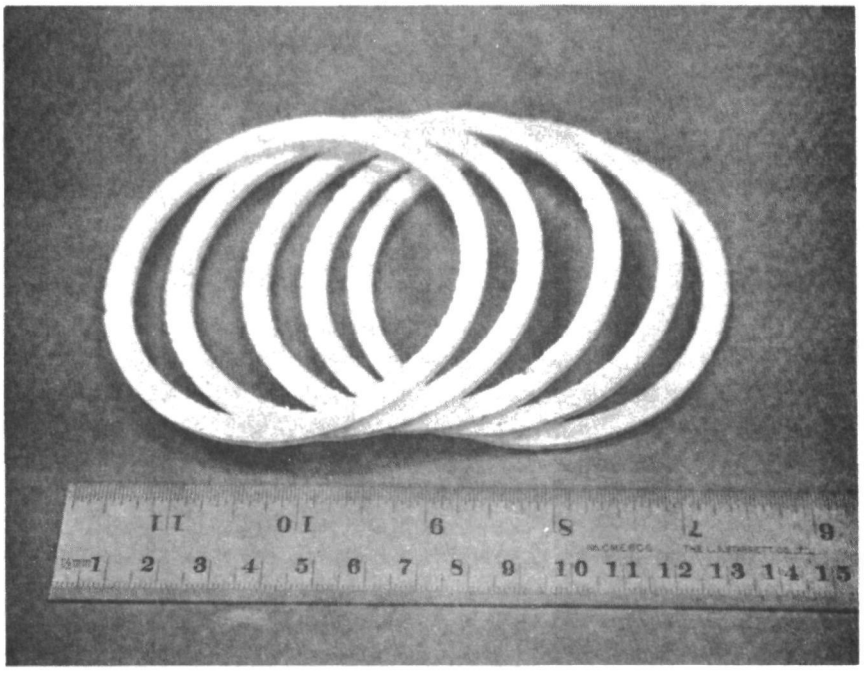

Fig. 30. Photograph of Isostatically Pressed $LiAlO_2$ Insulator Rings

In summary, the development of ceramic insulators is proceeding satisfactorily. Lithium aluminate insulator rings have been produced and will be tested in operating cells. Development work will now concentrate on the methods for producing Y_2O_3-, BeO-, and AlN-based ceramics and testing these pieces in operating cells. In addition, this task will be broadened to incorporate the development of ceramic insulators and feedthroughs which may be required in a battery.

E. Cathode Current Collector Development
(R. Rubischko)

A modification of the cathode design of Fig. 15 is being investigated. The purpose of this modification is to eliminate the molybdenum foam sheathing that prevents sulfur from dispersing into the electrolyte. An effort is currently being pursued to achieve a cathode structure of porous graphite into which chromium has been vapor-deposited so that the surfaces of the large, interconnected pores are coated with chromium. This structure will be partially filled with sulfur, which is expected to be located in small uncoated pores and the remaining volume will be filled with electrolyte, which is expected to wet the chromium-coated surfaces. The potential advantages are twofold. First, the electrolyte-filled pores are expected to provide a means of containing the sulfur without resorting to the porous metal elements in the cathode. Secondly, the number of sulfur-electrolyte-current collector reaction sites is expected to be greatly increased, which might result in greater sulfur utilization.

Fabrication of such a cathode structure has been attempted by thermally decomposing dicumene-chromium (DCC) vapor as it passed through porous graphite with a heated carrier gas. The apparatus consisted of an argon flow control unit, an argon heater, a DCC vapor generator, a quartz reaction tube, and an after condenser. A discussion of this technique of vapor deposition of chromium can be found in the literature.[25] It appears that dicumene-chromium, $Cr(C_6H_5CH(CH_3)_2)_2$, is one of a class of organo-chromium compounds which can be utilized. Other materials which may be applicable are dibenzene chromium, $Cr(C_6H_6)_2$, and chromocene, $Cr(C_5H_5)_2$. The technique may also provide a method for producing chromium-plated aluminum or aluminum alloy cell housings.

A sample of Union Carbide "Pyrofoam" Graphite, Grade FPA-20, was partially plated with chromium utilizing the dicumene-chromium vapor decomposition technique. The sample was not chromium-plated as desired because of non-uniform heating of the sample and leakage of the vapor past the porous graphite sample. The test did, however, demonstrate the feasibility of the technique. Microscopic examination of the sample and a mounted section of the sample revealed chromium deposits on the forward surface of the graphite and on surfaces of approximately 20% of the pores throughout the porous structure.

Changes have been made in the equipment design to remedy the above deficiencies. Samples are now being coated, and process control is of immediate concern. Suitably coated samples will be included in future cell tests to establish the performance characteristics of these current collectors.

V. ELECTRIC AUTOMOBILE PERFORMANCE CALCULATIONS

Calculations of the performance characteristics that might be obtained from an electric automobile powered by a lithium/sulfur battery have been made. These calculations, entailing extrapolation of laboratory cell data to full-sized batteries, are useful in that they place the cell performance now achievable in perspective relative to the intended application, and help to point out areas in which increased cell performance is necessary to achieve the ultimate aims of the program.

A. Cell Design
(R. Rubischko)

Early in the development of an electrochemical system, it is often useful to consider those problems associated with transferring the technology from small laboratory test cells to practical large-scale cells. An understanding of the ways in which the specific energy and specific power of large-scale cells are affected by variations of parameters in the laboratory cells permits investigators to design more meaningful experiments. A first approximation to large-scale cell performance is obtained from linear extrapolation of cell performance data (on the basis of identical performance per unit area of electrode) from laboratory cells to cells of a practical size for automobile propulsion.

A scaled-up lithium/sulfur cell was analyzed to determine the effects of cell size (area and thickness), materials, electrolytes, and configuration upon the specific energy of a battery. The configuration that was evaluated is not intended to be considered as a final design but rather to serve only as a means of evaluating the manner in which design can affect performance. The purpose of these studies was to estimate the values of the design parameters necessary to achieve a sealed cell with a specific energy in excess of 220 W-hr/kg and to provide quantitative data relating cell parameter variation to specific energy.

The assumptions used in the specific energy calculations were a sulfur utilization of 50% and an average cell voltage of 1.8 V. The electrolyte was assumed to be LiCl-KCl eutectic with a density of 1.67 g/cm^3 at 400°C. The overall cell reaction was assumed to be $2Li + S \rightarrow Li_2S$. The densities of lithium, sulfur, and Li_2S at a cell temperature of 400°C were taken as 0.49, 1.64, and 1.6 g/cm^3, respectively. Thus, since 0.433 g of lithium reacts with each gram of sulfur, 1.449 cm^3 of lithium reacts for each cubic centimeter of sulfur utilized. The battery weight on which the specific energy was based did not include outer battery cases, battery connectors, or outer thermal insulation. It did take into consideration the cell heaters and thermal insulation around the individual cells.

The design was that of a square cell with a laminated cathode, as shown in Fig. 31. The square shape was chosen since it is expected that fabrication of a cell with a laminated cathode would be simplest with this shape. The cathode was located below the anode so that, as the lithium is consumed, the electrolyte would remain in position. The anode housing material was assumed to be 0.25-mm-thick stainless steel, and the cathode housing material was assumed to be an aluminum alloy of 0.5-mm thickness. The anode current collector was taken to be 95%-porous stainless steel, and the laminated cathode

was assumed to be composed of 1-mm-thick elements of 91%-porous graphite filled with sulfur and 90%-porous aluminum alloy filled with LiCl-KCl. The specific energy of the cell was calculated as a function of cathode thickness and electrode area. The effect of electrode area upon specific energy is not large for cells of electrode area greater than 400 cm^2. Beyond this size, the increase in specific energy would not be expected to be balanced by the increased difficulties encountered in the use of the larger components. Increasing the cathode thickness increases the specific energy at a decreasing rate. If we consider a cell of 350-cm^2 electrode area and 0.5-cm cathode thickness, a specific energy of 204 W-hr/kg is expected. A cell having the same electrode area and a cathode thickness of 1.2 cm would have a specific energy of 234 W-hr/kg (an increase of ∿15%).

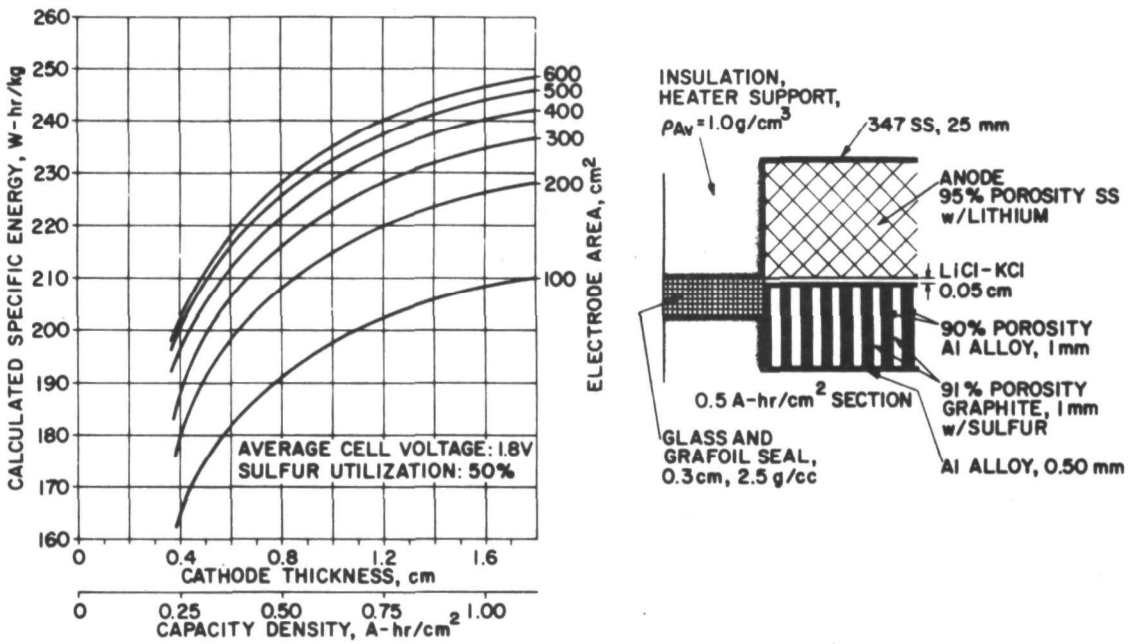

Fig. 31. Specific Energy and Schematic Design of a Li/LiCl-KCl/Li in S Square Laminated Sealed Cell

It is concluded from the design calculations that the cell housing materials must be on the order of 0.25-mm-thick stainless steel or 0.5-mm-thick aluminum since the use of heavier case materials would reduce the specific energy. It is desirable to investigate chromium plating of aluminum and magnesium to combine their low densities with the excellent corrosion resistance of chromium. It is also apparent that electrolyte elements in the cathode must have a density not much greater than that of aluminum. The use of an aluminum alloy which is adequately corrosion resistant to the cathode material and products would be desirable. High-porosity graphites such as Union Carbide Corp., Grade FPA-20, which is 91% porous with a 26-80 μm pore size, should be evaluated.

B. Method of Calculating Automobile Performance
(M. L. Kyle, E. J. Cairns)

Various estimates of the performance of electric automobiles are available,[26] but they commonly assume a certain deliverable battery energy, independent of the manner in which the automobile is driven. This assumption is incorrect for battery-powered automobiles because the deliverable energy of any battery is a function of the operating power level of the battery. In practice, the power level is related to the mode of driving (commonly termed the driving profile), and consequently must be incorporated properly in the vehicle range calculations. The effect of the details of the driving profile on the vehicle range is significant. For example, our calculations estimate a range of 530 km (329 miles) when a specified vehicle is operated at a constant velocity of 45 km/hr (28 mph). The range of this same vehicle drops to about 158 km (98 miles) on a driving profile typical of urban driving conditions with frequent stops, starts, low-speed driving, and accelerations. Regenerative braking, if used to charge the battery, could increase the vehicle range appreciably.

The calculations of expected vehicle performance reported here have eliminated the assumption of constant delivered specific energy. The vehicle parameters (weight, accessory requirements, frontal area, etc.) were based on OAP recommendations. The vehicle characteristics used for this study are presented in Table XXII. The test weight of the vehicle is 2086 kg (4600 lb).

TABLE XXII. Electric Automobile Characteristics[a]

Curb weight of vehicle	1950 kg	4300 lb
Vehicle test weight (W)	2086 kg	4600 lb
Weight of power plant (included in curb weight)		
Motors	68.0 kg	150 lb
Controls	90.7 kg	200 lb
Transmission and drive train	31.8 kg	70 lb
Air conditioner and heater	36.3 kg	80 lb
Miscellaneous	11.3 kg	25 lb
Battery	487.6 kg	1075 lb
Total	725.7 kg	1600 lb
Air drag coefficient (C_D)	0.5	
Frontal area of vehicle (A_f)	2.23 m^2	24 ft^2
Efficiency (battery output to wheels, $E_m \cdot E_e$)	0.82[b]	
Total accel./linear accel.	1.1	
Air density (ρ_A)	9.6×10^{-9} kg-hr^2/m^4	
Accessory power		
None	0 kW	
Lights, windshield wipers, blower, etc.	0.250 kW	0.33 hp
Above plus air-conditioning	2.983 kW	4 hp

[a]The assumptions and estimates used in the electric vehicle calculations do not necessarily represent the opinion of the Office of Air Programs.
[b]The transmission efficiency of 0.82 is probably optimistic for urban and suburban driving conditions; data for efficiencies under various driving cycles are not now available but should be in the near future.

The complete power plant weighs 726 kg (1600 lb) and includes a 488-kg (1075-lb) battery. A breakdown of the components of the power plant was made on the basis of information in the literature.[27,28] Performance estimates were made at three different accessory power levels: 0 kW, 0.250 kW (sufficient to operate service lights, windshield wipers, radio, and other normal automobile accessories exclusive of air-conditioning), and 2.983 kW (which includes air-conditioning).

The conceptual battery design used in these calculations is composed of 498 cells of the type depicted in Fig. 32. The square cell is of the enclosed laminated cathode design which has performed well in laboratory experiments. The cathode compartment is 0.5 cm deep, and both the sulfur and electrolyte elements are 1 mm thick. The sulfur elements consist of 91%-porous graphite filled with sulfur and the electrolyte elements are 90%-porous low-density metal (e.g., an aluminum alloy) filled with the LiCl-KCl eutectic salt mixture. The lithium anode of the cell is impregnated in a 95%-porous stainless steel current collector. Each cell is approximately 20 cm (7.9 in.) square, has a projected active area of 350 cm^2 (54 $in.^2$), weighs about 0.91 kg (2 lb), and is 1.33 cm (0.5 in.) thick. In the battery, the cells are connected in series-parallel and contained in an insulated 46 × 67 × 117 cm case (18 × 26 × 46 in.) having a volume of 0.36 m^3 (12.7 ft^3).

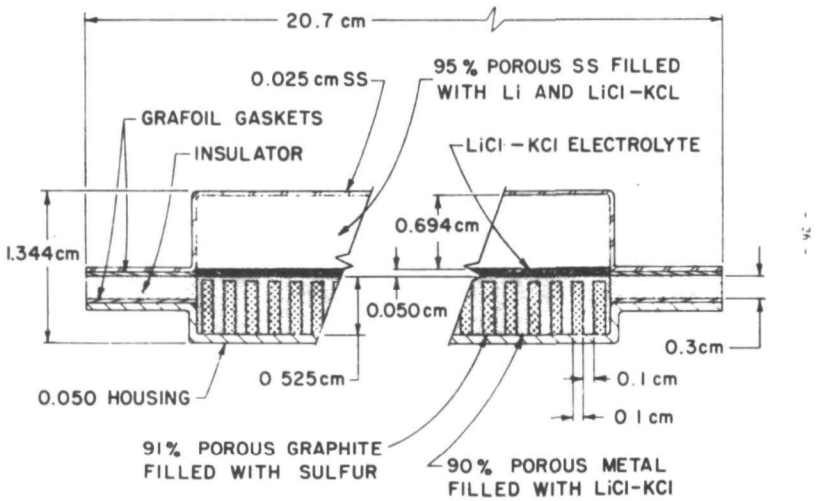

Fig. 32. Conceptual Li/S Cell Design Used in Automobile Performance Calculations

A cost analysis of the conceptual cell and battery design was performed to estimate both the current materials cost for one of these batteries and the anticipated materials cost if mass-production techniques were employed in production of the battery components. This analysis is also useful for identifying the battery components that need significant cost reductions to produce a battery with an overall cost near $2.20/kg ($1.00/lb). (The existing cost goal of $10/kW-hr of electrical storage capacity is equivalent to $2.20/kg if the battery specific energy is 220 W-hr/kg.) The results of these materials cost estimates are shown in Table XXIII.

TABLE XXIII. Weight and Material Cost Breakdown for Conceptual Cell and Battery Design

	Material	Weight, kg	Unit Cost, $/kg		Cost per Cell, $	
			Present	Projected	Present	Projected
Cell components						
Electrical insulator	BN	0.062	77.	a	$ 4.77	$0.30
Anode current collector	SS or Ni	0.090	30.	3.	2.70	0.27
Electrolyte	LiCl-KCl	0.335	4.	2.	1.34	0.67
Anode material	Li	0.053	19.	10.	1.01	0.53
Cathode current collector	Porous Graphite	0.049	11.	3.	0.54	0.15
Housing	Treated Al & SS	0.145	3.	2.50	0.44	0.36
Seal	Treated Al & SS	0.054	3.	b	0.16	b
Cathode material	S	0.122	0.40	0.40	0.05	0.05
Total cell cost					$11.01	$2.33

	Material	Weight, kg	Unit Cost, $/kg		Cost per Battery, $	
			Present	Projected	Present	Projected
Battery components						
498 cells	-	453.2	11.01[c]	2.33[c]	$5482.	$1160.
Inner can	Al	6.1	0.14	0.14	1.	1.
Outer can	Al	6.8	0.14	0.14	1.	1.
Thermal insulator	Various	12.0	50.	25.00	600.	300.
Supports, connectors, etc.	Various	7.5	2.00	2.00	15.	15.
Feedthroughs	Y_2O_3 & Al	2.0	50.00	6.00	100.	12.
Total battery cost					$6199.	$1489.

[a]Replaced by feedthrough.
[b]Not required if feedthrough is used.
[c]Cost per cell.

The goal for the cost of the conceptual cell used in the vehicle calculations is about $2.00. The present cost for materials only is about $11.00, and in mass production it would approach $2.33 if the cell electrical insulator used in this design were replaced by an electrical feedthrough. In order to reach the cost goal, further cost reductions will be required, associated primarily with cell design, in such areas as reduction in the quantity of electrolyte in each cell and replacement of the anode current collector with a less expensive porous current-collector material. These changes appear reasonable since the conceptual cell described above was designed from the current state of cell development, and advances in both design and performance are anticipated.

The calculation of vehicle performance was based upon the requirements for the battery to provide power levels sufficient to overcome tire-rolling resistance (friction between the tires and the road surfaces) and aerodynamic drag, to provide power for hill climbing and acceleration and to operate accessories.

The retarding effect of the rolling resistance was calculated by the following expression:

$$R_r = \frac{W}{65} [1 + (1.3 \times 10^{-3} V) + (10^{-5} V^2)]^* \quad (1)$$

where

R_r = rolling resistance, kg_f
W = weight of fully loaded vehicle, kg_f
V = vehicle velocity, km/hr

Aerodynamic drag resistance was approximated by the following expression:

$$R_w = \rho_A C_D A_f \frac{V^2}{2} \quad (2)$$

where

R_w = wind resistance, kg_f
ρ_A = air density, $kg_f\text{-}hr^2/m^4$
C_D = air-drag coefficient, dimensionless
A_f = frontal area of vehicle, m^2
V = velocity of vehicle, km/hr

The grade resistance, the downhill component of vehicle weight, was calculated from

$$R_g = W \sin \theta \quad (3)$$

where θ is the angle of the grade.

The acceleration resistance is represented by the following relation:

$$R_a = \frac{W}{g} \frac{dV}{dt} \quad (4)$$

where

g = gravitation constant, km/hr^2
t = time, hr

The acceleration required was obtained from the various driving profiles used in these calculations. The above relation applies only to linear acceleration. Some parts of the vehicle (such as the wheels, driveshaft, and motor) require rotational acceleration that is not accounted for in the above relation. Therefore it was assumed that an additional 10% of the value for linear acceleration is necessary.

The power that must be provided to overcome the various forces can be obtained by multiplying the sum of these forces by the vehicle velocity:

---

*Derived from an CAP suggested equation by conversion from English to metric units.

$$P_r = V(R_r + R_w + R_g + 1.1\ R_a) \tag{5}$$

This power requirement represents the power that must be delivered to the wheels and does not include losses resulting from electrical and mechanical inefficiencies nor the power required to operate the accessory load. Consequently, the power that must be delivered by the battery is

$$P_b = \frac{P_r}{E_m \cdot E_e} + \frac{P_a}{E_{ae}} \tag{6}$$

where

P_b = required battery power, kW
P_a = accessory power requirement, kW
E_m = mechanical efficiency
E_e = electrical efficiency of the drive system
E_{ae} = electrical efficiency of accessories

The range of an automobile depends upon the design, the driving profile that is assumed, and the energy-storage capability and operating power level of the battery. To estimate the battery performance, data on the voltage-capacity density relationships (taken from constant-current discharges) from several laboratory cells were combined and fitted by the empirical equation:

$$V = 2.18621603 - 5.97476987\ i + 13.48490411\ i^2 +$$

$$0.04421195\ q - 595.18189456\ iq + 867.25499666\ i^2q +$$

$$10116.62994535\ iq^2 + 17990.37652883\ i^2q^2 -$$

$$39707.09967978\ iq^3 - 1231165.26761080\ i^2q^3$$

This equation, which is quadratic in i (current density) and cubic in q (capacity density), relates V (voltage), q, and i for the laminated-cathode cell design. This relationship and some of the data used in its derivation are plotted in Fig. 33 where V is a function of q at various values of i. It should be noted that the electrode area used in calculating current densities and capacity densities in this case is the actual interfacial area between the electrolyte and sulfur-bearing elements of the laminated cathode and not the projected area of the cathode that faces the anode. The interfacial area was used because a better correlation of the data from several cells was obtained, as might be expected.

The equation represented by the curves in Fig. 33 was used in the calculation of the range of the vehicle. Each driving profile was divided into 1- to 15-sec segments, and the power and energy requirement for each segment was calculated. The battery current necessary to provide the desired power level was determined from the empirical equation. The energy requirement was the power level multiplied by the time interval. The capacity density (q) of the battery was incremented by this amount before the next interval was calculated. The range of the vehicle was then computed as the distance traveled before the battery was unable to deliver sufficient power for the next profile

interval. For the purpose of these calculations, individual cell voltages in the range of 2.2 to 1.0 V were considered acceptable.

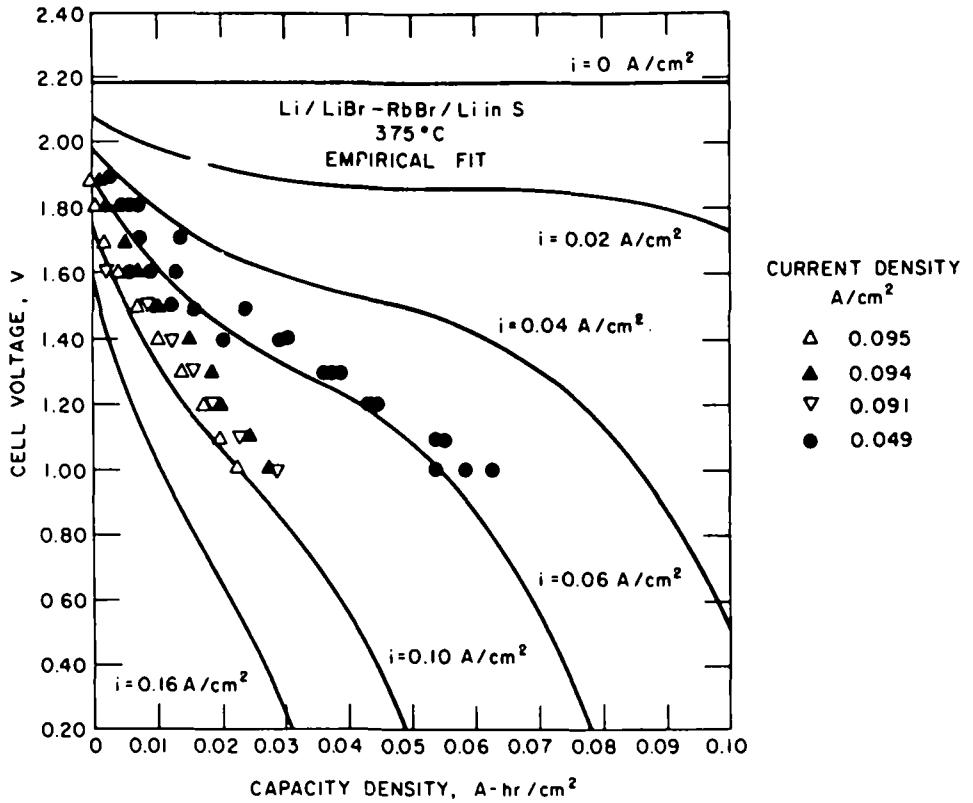

Fig. 33. Voltage-Capacity Density Data and Empirical Curves for Li/S Cells With Laminated Cathodes

In most cases, a significant amount of energy remained in the battery at the range reported. This energy was available at the required power levels; however, only at cell voltages below 1 V. This lower level of acceptable cell voltage was chosen because it is thought that a practical control system would not operate over a range of input voltages greater than about a factor of two. Some of this variation could be eliminated by parallel-series switching circuits in the control system, but this degree of complexity is beyond the intent of the current calculations.

The driving profile is an important determinant of vehicle range. Eight different profiles were used in the calculations to estimate the vehicle range under a variety of driving conditions. Four of the profiles (Urban I; Federal Register, July 15, 1970, and Nov. 10, 1970; and Public Health Service) represent urban driving conditions. Two are suburban driving profiles, and two are high, relatively constant-velocity profiles. The velocity and power requirements* of the profiles are shown in Fig. 34. The driving profiles differ in the number of starts and stops in a given time period, in the length of time at selected vehicle velocities, and in the acceleration required to complete the profile. These various driving conditions are reflected in different battery requirements of average power and peak power.

*The power requirements were based on a vehicle test weight of 4600 lb and an accessory power requirement of 2983 W.

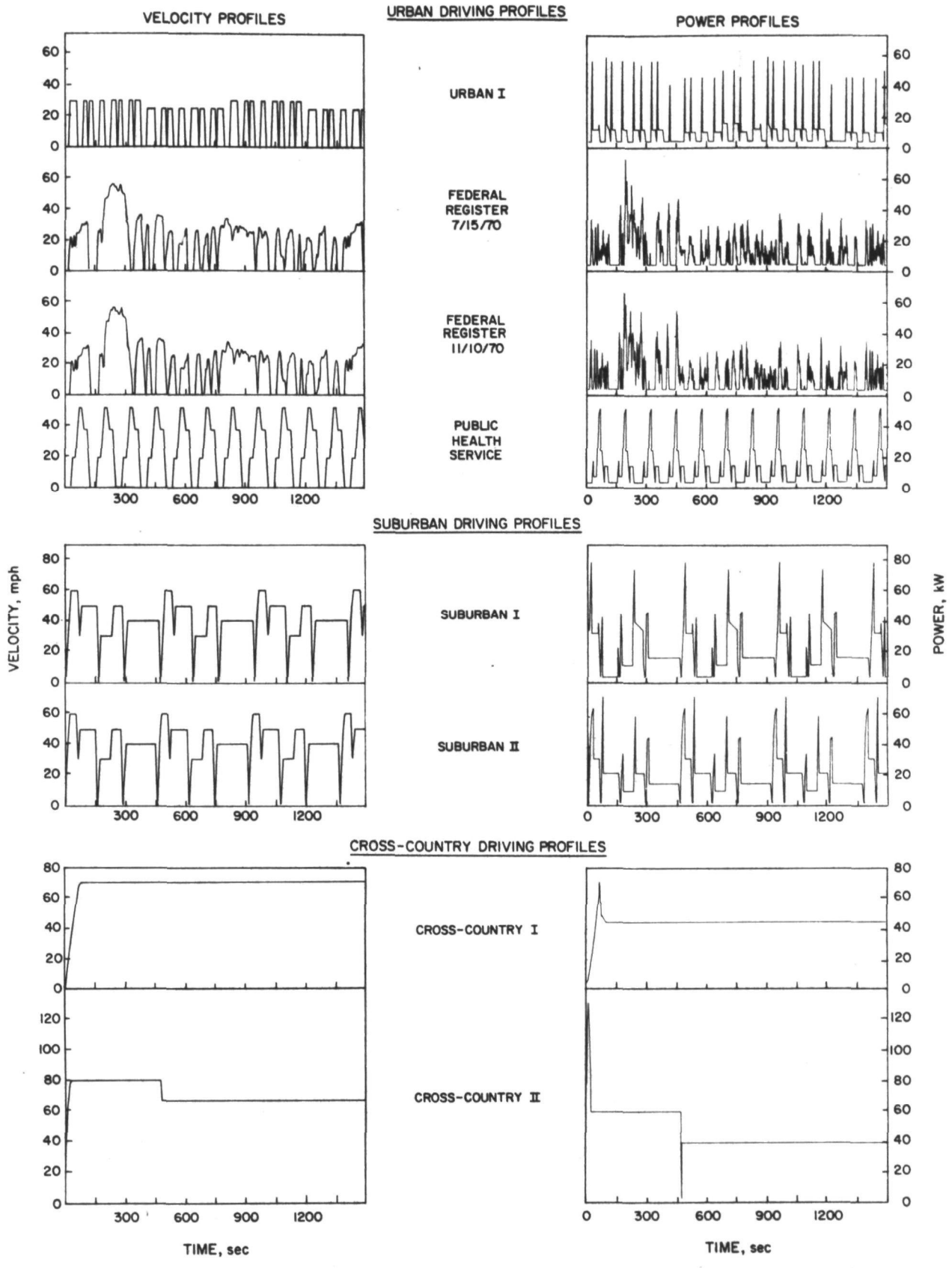

Fig. 34. Driving Profiles With Corresponding Power Profiles for the Automobile of Table XXII

C. Results and Discussion
(M. L. Kyle, E. J. Cairns)

The results of the calculations are shown in Table XXIV. The effect of accessory power requirements and driving conditions on the range of the vehicle for three of the driving profiles depicted in Fig. 34 are shown in Fig. 35. Under urban driving conditions averaging around 32 km/hr (20 mph) and for an accessory load of 2.983 kW (4 hp), the vehicle range is 158 to 248 km (98 to 154 miles) depending upon the exact driving conditions. At the lower accessory load of 0.250 kW, the range increases to around 322 km (200 miles). Urban driving requires peak power levels of 99 to 150 W/kg (45 to 68 W/lb); the battery delivers 120 to 195 W-hr/kg (54 to 89 W-hr/lb) with the greater energy capability and longer ranges obtained at the lower power levels.

Suburban driving averages around 64 km/hr (40 mph) and requires higher peak power levels of up to 162 W/kg (73 W/lb). The higher power levels reduce the delivered specific energy of the battery (at the 2.983-kW accessory power level) to as low as 97 W-hr/kg (44 W-hr/lb) and the vehicle range drops to 142 to 206 km (88 to 128 miles).

Constant-speed driving, even at the higher velocities of 96 to 113 km/hr (60 to 70 mph), is not as demanding on the battery as some of the other profiles because the average power level is lower. Once the initial power required to accelerate the vehicle to its velocity has been satisfied, the power requirement drops off so that, at a constant velocity of 113 km/hr (70 mph) and an accessory load of 2.983 kW, the range of the vehicle increases to 277 km (172 miles). At lower constant velocities of 32 to 40 km/hr (20 to 25 mph), the vehicle's range is over 483 km (300 miles). The effect of (constant) velocity on vehicle range is shown in Fig. 36 for constant velocities of 16 to 113 km/hr (10 to 70 mph) and a 2.983-kW (4-hp) accessory load. The range falls off rapidly at velocities above 88 km/hr (55 mph) primarily because of the increased retarding effect of wind.

The possible benefits obtainable from regenerative braking were investigated briefly. The automobile has a calculated range of about 187 km (116 miles) when driving according to the Urban I driving profile. This same vehicle would have a range of about 232 km (144 miles), a 24% increase, if 50% of the energy dissipated during braking could be recovered. A similar automobile, driven according to the Federal Register, Nov. 10, 1970, urban driving profile, increases about 12% in range from 193 km (120 miles) to 217 km (135 miles) if regenerative braking is employed. The calculations suggest that regenerative braking should be considered for any electric automobile powered by a lithium/sulfur battery. Regenerative braking is attractive because of the lithium/sulfur battery's ability to accept recharge at a rapid rate. The increased range obtained is significant even if some weight must be added to the vehicle to provide the regenerative-braking capability.

The conclusions that can be drawn from these calculations are that lithium/sulfur cells possess the potential for powering an all-electric vehicle. Laboratory cells have been shown to have a sufficient power density to accomplish all driving profiles tested. Energy storage, however, should be improved to increase the range of the vehicle. Two different methods of increasing the energy storage are available, namely, (1) increasing the capacity density

TABLE XXIV. Electric Automobile Performance Under Selected Driving Profiles[a]

Driving Profile (Average Velocity)	Average Energy/ Ton-Mile, kW-hr	Accessory Power, W	Delivered Specific Energy, W-hr/kg	Peak Power Interval, sec	Peak Power, W/kg	Peak Power Density, W/cm^2	Capacity Density, > 1 V, $A\text{-}hr/cm^2$	Range miles	Range km
Federal Register	0.18	0	157	1	128	0.36	0.22	187	301
Nov. 10, 1970	0.18	250	156	1	129	0.36	0.22	179	288
(19.5 mph)	0.26	2983	146	1	135	0.38	0.20	120	193
Federal Register	0.18	0	132	1	142	0.39	0.18	158	254
July 15, 1970	0.18	250	131	1	142	0.40	0.18	150	241
(19.6 mph)	0.26	2983	120	1	149	0.41	0.16	98	158
Urban I	0.21	0	185	4	112	0.31	0.27	186	299
(15.7 mph)	0.22	250	185	4	113	0.31	0.27	179	288
	0.31	2983	170	4	120	0.33	0.24	116	187
Public Health	0.20	0	215	7	99	0.28	0.32	225	362
Service	0.21	250	213	7	100	0.28	0.32	217	349
(23.9 mph)	0.27	2983	195	7	107	0.30	0.29	154	248
Suburban I	0.20	0	105	1	154	0.43	0.15	114	183
(41.3 mph)	0.20	250	102	1	155	0.43	0.15	109	175
	0.23	2983	97	1	162	0.45	0.14	88	142
Suburban II	0.21	0	164	14	121	0.34	0.29	169	272
(40.3 mph)	0.21	250	162	14	122	0.34	0.29	164	264
	0.25	2983	148	14	129	0.36	0.22	128	206
Cross-Country I	0.25	0	256	10	145	0.40	0.40	213	343
(70 mph)	0.26	250	254	10	146	0.40	0.40	209	336
	0.28	2983	225	10	152	0.42	0.36	172	277
Cross-Country II	0.24	0	219	5	262	0.73	0.32	193	310
(67.2 mph)	0.24	250	221	5	262	0.73	0.33	193	310
	0.26	2983	240	5	269	0.75	0.37	193	310

[a]The transmission efficiency of 0.82 used in these calculations is probably optimistic for the urban and suburban driving profiles; data for efficiencies under various driving cycles are not now available but should be in the near future. An approximate correction for the listed ranges for small variations of the transmission efficiency can be estimated from $R_E = (3.75E - 2.1)R_{82}$ where R_E = range of vehicle at transmission efficiency E, km; E = transmission efficiency, fraction; R_{82} = range of vehicle at transmission efficiency of 0.82, km.

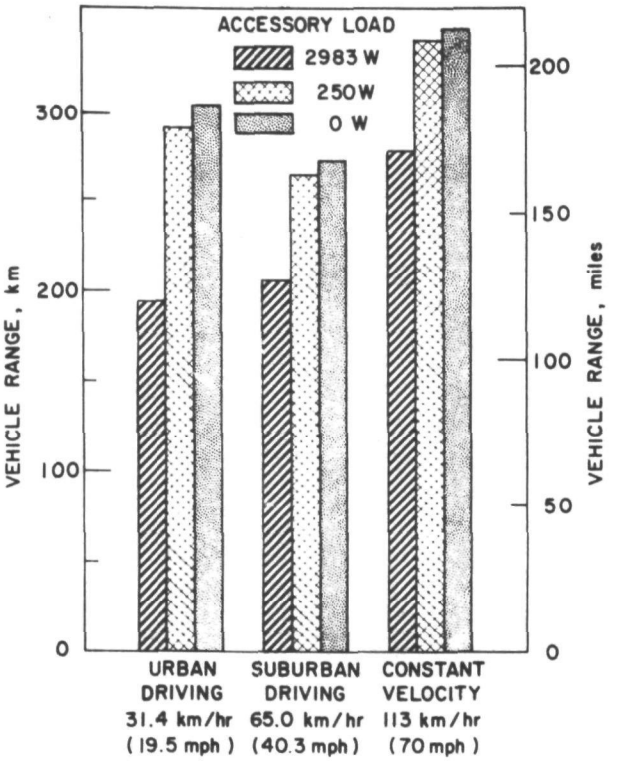

Fig. 35. Electric Automobile Ranges for Selected Driving Profiles

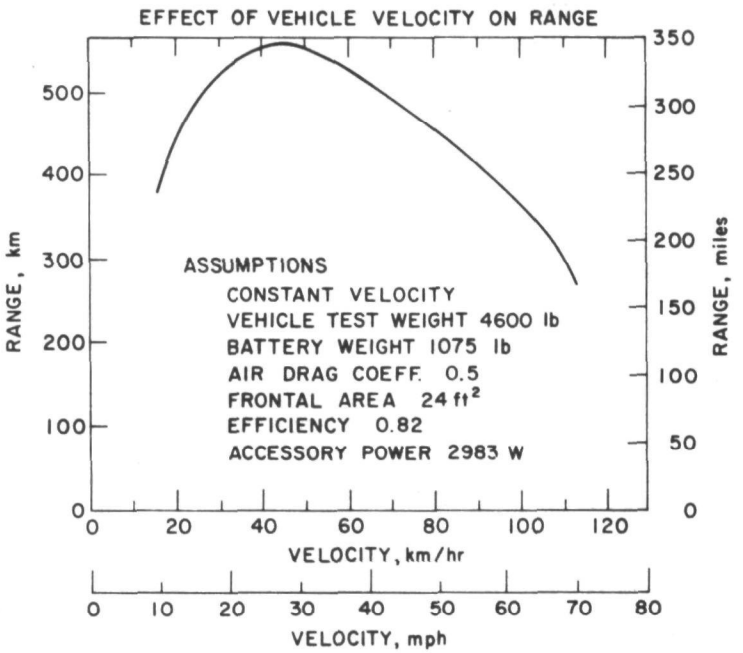

Fig. 36. Effect of Automobile Velocity on Range for Constant Velocity Driving

and capacity per unit volume of the cells and (2) increasing the average voltage of the cell during discharge by reducing the diffusional and resistive overvoltages. Both of these areas are under active investigation in the cell program, and it is hoped that these improvements in cell operation will result in projected vehicle ranges in excess of 325 km (200 miles).

D. Lithium Reserves
(M. L. Kyle)

The availability of lithium ore reserves capable of supporting an electric automobile industry utilizing lithium/sulfur batteries has been investigated.* The resources were subdivided into three categories: (1) measured and indicated resources, (2) resources inferred from current operations, and (3) potential resources, which include low-grade ores of currently uneconomic recovery potential. Estimates of lithium available from these sources are shown below:

Source	Kg of Li as Metal
Measured and indicated	4.3×10^9
Inferred	7.3×10^8
Potential resources	1.7×10^{10}
Total	2.2×10^{10}

There has been little economic incentive for locating additional lithium-bearing deposits because the known reserves are adequate for many years at the present rate of usage. Production statistics for lithium are not released to the public, but it is our estimation that the measured reserves represent a substantial supply at the current rate of lithium usage. (The 1965 edition of the U. S. Bureau of Mines' Minerals Yearbook estimates the world's production of lithium ores to be only about 6×10^7 kg/year.) The chances that a persistent exploration effort would yield further discoveries of lithium ores must be recognized since this has proved to be true for other minerals.

The automobile described previously is powered by a lithium/sulfur battery containing about 46.7 kg of lithium metal or equivalent. This value assumes that LiCl-KCl is the cell electrolyte and $LiAlO_2$ is the primary cell insulator. The measured reserves are sufficient to produce about 10^8 batteries of this size. Total reserves are sufficient to produce about 5×10^8 batteries of this size.

Lithium availability does not appear to be a hindrance to the utilization of lithium/sulfur batteries as electric vehicle propulsion devices. The present supply seems ample for any foreseeable application and, given an economic incentive to develop new sources, additional reserves could probably be located.

---

*The figures quoted were supplied by Dr. H. R. Grady of the Foote Mineral Company.

VI. STATUS AND FUTURE PLANS

The lithium/sulfur cell program has been, until now, essentially a laboratory program to determine if these cells show promise for use in a high-specific-energy, high-specific-power battery. At this stage in its development, the Li/S cell still appears promising, and many of the problems that must be solved to make the Li/S battery both technically and economically attractive have been identified. Laboratory cells of less than 10-cm^2 electrode area have demonstrated capacity densities (at the 1-hr rate) of 0.4 A-hr/cm^2 and lifetimes of over 800 cycles and 1100 hr (at reduced capacity densities). No cell operated to date, however, has achieved the required high performance levels over an extended lifetime. The sulfur electrode limits cell performance -- the capacity per unit volume and sulfur utilization must be improved to provide a viable battery. Sulfur electrode design modifications, additives to the sulfur, and the proper choice of electrolyte are all capable of increasing the cell performance.

The cells operated to this time have been relatively small ($\lesssim$10-cm^2 electrode area) and unsealed. The full-scale cells will be much larger ($\sim$ 350 cm^2) and must be sealed. Initial scale-up efforts are necessary to provide information on problem areas peculiar to the sealing, design, construction, and operation of larger cells. Materials are available for laboratory and first-generation, scaled-up cells, but the applicability of low-cost, lightweight construction materials that are necessary for a high-energy-density, high-power-density, low-cost battery is yet to be demonstrated. Finally, the assembly of cells into batteries will present new problem areas of cell matching, safety, reliability, long-term hermetic sealing, and temperature control. The program until now has been a laboratory effort to demonstrate the technical feasibility of lithium/sulfur cells. A great deal of research and development remains to be done to reach the stage of a reliable battery.

The FY 1972 OAP program at ANL for the development of lithium/sulfur batteries will be concentrated in three main areas of activity: a laboratory program for the support of the other portions of the program, a materials program for the development and testing of materials and components of cells and batteries, and a cell-development program centering around the improvement of cell performance and the development of sealed, scaled-up cells, leading into battery development in FY 1973.

The laboratory program will provide the necessary physicochemical information to the materials and cell-development programs. This information will include the measurement of the solubility of cathode materials in molten-salt electrolyte of various compositions and the physicochemical properties of electrolytes, the preparation of electrolytes, the investigation and synthesis of solid electrolytes having high lithium-ion conductivity, the study of the electrochemistry and chemistry of the lithium/sulfur cell, the evaluation of new current collector and electrode structures, and safety studies.

The materials program will have as its objective the identification and synthesis, as necessary, of corrosion-resistant metals and ceramics and the construction of certain cell components such as current collectors and electrical feedthroughs. Both short- and long-term corrosion tests will be carried

out. The promising materials will be obtained in appropriate forms for current collectors, housings, and other components, or these forms will be prepared at ANL. Insulating seals and feedthroughs will be prepared for corrosion testing and for use in cells. Suppliers for the seals and feedthroughs will be identified.

The cell development program for FY 1972 will center around the improvement of cell life at high capacity density and the scale-up of cells to larger sizes. Small-scale cell studies will be performed to test new electrode structure ideas, to improve cell lifetime, and to develop cell sealing techniques. The cell scale-up work will involve the preparation and testing of larger-area electrodes ($\sim$30-60 cm^2), and the construction and testing of larger-size sealed cells, preparatory to work on a 1-2-kW battery.

REFERENCES

1. C. E. Johnson, M. S. Foster, and M. L. Kyle, Purification of Inert Atmospheres, Nucl. Appl. 3, 563 (1967).
2. E. R. Van Artsdalen and I. S. Yaffe, Electrical Conductance and Density of Molten Salt Systems: KCl-LiCl, KCl-NaCl, and KCl-KI, J. Phys. Chem. 59, 118 (1955).
3. G. H. Kucera, P. T. Cunningham, Argonne National Laboratory, private communication (1970).
4. C. E. Johnson, Argonne National Laboratory, private communication (1970).
5. S. I. Berezina, A. G. Bergman, and E. L. Bakumskaya, Phase Diagram of the System KCl-LiCl-KF-LiF, Zh. Neorgan. Khim. 8 (9), 2140 (1963).
6. H. Shimotake, M. L. Kyle, V. A. Maroni, and E. J. Cairns in Proc. 1st Intern. Electric Vehicle Symp., Nov. 5-7, 1969, Pheonix, Ariz., Electric Research Council.
7. A. S. Dworkin, H. R. Bronstein, and M. A. Bredig, Miscibility of Metals with Salts. VI. Lithium-Lithium Halide Systems, J. Phys, Chem. 66, 572 (1962).
8. E. J. Cairns, G. H. Kucera, and P. T. Cunningham, Thermodynamic Studies of the Lithium-Selenium System by an EMF Method, presented at the CITCE Meeting, Prague, Sept. 28-Oct. 2, 1970; see also Extended Abstracts.
9. P. T. Cunningham, Argonne National Laboratory, private communication (1971).
10. V. A. Maroni, Argonne National Laboratory, private communication (1970).
11. H. A. Laitinen and C. H. Liu, An Electromotive Force Series in Molten LiCl-KCl Eutectic, J. Amer. Chem. Soc. 80, 1015 (1958).
12. C. H. Liu and S. Shen, Argentometric Titration of Sulfide in Alkaline Solution, Anal. Chem. 36, 1652 (1964).
13. P. O. Bethge, On the Volumetric Determination of Hydrogen Sulfide and Soluble Sulfides, Anal. Chim. Acta 10, 310 (1954).
14. R. Collongues, Les Phénomènes d'Ordre-désordre en Chimie Minérale, Ann. Chim. (France) 8, 395 (1963).
15. R. S. Roth and S. Hasko, Beta-Alumina-Type Structure in the System Lanthana-Alumina, J. Amer. Ceram. Soc. 41(4), 146 (1958).
16. L. Hsueh and D. N. Bennion, Ionic Conduction in Beta-Alumina, Interim Technical Report No. 6, Report No. 69-68, Dept. of Army, Mobility Equipment Research and Development Center, Ft. Belvoir, Va.
17. A. Imai and M. Harada, Ionic Conduction in Impurity Doped ß-Alumina, Abstract No. 277, Extended Abstracts, The Electrochemical Society, 137th National Meeting, May 1970.
18. F. A. Shunk, Constitution of Binary Alloys, Second Supplement, p.344, McGraw-Hill Book Co., N. Y. (1969).
19. G. Kullerud and H. S. Yoder, Pyrite Stability Relations in the Fe-S System, Economic Geology 54(4), 533 (1959).
20. A. A. Velikanov and V. A. Tertykh, Electrical Conductivity, Polarization, and Electrolysis of Thallium-Sulfur Melts, Zh. Fiz. Khim. 43, 2580 (1969).
21. M. Hansen and K. Anderko, Constitution of Binary Alloys, p.1168, McGraw-Hill Book Co., N. Y. (1958).
22. R. K. Steunenberg, C. Trapp, R. M. Yonco, and E. J. Cairns, Electrical Conductivity of Liquid Sulfur and Sulfur-Phosphorus Mixtures, presented at Third Annual Mardi Gras Symposium on Sulfur Chemistry and Theoretical Chemistry, New Orleans, February 18-19, 1971.
23. R. W. Flournoy, Reynolds Aluminum Corp., private communication (Dec. 28, 1970).

24. D. W. Strickler and R. Roy, Studies in the System Li_2O-Al_2O_3-Fe_2O_3-H_2O, J. Amer. Ceram. Soc. 44(5), 225 (1961).
25. J. E. Knap, B. Pesetsky, and F. N. Hill, Vapor Plating With Dicumene-chromium Preparation and Properties of the Chromium Plate, Plating 53, 772 (1966).
26. J. H. B. George, L. J. Stratton, and R. G. Acton, Prospects for Electric Vehicles, A Study of Low-Pollution-Potential Vehicles--Electric, Arthur D. Little, Inc. report to the U. S. Department of Health, Education and Welfare, National Center for Air Pollution Control (May 1968).
27. P. D. Agarwal, I. M. Levy, A High-Performance A. C. Electric Drive System, SAE preprint 670178, Annual Meeting, January 1967.
28. E. A. Rishaun, W. D. Bond, and T. A. Zechin, Electrovair - A Battery Electric Car, SAE preprint 670175, Annual Meeting, January 1967.

APPENDIX: SUMMARY OF PERFORMANCE OF CELLS OPERATED IN FISCAL YEAR 1971

CELLS OPERATED IN FISCAL YEAR 1971

Cell No.	Cell[a] Type	Cathode: Sulfur-Containing Element: Material[b]	Porosity, %	Pore Size, μm	Thickness, cm	Cathode: Electrolyte-Cont. Element: Material[b]	Porosity, %	Pore Size, μm	Thickness, cm	Mo Foam Sheath[c]: Porosity, %	Pore Size, μm	Thickness, cm	Active Material: Li, g	S, g	Electrolyte[d]	Cathode Area,[e] cm²	Theoretical Capacity Density,[f] A-hr/cm²	Capacity Density, > 1 V, A-hr/cm²	Capacity per Unit Volume Cathode,[g] A-hr/cm³	Current Density, A/cm²	Percent of Theoretical Capacity	Average Voltage,[h] V	Cell Life: No. of Cycles	Cell Life: Time, hr
28	L	SSH	80	30	0.16	SSH	80	30	0.16	---- None ----			1.0	1.23	A	1.59	1.29	0.33	0.30	0.30	26	1.4	6	100
29	R	SSH	80	30	0.16	--------- None --------				---- None ----			0.5	0.30	A	1.2	0.42	---------- Cell shorted ----------					0	<1
30	L	SSB	85	40	0.071	SSH	80	30	0.16	---- None ----			0.5	0.51	A	1.70	0.50	0.16	0.14	0.29	31	1.3	3	2
31	L	SSB	85	40	0.071	SSB	85	40	0.071	---- None ----			0.5	1.06	A	1.64	1.08	0.23	0.21	0.30	21	1.4	4	5
32	R	SSH	80	30	0.16	--------- None --------				---- None ----			0.2	0.30	A	1.2	0.40	0.03	0.16	0.33	8	1.4	1	0.3
33	L	SSH	80	30	0.16	SSB	85	40	0.071	---- None ----			0.5	1.24	A	1.09	1.90	0.23	0.21	0.37	12	1.4	1	1
34	L	SSH	80	30	0.16	SSB	85	40	0.071	---- None ----			0.5	1.27	A	1.09	1.95	0.18	0.16	0.38	9	1.4	3	1
35	L	SSH	80	30	0.16	SSH	80	30	0.16	---- None ----			0.5	1.18	A	1.58	1.25	0.29	0.26	0.32	24	1.5	3	3
36	L	SSH	80	30	0.16	SSB	83	25	0.045	---- None ----			0.5	1.16	A	0.96	2.01	0.02	0.018	0.52	1	1.2	1/2	0.1
37	L	SSH	80	30	0.16	SSB	83	25	0.045	---- None ----			1.0	1.18	A	0.96	2.06	0.52	0.47	0.52	25	1.5	3	5
38	L	SSB	83	25	0.05	SSB	83	25	0.05	---- None ----			1.0	0.68	A	0.97	1.17	---------- Cell shorted ----------					0	0.1
39	L	SSH	80	30	0.09	SSH	80	30	0.09	---- None ----			0.3	0.74	A	0.92	1.34	0.27	0.25	0.54	20	1.3	4	3
40	L	SSH	80	30	0.09	SSH	80	30	0.09	---- None ----			0.3	0.77	A	0.92	1.39	0.13	0.12	0.54	9	1.5	2	0.9
41	L	SSH	80	30	0.09	SSH	80	30	0.09	---- None ----			0.5	0.77	A	0.92	1.39	0.19	0.18	0.54	14	1.5	1/2	0.5
42	L	POCO AX	63	1.4	0.09	SSH	80	30	0.16	---- None ----			0.5	0.62	A	1.33	0.79	0.02	0.019	0.26	1	1.5	1/2	0.1
43	L	POCO AX	63	1.4	0.09	SSH	80	30	0.16	---- None ----			0.6	0.59	A	1.33	0.74	0.21	0.20	0.38	28	1.4	2	2
44	L	POCO AX	63	1.4	0.09	SSH	80	30	0.16	---- None ----			0.6	0.60	A	1.31	0.76	0.33	0.30	0.25	44	1.3	6	18
45	C	POCO AX	63	1.4	1.3	--------- None --------				---- None ----			0.7	1.64	A	1.89	1.45	0.40	0.23	0.53	27	1.5	4	7
46	C	POCO AX	63	1.4	1.3	--------- None --------				---- None ----			0.7	1.55[j]	A	1.89	1.08	0.30	0.18	0.32	28	1.5	3	5
47	L	POCO AX	63	1.4	0.094	Mo	75	20	0.17	---- None ----			0.7	0.66[j]	B	1.75	0.50	0.09	0.05	0.32	17	-	17	15
48	L	FC-14	49	3.5	0.17	Mo	75	20	0.17	---- None ----			1.7[k]	0.71	B	1.71	0.56	0.04	0.03	0.25	8	-	1	2
49	L	POCO AX	63	1.4	0.09	Mo	75	20	0.09	---- None ----			0.7	1.27[j]	B	2.43	0.69	0.07	0.06	0.25	9	-	35	152
50	R	POCO AX	63	1.4	0.06	--------- None --------				---- None ----			0.6	0.89	B	1.00	1.48	0.28	0.20	0.30	19	2.0	6	5

CELLS OPERATED IN FISCAL YEAR 1971 (cont.)

Cell No.	Cell[a] Type	Cathode: Sulfur-Containing Element: Material[b]	Porosity, %	Pore Size, μm	Thickness, cm	Electrolyte-Cont. Element: Material[b]	Porosity, %	Pore Size, μm	Thickness, cm	Mo Foam Sheath[c]: Porosity, %	Pore Size, μm	Thickness, cm	Active Material: Li, g	S, g	Electrolyte[d]	Cathode Area,[e] cm²	Theoretical Capacity Density,[f] A-hr/cm²	Capacity Density, 1 V, A-hr/cm²	Capacity per Unit Volume Cathode,[g] A-hr/cm³	Current Density, A/cm²	Percent of Theoretical Capacity	Average Voltage,[h] V	Cell Life: No. of Cycles	Cell Life: Time, hr
51	L	POCO AX	63	1.4	0.09	Mo	75	20	0.09	------ None ------			0.7	0.28	B	1.47	0.32	0.10	0.19	0.20	31	1.7	7	3
52	ER	FC-14	49	3.5	0.16	---------- None --------				78.2	25	0.3	1.0	3.82	B	1.24	5.14	0.45		0.24	9	1.7	1	3
53	ER	FC-14	49	3.5	0.2	---------- None --------				90	67	0.4	0.4	0.98	C	0.28	6.01	0.095	0.046	0.28	2	-	1	1
54	ER	FC-14	49	3.5	0.3	---------- None --------				90	67	0.3	0.3	0.98	B	1.00	1.63	0.15	0.13	0.25	9	1.6	9	26
55	EL	POCO AX	63	1.4	0.15	Mo	78.2	25	0.19	78.2	25	0.3	0.7	0.51	D	2.53	0.33	0.17	0.14	0.20	50	1.8	803	1100
56	ER	FC-14	49	3.5	0.3	---------- None --------				78.2	25	0.4	0.7	1.22	D	1.00	2.04	0.55	0.33	0.17	27	1.6	600	750
57	ML	PG-60	48	33	0.4	Mo	78.2	25	0.2	78.2	25	0.6	14.4	19.4	D	20.0	1.60	0.60	0.30	0.20	20	1.9	23	30
58	ML	POCO AX FC-14	63 49	1.4 3.5	0.3	Mo	78.2	25	0.2	78.2	50	0.48	13.9	16.1	D	27.6	0.97	0.18 0.15	0.17 0.14	0.18 0.25	19	1.9	7	25
59	ER	---------- None ----------				---------- None --------				78.2	25	0.16	0.7	1.18	B[+]	1.0	1.97	0.13 0.21	0.18 0.28	0.20 0.10	7	1.8 1.7	141	184
60	ER	PG-25	48	120	0.3	---------- None --------				78.2	25	0.16	0.7	1.52	B[+]	1.0	2.54	0.57	0.51	0.10	22	1.9	29	89
61	ER	PG-25	48	120	1.0	---------- None --------				78.2	25	0.16	0.7	0.74	B[+]	1.0	1.24	0.51 0.048	0.52 0.05	0.10 0.20	41	1.7	253	90
62	ER	FC-14	49	3.5	0.25	---------- None --------				78.2	25	0.33	0.7	1.24	D	1.0	2.07	0.17	0.09	0.20	8	1.9	131	175
63	ER	PG-25	48	120	0.32	---------- None --------				78.2	25	0.64	0.8	11.8	D	2.6	7.58	0.23	0.05	0.32	11	1.6	1/2	5
64	LY	Nb	90	12/35	0.16	Nb	90	12/35	0.16	78.2	25	0.16	0.8	0.71	D	1.0	1.19	0.13 0.14	0.29 0.30	0.20 0.10	11 11	1.7	36	117
65	LY	GF	97.3	-	0.6	---------- None ----------				78.2	25	0.39	0.8	8.34	B[+]	1.8	7.61	0.58	0.20	0.10	8	0.6	7	27
66	ER	PG-25	48	120	1.3	---------- None ----------				78.2	25	0.64	0.8	9.43	D	2.6	6.15	0.70 0.75	0.24 0.26	0.20 0.10	11 12	1.9	11	70
		Metal		Carbon		Electrolyte		Sulfur																
		Wt, g	Vol %	Wt, g	Vol %	Wt, g	Vol %	Wt, g	Vol %															
67	M	0.226	0.40	0.51	5.1	3.95	48.5	4.59	46.0	78.2	25	0.15	2.11	4.59	B[+]	2.55	3.0	0.218	0.114	0.1	8	1.8	82	230
68	M	2.0	4.4	0.8	10.0	2.69	43.5	3.2	42.1	78.2	25	0.15	1.85	3.2	B[+]	2.55	2.1	0.257	0.172	0.1	12	1.6	3	42

FOOTNOTES FOR APPENDIX TABLE

[a]Cell type classification:
L = laminated, C = comb, R = reservoir, ER = enclosed reservoir, EL = enclosed laminated, ML = multilayered, LY = layered, M = mixed.

[b]SSH = Type 302 stainless steel Feltmetal, Huyck; SSB = Type 304 stainless steel Brunspore Fibermetal, Brunswick; POCO AX = porous graphite, Poco Graphite; FC-14 = porous carbon, Pure Carbon; PG-25, PG-60 = porous graphites, Union Carbide Corp.; NB = niobium; GF = graphite felt.

[c]Molybdenum foam = a product of Spectra-Mat, Inc. In Cells No. 53 and 54, Type 347 stainless steel Feltmetal was used.

[d]Electrolytes (in mol %):
A = 59 LiBr-41 RbBr (mp = 278°C), B = 58.5 LiCl-41.5 KCl (mp = 352°C), C = 11.7 LiF-29 LiCl-59.3 LiI (mp = 342°C), D = 8.5 LiCl-59.0 LiI-32.5 KI (mp = 265°C), B^+ = 3.5 LiF-56 LiCl-40.5 KCl (mp ∿345°C).

[e]Cathode area: projected electrode area facing the anode.

[f]Theoretical capacity density: calculated based on Li_2S as the final discharged product.

[g]Capacity per unit volume of cathode: based on the volume of reactants and current collectors excluding housing and sheath.

[h]Average voltage = $\frac{\int V\,dt}{\Delta t}$ where V = cell terminal voltage, t = discharge time (cut-off voltage = 1 V).

[j]In these cells P_4S_{10} was used instead of S.

[k]In this cell a Li-Al alloy was used instead of Li.